Physics – Uspekhi **60** (12) 1197 – 1235 (2017)

REVIEWS OF TOPICAL PROBLEMS PACS numbers: 52.20.Dq, 52.20.Fs, 52.25.Dg, 52.50.Sw

Electron–ion collisions in strong electromagnetic fields

A A Balakin, G M Fraiman

DOI: https://doi.org/10.3367/UFNe.2017.02.038075

Contents

Abstract. The current status of the problem of electron–ion collisions in strong electromagnetic fields is presented. The collision operator is expressed in terms of an integral over test particle trajectories for an arbitrary alternating field. The equation for test particles is analyzed. It is shown that none of the energy processes involved (Joule heating, bremsstrahlung and fast electron generation) diminishes as the electromagnetic field amplitude increases. The collision frequency, the momentum distribution of fast electrons, and the electron–ion collision operator are calculated in the classical framework.

Keywords: electron–ion collisions in plasma, strong electromagnetic fields, collision operator (integral)

1. Introduction

Recent years have seen considerable progress in the production of superstrong laser pulses with focal intensities of $10^{18}-10^{21}$ W cm^{-2} and higher. At such field intensities, in the laser wavelength range the plasma electrons oscillate with velocities that far exceed their thermal velocities, which opens up brand-new, previously unexplored possibilities for studying radiation–plasma interactions. In this case, one of the key issues is the question of the importance of collisions in these interactions.

Investigations of collisional absorption of superstrong laser pulses in plasmas are required for several applications. To the latter one can attribute thermonuclear fusion using ultrashort high-intensity laser pulses for the fast ignition of fusion reactions, X-ray lasers, and the conversion of laser energy to the coherent radiation at fundamental frequency harmonics in the superstrong laser pulse–plasma interaction.

Theoretical studies of electron collisions in strong electromagnetic (EM) fields have been traditionally performed on the basis of three models: small-angle electron scattering [1–22], Born [15, 23–30], and low-frequency [14, 31] approximations. The approximation employed in Refs [3–5] has been historically referred to as small-angle. However, this approximation would be more properly termed the straight line approximation, since it implies that the drift trajectories of scattered particles are nearly straight lines. By drift trajectory is meant a trajectory resulting from the subtraction of particle oscillations from the particle trajectory in the laboratory frame of reference. We note that in drift coordinates the electron motion unperturbed by the Coulomb potential describes a straight line and that ions oscillate. By contrast,

A A Balakin, G M Fraiman Institute of Applied Physics, Russian Academy of Sciences, ul. Ul'yanova 46, 603950 Nizhny Novgorod, Russian Federation
E-mail: balakin@appl.sci-nnov.ru, fraiman@appl.sci-nnov.ru

Received 24 October 2016, revised 20 February 2017
Uspekhi Fizicheskikh Nauk **187** (12) 1289 – 1328 (2017)
DOI: https://doi.org/10.3367/UFNr.2017.02.038075
Translated by E N Ragozin; edited by A Radzig

in the laboratory reference system, the ions are at rest and the electron motion reduces to a slow drift of oscillations. Calculated in the Born approximation are similar small corrections to the Volkov wave function, which represents a plane wave in the drift coordinates. In the low-frequency approximation, the scattering by an ion is described more precisely, but the electron impact on the ion is implied to be unique.

All these approximations have yielded results which differ only by logarithmic factors. The main reason for this coincidence supposedly lies with the general assumptions that the instants of collisions are uncorrelated and that the electron trajectory cannot twist (be attracted to the ion) in the course of multiple oscillations in the vicinity of the ion. This was demonstrated with extraordinary clarity by Silin [32, 33], who obtained the same logarithmically accurate results directly from the kinetic equation with the Landau collision integral. Recall [5] that the derivation of the Landau collision integral relies on the assumptions of the uniform distribution of the instants of collisions and the determinative contribution of distant (almost straight-line, without a change in the impact parameter) collisions. It is likely that the coincidence of the three different — on the face of it — approximations became the reason why interest in this research area was lost for more than 30 years.

More recently, attempts have been made to develop numerical codes for modeling the energy exchange processes in plasmas with the inclusion of electron–ion collisions in strong laser fields [34, 35]. In particular, even the results of Ref. [34] are at variance with traditional ones. At the same time, experimental data appeared which could not be explained in the framework of traditional notions.

What effects are, in our opinion, omitted from the traditional models? Consider how collisions are usually described. In the absence of a Coulomb ion field, the particle motion comprises oscillations in the EM wave field with an oscillatory velocity $v_{\rm osc} = eE/(m\omega_0)$ (where ω_0 and E are the frequency and amplitude of the EM wave field, respectively) superimposed on a slow drift with a constant drift velocity $\mathbf{v}$. It is commonly assumed [3, 4] that the drift occurs in a straight line throughout the collision period and merely 'delivers' a particle to the interaction domain. A particle collision then happens with the ion, which is differently described in different models. In this case, prior to the collision, the particles are assumed to be uniformly distributed in space. After the collision the particle is assumed to have abandoned the scattering domain forever.

The assumption that particles are uniformly distributed in the collision phase is justified for fast particles, $v \gg v_{\rm osc}, \omega_0 b_v$, when the particle transits the domain $b_v = e^2Z/(mv^2)$ of significant scattering[1] in a time much shorter than the field oscillation period and never returns to this ion. The formal transference of this assumption to the case of slow particles, $v < v_{\rm osc}$, with the corresponding estimate of the scattering domain as $b_{\rm osc} = e^2Z/(mv_{\rm osc}^2)$, is illegitimate, because the particle flies over the ion many times (during many field cycles) and may be pulled closer to the ion. As a consequence, the assumption of uniform particle distribution may be inapplicable. In particular, it was shown in Refs [37–44] that the inclusion of electron returns to the ion entails a significant change in the scattering pattern.

[1] Particles moving with velocity v and impact parameter $b_v = e^2Z/(mv^2)$ are scattered through an angle $\pi/2$ [36].

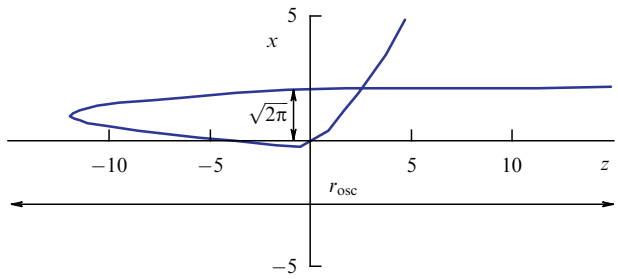

Figure 1. Trajectory of a particle pulled to an ion during one cycle of field oscillations.

Numerical simulations do reveal different dynamics of particle scattering. In a strong field, owing to the large oscillation radius, $r_{\rm osc} = eE/(m\omega_0^2) \gg b_{\rm osc}$, the particle repeatedly returns to the same ion to experience many distant collisions, which are referred as small-angle in total velocity, during the scattering time. As this takes place, the particle energy hardly changes, but its drift trajectory twists [37, 38]. Furthermore, a similar picture of the attraction of the electron wave function to a scatterer ion during many cycles of the external field variation is also observed in the quantum-mechanical description of particle collisions in strong fields [42–44].

Shown in Fig. 1 by way of example is the trajectory of a particle which was pulled closer to the ion during a half-cycle of EM field oscillations (during one flight over the ion). As a result, prior to the last impact, which actually changes the particle energies, the particles find themselves much closer to the ion than in the straight drift motion, so the changes in particle energies in the scattering become much larger and a wealth of new effects show up, whose consideration is the concern of our review.

The layout of our review is as follows. In Section 2, we introduce general notions and give a general form of the pairwise collision operator in alternating EM fields. It is shown, in particular, how the kernel of the collision operator is determined by test particle trajectories. We consider the relation of the resultant integral to the collision operator in the straight-line approximation. In Section 3, we analyze the equations governing the motion of test particles. Discussed in Sections 4–6 are the features of test particle dynamics in the high-velocity domain, of the averaged description, and of multiple returns. Analytical results for point mapping of the coordinates and momenta of test particles through a cycle are outlined in Section 7. The integral characteristics of electron–ion collisions in strong fields are considered in Sections 8 and 9. Section 10 is concerned with collisions in relativistically strong fields. The final form of the collision operator in strong EM fields is given in Section 11. Considered in Section 12 are the applicability conditions for the results obtained.

2. Collision operator in alternating electromagnetic fields

In this section, we give general relations for the kinetic equations used for describing nonequilibrium processes in fully ionized plasmas. These relations were obtained from the Liouville equation using a method introduced by Bogoliubov [45]. They permit, first, determining the boundaries of applicability of the Boltzmann, Landau, and other collision operators and, second, finding new collision operators in the

future, when it becomes necessary to take into account fast processes and describe particle collisions in a plasma embedded in strong EM fields.

2.1 Kinetic equation in the canonically invariant form

The most complete description of a plasma of N particles is provided by the N-particle distribution function $D_N(t, \zeta_1, \ldots, \zeta_N)$. Here, $\zeta_i = \{\mathbf{r}_i, \mathbf{p}_i\}$ are the coordinates and momentum of the ith particle. The physical meaning of the function D_N is that the quantity $D_N \, \mathrm{d}\zeta_1 \ldots \mathrm{d}\zeta_N$ gives the probability that the parameters of the particles $(i = 1, \ldots, N)$ fall within the range from ζ_i to $\zeta_i + \mathrm{d}\zeta_i$. For a normalization of D_N in a closed system, one can choose the condition $\int D_N \, \mathrm{d}\zeta_1 \ldots \mathrm{d}\zeta_N = 1$. The D_N function satisfies the Liouville equation

$$\partial_t D_N + [\mathcal{H}_N^{\Sigma}, D_N] = 0 \,, \tag{1}$$

which is reflective of the fact that a variation of the particle distribution probability in a given phase volume is possible only due to the transit of particles through its boundaries. Here, $\partial_t f = \partial f / \partial t$, $[\ldots, \ldots]$ are the Poisson brackets:

$$[f, g] = \sum_i \frac{\partial f}{\partial \mathbf{r}_i} \frac{\partial g}{\partial \mathbf{p}_i} - \frac{\partial f}{\partial \mathbf{p}_i} \frac{\partial g}{\partial \mathbf{r}_i} \,.$$

If it is assumed that only pairwise interactions occur between particles,[2] the Hamiltonian $\mathcal{H}_N^{\Sigma}$ of a system of N particles may be represented as

$$\mathcal{H}_N^{\Sigma} = \sum_i \mathcal{H}_i + \sum_{j>i} \mathcal{V}_{ij} \,, \tag{2}$$

where $\mathcal{H}_i$ is the Hamiltonian of a free particle, and $\mathcal{V}_{ij}(\mathbf{r}_i - \mathbf{r}_j, t)$ is the interparticle interaction potential. So simple a form of the interaction potential takes place only for nonrelativistic particles. For the sake of simplicity, in the subsequent discussion we restrict ourselves to precisely this form. In the relativistic case, the potential would also depend on the particle momenta (see Section 9.1), which would call for a slight generalization of derivations.

Equation (1) is complicated, because it defines the temporal evolution of the function of $6N$ variables (where $N \sim 10^{23}$ is the total number of plasma particles). On the other hand, owing to the relative smallness of the average interaction energy in comparison with the kinetic energy of the particles, a large role should be played by the notions that pertain to individual particles. Introduced for their description are s-particle distribution functions:

$$D_s = V^{(s)} \int D_N \, \mathrm{d}\zeta_{s+1} \ldots \mathrm{d}\zeta_N \,, \tag{3}$$

where V is the plasma volume. The equations for each of these functions, which are referred to as the Bogoliubov chain [45], originate from the higher-order distribution function:

$$\partial_t D_1 + [\mathcal{H}_1, D_1] = -\int \frac{\mathrm{d}\zeta_2}{V} \, [\mathcal{V}_{12}, D_2] \,, \tag{4}$$

$$\partial_t D_2 + [\mathcal{H}_1 + \mathcal{H}_2 + \mathcal{V}_{12}, D_2] = -\int \frac{\mathrm{d}\zeta_3}{V} \, \big([\mathcal{V}_{13}, D_3] + [\mathcal{V}_{23}, D_3]\big) , \tag{5}$$

[2] This is knowingly true for nonquantum plasmas [5].

etc. It should be emphasized that the EM fields in these equations are given by sources external to the plasma without taking into account the plasma action.

Since $D_n = \prod_{i=1}^{n} D_1(\zeta_i)$ in the absence of correlations (interaction), there is a good reason to explicitly single out in the functions $D_2, D_3, \ldots$ the terms responsible for correlations:

$$D_1(\zeta_a) = \frac{V}{N_a} f_a \,, \quad D_2(\zeta_a, \zeta_b) = \frac{V^2}{N_a N_b} \big(f_a f_b + g_{ab}\big) \,,$$
$$D_3(\zeta_a, \zeta_b, \zeta_c) = \frac{V^3}{N_a N_b N_c} \big(f_a f_b f_c + f_a g_{bc} + f_b g_{ac} + f_c g_{ab} + d_{abc}\big) \,. \tag{6}$$

Hereinafter, the subscripts indicate the coordinate dependence of the corresponding function [for instance, $g_{ab} \equiv g_{ab}(\zeta_a, \zeta_b)$].

We substitute definitions (6) in Eqn (4) to obtain the kinetic equation for the distribution function f_a:

$$\partial_t f_a + [H_a, f_a] = \sum_b \mathrm{St}_{ab}[f_a] \equiv -\sum_b \int \mathrm{d}\zeta_b \, [\mathcal{V}_{ab}, g_{ab}] \,. \tag{7}$$

In this case, the Hamiltonian on the left-hand side of Eqn (7) contains an already self-consistent (acting) field in the plasma:

$$H_a = \mathcal{H}_a + \sum_b \int f_b \mathcal{V}_{ab} \, \mathrm{d}\zeta_b \,.$$

The integral on the right-hand side of Eqn (7) is termed the collision operator $\mathrm{St}_{ab}[f_a]$ with particles of sort b. Its determination calls for knowledge of the pair correlation function g_{ab}. The equation for the function g_{ab} is obtained by simple transformations from expression (5) in view of definitions (6):

$$\partial_t g_{ab} + [H_a + H_b + \mathcal{V}_{ab}, g_{ab}] = -[\mathcal{V}_{ab}, f_a f_b] \,. \tag{8}$$

Omitted in this case were the terms $\int \mathrm{d}\zeta_c \big([\mathcal{V}_{ac}, f_a g_{bc}] + [\mathcal{V}_{bc}, f_b g_{ac}]\big)$ responsible for dynamic plasma polarization (Debye screening), which are significant at distances from the charge exceeding the Debye radius r_{D}, $r \geqslant r_{\mathrm{D}} = \sqrt{T/(8\pi e^2 n_{\mathrm{e}})}$. The three-particle correlation term d_{abc} in Eqn (8) was also discarded assuming that the probability of simultaneous collision of three particles at one point in space is low.

Equation (8) is of the hyperbolic type, and its solution is easily found considering the smoothness of the distribution functions on the collision scale:

$$\partial_t f_a f_b + [H_a + H_b, f_a f_b] \ll [\mathcal{V}_{ab}, f_a f_b]$$

and the feasibility condition $\lim_{t \to -\infty} g_{ab} = 0$ indicating the absence of correlations 'prior to the interaction', which was proposed by Bogoliubov [45]. As a result, we obtain

$$g_{ab} = -f_a f_b \big|_{\mathrm{tr}} \equiv -f_a\big(\zeta_{0a}(\zeta_a, \zeta_b)\big) \, f_b\big(\zeta_{0b}(\zeta_a, \zeta_b)\big) \,. \tag{9}$$

The right-hand-side of expression $f_a f_b|_{\mathrm{tr}}$ should be interpreted as the dependence on the 'current' coordinates and momenta ζ in the trajectory of test particles, which in turn depend on the 'initial' coordinates and momenta ζ_0. To denote this dependence, in what follows we make use of the function $\tilde{\zeta}_a(\zeta_{a0}, \zeta_{b0}, t)$. The term test particles is referred to the

particles which move in a system with the Hamiltonian $H_\Sigma = H_a + H_b + U_{ab}$.

Substituting expression (9) into expression (7) yields the collision operator in the form

$$\mathrm{St}_{ab}[f_a] = \int \mathrm{d}\zeta_b \left[\mathcal{V}_{ab}, f_a f_b\big|_{\mathrm{tr}}\right]. \tag{10}$$

Expression (10) can be brought to the classical form of the integral operator with the kernel $w_{ab}(\zeta_a, \zeta_a^0)$:

$$\mathrm{St}_{ab}[f_a] = \int f(\zeta_{a0})\, w_{ab}(\zeta_a, \zeta_{a0}, t)\, \mathrm{d}\zeta_{a0}\,. \tag{11}$$

Using the Hamiltonian nature of the system, we obtain, in turn, a rather simple expression for w_{ab} [46]:

$$w_{ab}(\zeta_a, \zeta_{a0}, t) = \int f_b(\zeta_{b0})\, \frac{\mathrm{d}}{\mathrm{d}t}\, \delta\big(\tilde{\zeta}_a(\zeta_{a0}, \zeta_{b0}, t) - \zeta_a\big)\, \mathrm{d}\zeta_{b0}\,. \tag{12}$$

Expression (12) has a simple physical meaning: the variation of the distribution function upon collisions is only defined by the motion of particles along test particle trajectories. Accordingly, the momentum distribution comes out as the integral variation of test particles momenta in their motion along trajectories. To determine the collision operator, it is therefore necessary and sufficient to find the particle trajectories in the scattering and integrate the momentum variation distribution over all possible initial coordinates and momenta ζ_{b0}.

As a matter of fact, formulas (11) and (12) underlie the method of calculating the binary collision characteristics with the utilization of test particles. The heart of the method consists in the mental convergence of all plasma ions of the same kind into a single point A. In this regard, the totality of electron–ion collisions comes to sequential collisions of mutually noninteracting (test) particles with one ion residing at point A. The averaging over space (over collisions with different ions) is, in fact, replaced by averaging over time (sequential collisions with one ion). A sufficiently large number ($10^7 - 10^8$ for typical parameters) of test particles is taken in the numerical simulations. Random initial parameters $\zeta_0 = \{\mathbf{r}_0, \mathbf{p}_0\}$ are chosen for every particle and its trajectory is calculated in collision with the ion. The data of all collisions are then summed up by analogy with what is done in the Monte Carlo method. Therefore, formulas (11) and (12) substantiate the applicability of the test particle method for an arbitrary scattering potential, including a time-dependent one.

2.2 Kernel of the collision operator

It should be noted that Eqn (12) has a canonically invariant form, because it includes the displacements of particles in both momentum and coordinate spaces. Unfortunately, the direct use of Eqn (12) involves great difficulties, despite its relatively simple form. To simplify expression (12), we first ignore the variation of the spatial coordinate (it will be assumed that $\mathbf{r}_{a0} = \mathbf{r}_a$) in the collision owing to the smallness of collisional scales and concentrate on the momentum part. This disregard of the variation of particle coordinates upon the scattering has the effect that the collision operator (11), (12) loses canonical invariance, since the information about the scattering event is roughened. As a result, the collision operator acquires a diffusive character common for the Boltzmann collision integral.

In Section 2.1, we considered the collision operator for arbitrary (including relativistic) colliding particles. To avoid cumbersome mathematical manipulations in the general case, we consider at first the important special case of nonrelativistic electron–ion collisions. Practically all formulas are generalized to the case of relativistic collisions in a similar way, accurate to more complex expressions for the drift coordinates (see Section 9.1).

The Hamiltonian for two charged (test) particles in the nonrelativistic case is well known:

$$H_\Sigma = \frac{p_a^2}{2m_a} + \frac{p_b^2}{2m_b} + \frac{e_a e_b}{|\mathbf{r}_a - \mathbf{r}_b|} + \mathbf{E}(t)(e_a \mathbf{r}_a + e_b \mathbf{r}_b)\,.$$

For practical implementation, however, the Hamiltonian is conveniently written out in drift coordinates[3] $\mathbf{r}_{a,b}^{\mathrm{drift}} = \mathbf{r}_{a,b}^{\mathrm{lab}} - \mathbf{r}_{a,b}^{\mathrm{osc}}$, $\mathbf{p}_{a,b}^{\mathrm{drift}} = \mathbf{p}_{a,b}^{\mathrm{lab}} - \mathbf{p}_{a,b}^{\mathrm{osc}}$:

$$\begin{aligned} H_\Sigma &= \frac{p_a^2}{2m_a} + \frac{p_b^2}{2m_b} + U_{ab}\,, \\ U_{ab} &= \frac{e_a e_b}{\left|\mathbf{r}_a + \mathbf{r}_a^{\mathrm{osc}}(t) - \mathbf{r}_b - \mathbf{r}_b^{\mathrm{osc}}(t)\right|}\,. \end{aligned} \tag{13}$$

Here, $\mathbf{p}_{a,b}^{\mathrm{osc}} = \int e_{a,b}\mathbf{E}(t)\,\mathrm{d}t$ is the oscillatory momentum, $\mathbf{r}_{a,b}^{\mathrm{osc}} = \int \mathbf{p}_{a,b}^{\mathrm{osc}}/m_{a,b}\,\mathrm{d}t$ is the oscillatory radius, and e_a and e_b are the charges of the particles of sort a and b, respectively. This representation is convenient in view of the spatial localization of the scattering potential U_{ab}. This transformation was achieved at the expense of acquiring explicit time dependence by the potential U_{ab}. Furthermore, when one particle (the electron) is far lighter than the other (the ion), the oscillations $\mathbf{r}_b^{\mathrm{osc}}(t)$ of the heavy particle in the interaction potential may be ignored in view of the smallness of parameter m_a/m_b.

For a Hamiltonian in the form (13), only the relative distances $\mathbf{r} = \mathbf{r}_a - \mathbf{r}_b$ are of importance. We also assume that ion velocity changes in electron–ion collisions are small and disregard the variation of the coordinate part of the distribution functions f_a, f_b due to the change of particle positions in collisions. As a result, kernel (12) may be represented as

$$w_{ab} = n_b(\mathbf{r}_a)\delta(\mathbf{r}_a - \mathbf{r}_{a0}) \int \frac{\mathrm{d}}{\mathrm{d}t}\, \delta\big(\tilde{p}_a(\mathbf{r}, \mathbf{p}_{a0}, t) - \mathbf{p}_a\big)\, \mathrm{d}^3 r\,, \tag{14}$$

where $n_b = \int f_b\, \mathrm{d}^3 p_b$ is the concentration of particles of sort b at point r_a. In what follows, we omit $\delta(\mathbf{r}_a - \mathbf{r}_{a0})$ in expression (14) and assume all collisions to be local.

When H_a and $\mathcal{V}_{ab}$ are periodic functions of time (for instance, in the case of collisions in a plane EM wave) with a period $T = 2\pi/\omega_0$, the collision function and, accordingly, the collision operator should also be periodic functions of time. It is therefore of interest to find the average value and amplitudes of harmonics of the collision operator. The time average of the collision kernel is expressed as

$$\big\langle w_{ab}(\mathbf{p}, \mathbf{p}_0)\big\rangle = \frac{n_b}{T} \int_t^{t+T} w(\mathbf{p}, \mathbf{p}_0, t)\, \mathrm{d}t\,. \tag{15}$$

In what follows, the subscripts a of the momenta are omitted.

Let us go over to Cartesian coordinates ξ, ρ_1, and ρ_2 with the origin at the point of ion residence and the ξ-axis aligned

[3] In quantum mechanics, this transition is termed the Kramers–Henneberger transformation.

with the initial momentum $\mathbf{p}_0$. Using the condition of Hamiltonian periodicity with a period T, we write down the expression for the momenta at different points in time as $\xi \to -\infty$:

$$\mathbf{p}(t;\xi) = \mathbf{p}(t-T;\xi-\zeta), \quad \zeta = |\mathbf{v}_0|T. \tag{16}$$

Here, the initial velocity $\mathbf{v}_0$ is related to the initial momentum in the ordinary way: $\mathbf{v}_0 = \mathbf{p}_0/m$. Relation (16) for momenta permits representing function w (15) as

$$\begin{aligned}\langle w_{ab}(\mathbf{p},\mathbf{p}_0)\rangle &= \frac{n_b}{T}\sum_{n=-\infty}^{\infty}\iint_{n\zeta}^{(n+1)\zeta}\Big[\delta\big(\tilde{\mathbf{p}}(t+T)-\mathbf{p}\big)-\delta\big(\tilde{\mathbf{p}}(t)-\mathbf{p}\big)\Big]\,\mathrm{d}\xi\,\mathrm{d}^2\rho\\ &= \frac{n_b}{T}\lim_{\Xi\to-\infty}\iint_{\Xi}^{\Xi+\zeta}\sum_{n=-\infty}^{\infty}\Big[\delta\big(\tilde{\mathbf{p}}(t+(n+1)T)-\mathbf{p}\big)\\ &\quad-\delta\big(\tilde{\mathbf{p}}(t+nT)-\mathbf{p}\big)\Big]\,\mathrm{d}\xi\,\mathrm{d}^2\rho\\ &= \frac{n_b}{T}\lim_{\Xi\to-\infty}\iint_{\Xi}^{\Xi+\zeta}\Big[\delta\big(\tilde{\mathbf{p}}(+\infty)-\mathbf{p}\big)-\delta\big(\tilde{\mathbf{p}}(-\infty)-\mathbf{p}\big)\Big]\,\mathrm{d}\xi\,\mathrm{d}^2\rho\,,\end{aligned}$$

where Ξ is the distance between the incident particle and the scattering center. The initial momentum $\tilde{\mathbf{p}}(-\infty)$ is identical to $\mathbf{p}_0$, and so one has

$$\langle w_{ab}(\mathbf{p},\mathbf{p}_0)\rangle = \frac{n_b}{T}\lim_{\Xi\to-\infty}\iint_{\Xi}^{\Xi+\zeta}\big[\delta(\mathbf{p}_+-\mathbf{p})-\delta(\mathbf{p}_0-\mathbf{p})\big]\,\mathrm{d}\xi\,\mathrm{d}^2\rho\,, \tag{17}$$

where $\mathbf{p}_+ \equiv \tilde{\mathbf{p}}(+\infty)$. Therefore, the physical meaning of the period-averaged kernel of the collision operator lies in it being the particle velocity distribution density in the problem of monoenergetic beam scattering.

We revert to formula (11) to obtain the expression for the collision operator [46]

$$\begin{aligned}&\langle \mathrm{St}_{ab}[f]\rangle\\ &\quad= \frac{n_b}{T}\lim_{\Xi\to-\infty}\iint_{\Xi}^{\Xi+\zeta}\int f(\mathbf{p}_0)\big[\delta(\mathbf{p}_+-\mathbf{p})-\delta(\mathbf{p}_0-\mathbf{p})\big]\,\mathrm{d}^3p_0\,\mathrm{d}\xi\,\mathrm{d}^2\rho\,,\end{aligned} \tag{18}$$

which generalizes the Boltzmann collision integral to the case of scattering in a periodically time-varying potential. Thus, the distribution function variation upon collisions is *only* determined by the motion of particles along their trajectories. Accordingly, the momentum distribution results as the integral change of particle momenta in a trajectory motion.

Similarly, it is possible to find the expression for the amplitude of the kth harmonic of the kernel of the collision operator:

$$w_k^{ab} = \mathrm{i}k\omega_0\lim_{\Xi\to-\infty}\iint_{\Xi}^{\Xi+\zeta}\int_{-\infty}^{\infty}\delta\big(\tilde{\mathbf{p}}(\tau)-\mathbf{p}\big)\exp\left(\frac{\mathrm{i}2\pi\tau k}{T}\right)\mathrm{d}\tau\,\mathrm{d}\xi\,\mathrm{d}^2\rho\,. \tag{19}$$

We note one more important and more or less obvious property of expressions (17)–(19). The collision operator (18) gives the exact solution for the distribution function evolution over a period in quasimonochromatic EM fields, while expression (19) permits calculating the spectrum of its harmonics. Specifically, upon averaging over a period, only the term $\int \partial_t f\,\mathrm{d}t = f(t+T)-f(t)$ remains on the left-hand side of kinetic equation (7), while the collision operator (18) remains on the right-hand side. This permits constructing numerical methods (like the particle-in-cell technique) which fastly and accurately calculate the plasma evolution with a rather large time step equal to the EM-field cycle.

The collision operator (11) and expressions (17) and (19) for the function w make it possible to easily find the collision characteristics (moments), for instance, for the Joule heating of the plasma:

$$\frac{\mathrm{d}T_\mathrm{e}}{\mathrm{d}t} \equiv \frac{\mathrm{d}}{\mathrm{d}t}\int\frac{p^2}{2m}f(\mathbf{p},t)\,\mathrm{d}^3p = \frac{mv_\mathrm{osc}^2}{2}\int\nu_\mathrm{ei}(\mathbf{p}_0)f(\mathbf{p}_0)\,\mathrm{d}^3p_0\,. \tag{20}$$

Here, the effective collision frequency ν_ei is introduced as the cycle-averaged variation of plasma electron energy per unit time referred to the electron oscillatory energy:

$$\nu_\mathrm{ei}(\mathbf{p}_0) = \frac{2m}{\mathbf{p}_\mathrm{osc}^2}\frac{n_\mathrm{i}}{2m}\int p^2\langle w_\mathrm{ei}(\mathbf{p},\mathbf{p}_0)\rangle\,\mathrm{d}^3p\,, \tag{21}$$

where n_i is the ion concentration. With the use of formula (17), it is easy to obtain the expression for the collision frequency

$$\nu_\mathrm{ei}(\mathbf{p}_0) = \frac{n_\mathrm{i}}{T\mathbf{p}_\mathrm{osc}^2}\lim_{\Xi\to-\infty}\iint_{\Xi}^{\Xi+\zeta}(p_+^2-p_0^2)\,\mathrm{d}\xi\,\mathrm{d}^2\rho\,. \tag{22}$$

As shown by this expression, to calculate the energy variation in collisions, it is sufficient to find the variation in time $(-\infty,\infty)$ of the energies of test particles from one layer with width ζ along ξ.

By changing coordinates $\varphi = \zeta\xi/(2\pi) = p_0T\xi/(2\pi m)$, we represent formula (22) in a more convenient form:

$$\nu_\mathrm{ei}(\mathbf{p}_0) = n_\mathrm{i}v_0\sigma_\mathrm{eff}\,, \quad \sigma_\mathrm{eff}(\mathbf{p}_0) = \lim_{\Xi\to-\infty}\iint_0^{2\pi}\frac{p_+^2-p_0^2}{p_\mathrm{osc}^2}\,\mathrm{d}\varphi\,\mathrm{d}^2\rho\,. \tag{23}$$

The effective cross section σ_eff has the dimension of area and characterizes the ratio of the number of particles that changed their energy by a value of $p_\mathrm{osc}^2/(2m)$ to the incident particle flux density. It is precisely this quantity that will be employed for calculating the Joule heating of the plasma.

Similarly, it is possible to find out the electron beam current determined by collisions:

$$\frac{\mathrm{d}\mathbf{j}_\mathrm{ei}}{\mathrm{d}t} \equiv e\,\frac{\mathrm{d}}{\mathrm{d}t}\int\mathbf{p}\,\delta(\mathbf{p}-\mathbf{p}_0)\,\mathrm{d}^3p = en_\mathrm{i}\int\mathbf{p}\,w_\mathrm{ei}(\mathbf{p},\mathbf{p}_0,t)\,\mathrm{d}^3p\,. \tag{24}$$

When expression (19) for the w_ei function is substituted into expression (24), we obtain the expression for the Fourier spectrum of current $\mathbf{j}_\mathrm{ei}$:

$$\begin{aligned}\mathbf{j}_\omega &= \int\mathbf{j}_\mathrm{ei}\exp(\mathrm{i}\omega t)\,\mathrm{d}t\\ &= en_\mathrm{i}\lim_{\Xi\to-\infty}\iint_{\Xi}^{\Xi+\zeta}\mathbf{p}_\omega\left(\sum_{n=-\infty}^{\infty}\exp\left(\mathrm{i}\omega n\,\frac{2\pi}{\omega_0}\right)\right)\mathrm{d}\xi\,\mathrm{d}^2\rho\,.\end{aligned} \tag{25}$$

The sum on the right-hand side of expression (25) comprises the sum of δ functions:

$$\mathbf{j}_\omega = e\lim_{\Xi\to-\infty}\iint_{\Xi}^{\Xi+\zeta}\mathbf{p}_\omega\,\mathrm{d}\xi\,\mathrm{d}^2\rho\sum_{n=-\infty}^{\infty}\delta(\omega-n\omega_0)\,, \tag{26}$$

since the system's response (in particular, plasma response) to a periodic perturbation at the frequency ω_0 should be periodic with frequencies that are multiples of ω_0.

The external field has no effect on the electron–electron collisions. As a consequence, the electron–electron collision frequency ν_{ee} will almost always exceed the electron–ion collision frequency, and any anisotropy of the distribution function would be expected to smooth out in a time $1/\nu_{ee}$. So that the electron distribution function may be treated as isotropic under electron–ion collisions. An exception is provided by the domain $Zv_{osc} > v_T > v_{osc}$, where the electron–ion collision frequency is higher than the electron–electron collision frequency, as shown by Langdon [47, 48]. (Here, Z is the ion-to-electron charge ratio.) As a consequence, the electron distribution function becomes anisotropic.

It should be noted that, for an isotropic distribution function $f(|\mathbf{p}|)$, on the strength of the symmetry relation for $\xi \to -\infty$ one obtains

$$\mathbf{p}(t;\xi,\mathbf{p}_0) = \mathbf{p}\left(t+\frac{T}{2};-\xi,-\mathbf{p}_0\right) \tag{27}$$

and only odd harmonics of the frequency ω_0 will remain in the sum. As a result, formula (26) takes on the form

$$\mathbf{j}_\omega = en_{\mathrm{i}}v_0\chi_{\mathrm{coh}}(\mathbf{p}_0)\sum_{n=-\infty}^{\infty}\delta(\omega-n\omega_0)\,, \tag{28}$$

where we introduced the quantity χ_{coh}, which will be referred to as the coherent radiation cross section:

$$\chi_{\mathrm{coh}}(\mathbf{p}_0) = \lim_{\Xi\to-\infty}\iint_0^{2\pi}\mathbf{p}_\omega(\Xi+\varphi r_a,\boldsymbol{\rho})\,\mathrm{d}\varphi\,\mathrm{d}^2\rho\,. \tag{29}$$

Similarly, it is possible to derive expressions for other quantities. The transport cross section, characterizing the area from which particles are scattered through an angle of order $\pi/2$, has the form

$$\sigma_{\mathrm{tr}}(\mathbf{p}_0) = \lim_{\Xi\to-\infty}\iint_0^{2\pi}\left(1-\frac{\mathbf{p}_+\mathbf{p}_0}{p_+p_0}\right)\mathrm{d}\varphi\,\mathrm{d}^2\rho\,. \tag{30}$$

The incoherent radiation cross section, which has the dimension of area per energy, is defined as

$$\chi_{\mathrm{inc}}(\mathbf{p}_0) = \frac{4}{3c^3}\lim_{\Xi\to-\infty}\iint_0^{2\pi}p_\omega^2\,\mathrm{d}\varphi\,\mathrm{d}^2\rho\,. \tag{31}$$

While expression (26) for the collisional current takes into account the correlatedness of the powers of radiating sources, in expression (31) for the incoherent radiation these powers are summed ignoring possible correlation between them. This is the commonly accepted method for calculating the incoherent radiation intensity in the presence of collisions [49].

2.3 Perturbation method

Unfortunately, the exact analytical solution of the equation of motion of a test particle is rather hard to find. In some cases, however, attempts to develop a perturbation theory do meet with success when the particle trajectory departs only slightly from the straight one. This approximation is termed the small-angle or straight line approach [2–4, 15, 26, 31]. In essence, the approximation reduces to ignoring the term

$$[\mathcal{V}_{ab}, g_{ab}] \ll [\mathcal{V}_{ab}, f_a f_b] \tag{32}$$

in equation (8) for the correlation function:

$$\partial_t g_{ab} + [H_a + H_b, g_{ab}] = -[\mathcal{V}_{ab}, f_a f_b]\,. \tag{33}$$

It should be noted that assumption (32) alone imposes the rectilinearity condition for particle drift trajectories during collisions. This approximation is fully justified for high-energy particles, $v \gg v_{osc}$, which experience a single impact on an ion and never return to it, or for a repulsive interaction potential (for instance, in electron–electron or ion–ion collisions), when each successive collision is weaker than the previous one. However, for slower particles, $v \leqslant v_{osc}$, the situation in electron–ion collisions is not that unambiguous, because in this case the electron has a chance to return to the same ion a cycle later and experience a stronger impact. In particular, it was shown in Refs [38–43] that the inclusion of electron returns to the ion significantly changes the scattering picture.

So, let us focus on high-energy particles with $v \gg v_{osc}$. The solution of equation (33) is easily found in view of the zero value of the Poisson bracket $[H_a, \mathbf{p}_a]$ (i.e., for a constant drift momentum in the particle 'trajectory'):

$$g_{ab} = -f_b\int[\mathcal{V}_{ab}, f_a]\Big|_{\mathrm{tr}}\mathrm{d}t = f_b\,\frac{\partial f_a}{\partial\mathbf{p}}\int\frac{\partial\mathcal{V}_{ab}}{\partial\mathbf{r}}\bigg|_{\mathbf{r}\to\mathbf{r}+\mathbf{v}t}\mathrm{d}t\,.$$

By substituting this expression into operator (11), we obtain the collision operator, which is expressed in quadratures:

$$\mathrm{St}\,[f_a] = n_b\int\mathrm{d}^3r\left[\mathcal{V}_{ab},\frac{\partial f_a}{\partial\mathbf{p}}\int\frac{\partial\mathcal{V}_{ab}}{\partial\mathbf{r}}\bigg|_{\mathbf{r}\to\mathbf{r}+\mathbf{v}t}\mathrm{d}t\right]. \tag{34}$$

We emphasize that the quadratic dependence on the Coulomb potential (or on the ion charge), which emerged here only on the strength of approximation (32), is by no means a consequence (criterion) of binary collision approximation. Furthermore, a rigorous solution of equation (8) might yield any degree of its dependence on the ion charge, because the test particle trajectories depend on it in a transcendental way.

In the nonrelativistic approximation, when the interaction potential is independent of momenta (13), this integral may be calculated analytically. It is easily seen, indeed, that the collision operator in this case may be represented as

$$\mathrm{St}_{ab}\,[f_a] = \frac{\partial}{\partial p_j}\,B_{ij}\,\frac{\partial f(\mathbf{p})}{\partial p_i}\,, \tag{35}$$

where tensor B_{ij} is defined by the expression

$$B_{ij} = \iint\frac{\partial\mathcal{V}_{ab}}{\partial r_j}\bigg|_{\mathbf{r}\to\mathbf{r}+\mathbf{v}t}\mathrm{d}t\,\frac{\partial\mathcal{V}_{ab}}{\partial r_i}\,\mathrm{d}^3r\,. \tag{36}$$

Using the Fourier expansion for the Coulomb potential

$$\frac{1}{r} = 4\pi\int\frac{\exp(\mathrm{i}\mathbf{kr})}{k^2}\,\frac{\mathrm{d}^3k}{(2\pi)^3}\,,$$

we obtain

$$B_{ij}(t) = \frac{2Z^2e^4}{\pi}\int\frac{\mathrm{d}^3k}{k^4}\,k_ik_j\exp\left(-\mathrm{i}\mathbf{kr}_{\mathrm{osc}}(t)\right)$$
$$\times\int\exp\left(\mathrm{i}\mathbf{kv}t' - \mathrm{i}\mathbf{kr}_{\mathrm{osc}}(t')\right)\mathrm{d}t'\,. \tag{37}$$

In the laboratory frame of reference, this corresponds to V P Silin's collision integral [2]

$$B_{ij}(t) = \frac{2Z^2e^4}{\pi}\iint \frac{\mathrm{d}^3k\,\mathrm{d}t}{k^4}\,k_ik_j\exp\left[\mathrm{i}\mathbf{k}\big(\mathbf{v}+\mathbf{v}_{\mathrm{osc}}(t)\big)t\right]. \quad (38)$$

The form of integral (38) may be simplified within a logarithmic accuracy. With this aim, we note that in the case of high k (significant, for instance, for determining the efficient collision frequency) it is possible to ignore the variation of the total particle velocity with parameter $kv/\omega \equiv kr_{\mathrm{a}} \gg 1$ at the instant of scattering:

$$B_{ij}(t) \approx 2Z^2e^4\int\frac{\mathrm{d}^3k}{k^4}\,k_ik_j\,\delta(\mathbf{kV}) = 2\pi Z^2e^4\,\frac{\delta_{ij}V^2 - V_iV_j}{V^3}\ln\frac{r_{\mathrm{a}}}{b_v}, \quad (39)$$

where $\mathbf{V}(t) = \mathbf{v} + \mathbf{v}_{\mathrm{osc}}(t)$ is the total particle velocity at the instant of impact, δ_{ij} is the Kronecker delta, and r_{a} is the adiabaticity radius. In the domain of small k ($kr_{\mathrm{osc}} \ll kr_{\mathrm{a}} \leqslant 1$), the term $\mathbf{kr}_{\mathrm{osc}}(t)$ may be discarded in expression (37), which corresponds to the lack of the external field effect on distant collisions:

$$B_{ij} \approx 2Z^2e^4\int\frac{\mathrm{d}^3k}{k^4}\,k_ik_j\delta(\mathbf{kv}) = 2\pi Z^2e^4\,\frac{\delta_{ij}v^2 - v_iv_j}{v^3}\ln\frac{r_{\mathrm{D}}}{r_{\mathrm{a}}}. \quad (40)$$

Finally, for the collision operator in the applicability domain of the small-angle approximation we obtain

$$B_{ij} \approx 2\pi Z^2e^4\,\frac{\delta_{ij}V^2 - V_iV_j}{V^3}\ln\frac{r_{\mathrm{a}}}{b_v} + 2\pi Z^2e^4\,\frac{\delta_{ij}v^2 - v_iv_j}{v^3}\ln\frac{r_{\mathrm{D}}}{r_{\mathrm{a}}}. \quad (41)$$

The first term on the right-hand side of expression (41) corresponds primarily to the plasma energy variation in the particle interaction with the external electromagnetic wave field. The second term does not entail plasma energy variations and, as a rule, is not considered. It is responsible only for the transport characteristics of the scattering (by analogy with the Landau collision operator for electron–electron collisions).

Expression (41) for tensor B_{ij} is of a rather general form. In several specific cases, it becomes significantly simpler and is brought to some well-known formulas or permits drawing conclusions about the particle dynamics in these regimes. Let us consider them.

In the absence of an external field ($v_{\mathrm{osc}} \to 0$), the total particle velocity is equal to the drift velocity of the particle: $\mathbf{V}(t) \to \mathbf{v}$. Accordingly, B_{ij} goes over into the Landau tensor B^0_{ij} (40), which appears in the Landau collision integral:

$$B_{ij} \to 2\pi Z^2e^4\,\frac{\delta_{ij}v^2 - v_iv_j}{v^3}\left(\ln\frac{r_{\mathrm{a}}}{b_v} + \ln\frac{r_{\mathrm{D}}}{r_{\mathrm{a}}}\right) = 2\pi Z^2e^4\,\frac{\delta_{ij}v^2 - v_iv_j}{v^3}\ln\frac{r_{\mathrm{D}}}{b_v}. \quad (42)$$

Notice that the integral of a traditional form in the presence of the nonzero EM field [2] is devoid of such a passage.

For an opaque plasma, $\omega < \omega_{\mathrm{p}} \Leftrightarrow r_{\mathrm{a}} > r_{\mathrm{D}}$, tensor B_{ij} takes the form of the Landau tensor with replacement of the drift velocity by the total particle velocity:

$$B_{ij} = 2\pi Z^2e^4\,\frac{\delta_{ij}V^2 - V_iV_j}{V^3}\ln\frac{r_{\mathrm{D}}}{b_v}. \quad (43)$$

This tensor form is traditionally employed for defining the permittivity of opaque plasmas [5].

In the opposite limiting case of high-frequency fields, $r_{\mathrm{a}} < b_v$, tensor B_{ij} is identical to the Landau tensor (40) in the problem without the field:

$$B_{ij} = 2\pi Z^2e^4\,\frac{\delta_{ij}v^2 - v_iv_j}{v^3}\ln\frac{r_{\mathrm{D}}}{b_v}. \quad (44)$$

Notice that the same form of B_{ij} results from integral (37) also when the oscillatory radius is small in comparison with the Rutherford radius, $r_{\mathrm{osc}} \ll b_v$, irrespective of the drift-to-oscillatory velocity ratio. In both cases ($r_{\mathrm{a}}, r_{\mathrm{osc}} \ll b_v$), the part responsible only for the variation of particle momentum direction and not for the variation of particle energy remains in tensor B_{ij}. This signifies, in particular, that the *transport cross section remains Rutherfordian* in these ranges, to within a logarithmic factor. The absence of energy variation in expression (44) signifies that determining the effective frequency responsible for plasma energy variation in these ranges calls for the inclusion of larger-angle scattering [50, 51]. However, this does not necessary mean the absence of energy exchange in the domains under consideration, as is stated, for instance, in Ref. [15].

Lastly, in a transparent plasma in the domains

$$v \gg v_{\mathrm{osc}}, \quad b_v \ll r_{\mathrm{a}} \ll r_{\mathrm{D}} \quad (45)$$

tensor B_{ij} (41) contains both terms. The term responsible for energy variation [the first term in expression (41)] is of the form of the tensor first proposed by Silin [2], which is traditionally used in this domain.

The further generalization of the Silin collision integral (41) to the low-velocity domain should be performed with the inclusion of the finite curvature of the characteristics of the equation for the correlation function, i.e., should overstep the limits of the straight line approximation.

3. Equation of motion of a test particle. Numerical integration problems

Let us turn to the low-temperature plasma case, $v \ll v_{\mathrm{osc}}$. To calculate the collision operator (11), (18), one has to describe the motion of test particles. We consider in more detail the equation of motion corresponding to Hamiltonian (13). A uniform monochromatic electric field, which is called the pump field below, is imposed on plasma:

$$\mathbf{E}(t) = E\,\mathrm{Re}\left[\mathbf{e}_0\exp(\mathrm{i}\omega_0 t)\right].$$

The equations of motion may be written down in the dimensionless form:

• for the laboratory frame

$$\ddot{\mathbf{R}} = -\frac{\mathbf{R}}{|\mathbf{R}|^3} + \mathrm{Re}\left[\mathbf{e}_0\exp(\mathrm{i}\Omega t)\right]; \quad (46)$$

• for the drift coordinates $\mathbf{R} = \mathbf{r} - \mathbf{r}_{\mathrm{osc}}$

$$\ddot{\mathbf{r}} = -\frac{\partial}{\partial\mathbf{r}}\frac{1}{|\mathbf{r} - \mathbf{r}_{\mathrm{osc}}|}, \quad \mathbf{r}_{\mathrm{osc}} = \frac{1}{\Omega^2}\,\mathrm{Re}\left[\mathbf{e}_0\exp(\mathrm{i}\Omega t)\right]. \quad (47)$$

Here, we introduced the characteristic scales

$$r_E = \sqrt{\frac{eZ}{E}}\,, \quad \omega_E = \sqrt[4]{\frac{eE^3}{m^2 Z}}\,, \quad v_E = \sqrt[4]{\frac{Ze^3 E}{m^2}}\,, \tag{48}$$

where E is the amplitude of a pump field, and $\mathbf{e}_0$ is the complex vector which characterizes the polarization of the pump field. In particular, for linear (LP) and circular (CP) polarizations, it is conveniently taken in the form

$$\mathbf{e}_0^{\mathrm{LP}} = \{0,\, 0,\, 1\}\,, \quad \mathbf{e}_0^{\mathrm{CP}} = \{1, -\mathrm{i},\, 0\}\,. \tag{49}$$

In equations (46) and (47), *a unique* dimensionless parameter appears — the dimensionless frequency, which characterizes the pump field [38, 39]:

$$\Omega = \omega_0 \left(\frac{m^2 Z}{eE^3}\right)^{1/4} = \frac{\omega_0}{\omega_E}\,. \tag{50}$$

The amplitude E and the frequency ω_0 enter into parameter Ω as the combination E^3/ω_0^4. This signifies that collisions in strong high-frequency fields (for instance, of the laser range) are similar to collisions in weaker low-frequency fields (for instance, of the microwave range). Therefore, the phase-space structure and the expected effects are determined only by the Ω parameter and are fundamentally different in the high-frequency, $\Omega \gg 1$, and low-frequency, $\Omega \ll 1$, field domains [52].

For high Ω values, the phase-space structure will appreciably vary only in a small neighborhood of the separatrix which separates the transit trajectories from the captured (quasiperiodic) ones. As the field amplitude increases (and parameter Ω lowers), the volume of the stochastic layer increases and becomes of order $v_{\mathrm{osc}} = 1/\Omega \gg 1$ for $\Omega \ll 1$. In dimensional variables, this corresponds to the oscillatory radius in coordinate space, and to the oscillatory momentum in the momentum space. This evolution is qualitatively depicted in Fig. 2. From the standpoint of the scattering problem, this signifies that in weak fields ($\Omega \gg 1$), or as long as the drift (thermal) electron velocity is high in comparison with the oscillatory one, the particle dynamics are regular and the energy exchange with the field may be calculated by the Landau model. By contrast, in the strong field case ($\Omega \ll 1$), under conditions whereby the oscillatory velocity is far higher than the drift one, the domain of irregular dynamics becomes determinative in the phase space of the system. Even these simple considerations suggest that these effects could not be adequately included in the early papers of the 1960s–1970s, because the very notion of stochasticity was still in its infancy. Furthermore, this problem was also quite difficult from the standpoint of numerical solution.

The second parameter that determines the collisions of individual particles is the thermal electron velocity v_{Te}. Since the external electric field has no effect on electron–electron collisions, their frequency in strong fields will exceed the electron–ion collision frequency: $\nu_{\mathrm{ee}} \geqslant \nu_{\mathrm{ei}}, \nu_{\mathrm{ii}}$. Consequently, any inhomogeneity of electron velocities (for instance, due to electron–ion collisions) will be promptly (in parameter $\nu_{\mathrm{ee}}/\nu_{\mathrm{ei}}$) isotropized. Therefore, due to the isotropy of the distribution function, the directions of individual-electron velocities must have no effect on the result (averaging should be performed over them), i.e., the second parameter that defines the collision dynamics is the modulus of thermal electron velocity.

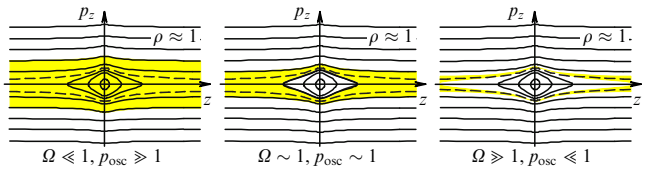

Figure 2. Variation of the stochasticity domain (shown qualitatively) in the phase space under variation of parameter Ω. The separatrix curve is shown with a dashed line.

Thus, collisions are only affected by two dimensionless parameters: the frequency $\Omega = \omega_0/\omega_E$, and the velocity $v = v_{Te}/v_E$. At the same time, it is possible to introduce three physically meaningful spatial parameters that affect the particle trajectory: b_v, r_{osc}, and b_{osc}, and the parameter r_{a} determining the character of particle energy variation by the pump field. We write them out in dimensional and dimensionless (in square brackets) forms:

$$\begin{aligned} b_v &= \frac{Ze^2}{mv^2} = \left[\frac{1}{v^2}\right], \quad r_{\mathrm{osc}} = \frac{eE}{m\omega_0^2} = \left[\frac{1}{\Omega^2}\right], \\ b_{\mathrm{osc}} &= \frac{Ze^2}{mv_{\mathrm{osc}}^2} = [\Omega^2], \quad r_{\mathrm{a}} = \frac{v}{\omega_0} = \left[\frac{v}{\Omega}\right]. \end{aligned} \tag{51}$$

Parameter b_v, which is termed the Rutherford radius, characterizes the size of a domain, such that an electron with a velocity v is scattered through the angle of about 1 rad (disregarding the pump field) on finding itself inside it. Similarly, $b_{\mathrm{osc}} \equiv b_v(v_{\mathrm{osc}})$ is the size of a domain, such that the electron with an oscillatory velocity will be scattered through the angle of about 1 rad on finding itself inside it. The oscillatory radius r_{ocs} is the electron oscillation radius in the pump field (disregarding the ion Coulomb field). The adiabaticity radius r_{a} characterizes the size of a domain in which the electron motion is not adiabatic, i.e., the time r_{a}/v taken to transit this domain is much shorter than the field period $2\pi/\omega_0$. We also give the expression for the normalization scale r_E (48) in terms of parameters (51):

$$r_E = \sqrt{r_{\mathrm{osc}} b_{\mathrm{osc}}}\,. \tag{52}$$

By comparing parameters (51) between themselves in the $\Omega \times \Omega v$ parameter plane, one can single out three domains (Fig. 3) representing fundamentally different dynamics of electron motion. We note that only two domains have traditionally been considered: the weak field domain with $v \gg v_{\mathrm{osc}}$, and the strong field domain with $v \ll v_{\mathrm{osc}}$.

We briefly consider all of them.

High-velocity domain. The particle trajectory in the high-velocity domain ($b_{\mathrm{osc}} \gg b_v \Leftrightarrow v \gg v_{\mathrm{osc}}$) is close to the Rutherfordian one, because the pump field is low, $v_{\mathrm{osc}} \ll v$, and so the effect of the external field on the trajectory may be neglected. The motion is regular. There are no particle captures, and the collisional current is absent. This is the best-studied parameter domain. Moreover, in the calculation of energy variation (the effective collision frequency) in the domain $r_{\mathrm{a}} \gg b_v$, use can be made of the small-angle approximation [2] (see Section 2.3). Outside this domain, the small-angle approximation is inapplicable. In the $r_{\mathrm{a}} \leqslant b_v$ domain, a more accurate calculation of energy variations with the inclusion of considerable electron attraction by the ion is required.

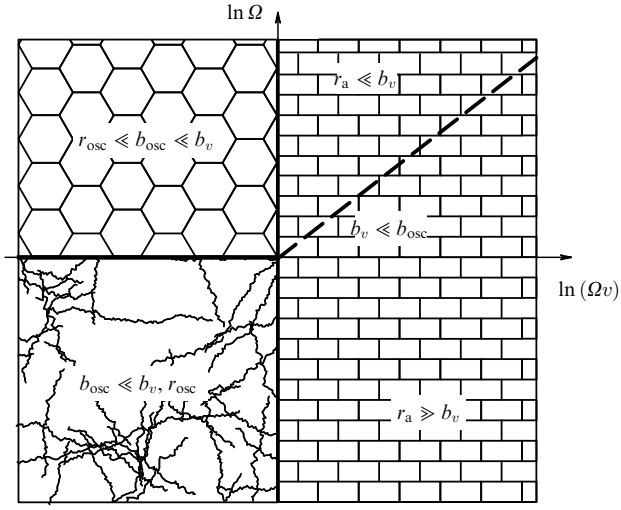

Figure 3. Division of $(\Omega \times \Omega v)$ parameter plane into domains of various electron dynamics.

Domain of averaged description. In the averaged description domain, where $r_{osc} \ll b_{osc} \ll b_v$, the effect of external field on the particle trajectory is significant, but it may be included by introducing an averaged potential in view of the high frequency of the pump field [50, 51]. The motion turns out to be regular once again. The possibility appears that a particle 'falls' on the center because of the nonpoint-like singularity of the averaged potential. Distant trajectories are close to the Rutherfordian ones. Correspondingly, close are the cross sections: the transport and incoherent radiation cross sections.

Domain of multiple returns. In the multiple return domain, where $b_{osc} \ll r_{osc}, b_v$ and $b_{osc} \ll b_v \Leftrightarrow v \ll v_{osc}$, the electron trajectory $\mathbf{r}_{osc}$ exhibits a slow oscillatory drift. This domain is most difficult to describe analytically. A wealth of new effects manifest themselves in this domain: the multiflow state, stochastic dynamics in the particle scattering, particle capture by ions, particle grouping (bunching) in the scattering, etc. It is precisely this domain that will receive the bulk of our attention below.

Numerical integration problems. The numerical data outlined below rely on the calculation of the moments of the collision operator and of the cycle-averaged collision function w_{ei} (17) by numerical integration. The integration was performed over the initial coordinates $\mathbf{r}_0$ using the Monte Carlo method. The electron trajectories were calculated by the Runge–Kutta method. Several difficulties are encountered in the numerical integration of the moments of the collision operator.

The first difficulty is due to the fact that a huge number of trajectories need to be calculated. Owing to a strong irregularity (see Section 6) of the integrands in formulas (23) and (29), a large number of trajectories emanating from the initial coordinates $\mathbf{r}_0$ have to be calculated for each point $\{\mathbf{p}_0, \Omega\}$:

$$N_{traj} \sim \frac{50}{\min(\Omega^4, v^4)} \max\left(20, \frac{1}{\Omega^2}\right). \tag{53}$$

This number was sometimes as high as 10^8.

The irregularity of the functions arises from the possibility that a particle acquires a substantial energy variation $\Delta w \sim v_{osc}^2 = 1/\Omega^2$ in comparison with its own energy. This signifies that a small fraction of particles ($\sim \Omega^2$) that changed their energy up to v_{osc}^2 make an appreciable contribution to the overall variation of particle energies and, accordingly, cross sections. To calculate the scattering characteristics correctly, a small fraction of these particles should also be taken into account.

Another limiting factor is the computer time required for calculating an individual trajectory. This applies especially to low-velocity electrons or a high-frequency pump field. The computation time (the number of steps in the solution of the equation of motion) may be estimated as

$$N_{step} \sim \Omega t_{pass} \equiv \frac{\Xi}{v}\,\Omega\,, \quad \Xi \geqslant \max\left(\frac{3v}{\Omega}, \frac{4}{v^2}, \frac{2}{\Omega^2}\right), \tag{54}$$

where the initial distance Ξ was taken as the longest of all characteristic scales of the problem.

Therefore, the complexity of numerically solving a problem with the number of operations on the order of $N_{traj} N_{step}$ at the very least increases with catastrophic speed with a decrease in parameter Ω — as a quantity proportional to $1/\Omega$ taken to the seventh power! The limitation of the computation domain is related to precisely this circumstance. Numerical simulations for small Ω ($\Omega < 0.1$) are practically lacking.

Mention should be made of two more problems in the numerical simulation of collisions in very strong (or, conversely, low-frequency) fields [52].

The first one shows up in particle-in-cell (PIC) simulations and is due to the fact that modern computers are capable of calculating only a finite (on the order of several dozen or hundred) number of particles in one cell.[4] In strong or low-frequency fields, the electron oscillation radius becomes large in comparison with the interparticle distance. This requires to either including a *very* high number of particles in a cell, which is so far unreal, or numerically 'tearing' the electron motion to pieces upon crossing the cell boundaries. The problem with such a discontinuous trajectory lies in the fact that a 'numerical' electron loses information about the variation of parameters in the motion in the other cell. At the same time, a real electron, owing to the continuity of its smooth trajectory, retains information about the scattering during the previous oscillation period and, for a sufficiently low drift velocity, will be able to accumulate the impact parameter variation for a qualitative change in its dynamics. This brings up the question: how distinct is this dynamics change? The data of numerical simulations suggest that it is considerable. This signifies that the description of particle collisions in plasmas by *any* of the existing PIC codes is invalid for a strong field. Ways of remedying this problem are described in Section 7. It should be noted that integration by calculating quantities from the numerically derived smooth trajectory of test electron scattering is devoid of the above drawback. In this case, the computer does not introduce random distortions to the particle trajectory that arise from crossing the cell boundaries.

The second problem consists in the complexity of a valid description of a particle motion about the ion and of large-

[4] A cell represents an artificially (by the programmer's will) selected space domain, in which the particle motion is calculated precisely and the contribution from the outside particles is determined by the mean-field method.

angle scattering [53–55]. Specifically, the equations of motion in the form of expression (46) have a singularity at the point of ion residence. As the electron approaches the ion, its velocity increases as

$$\frac{1}{\sqrt{r}} \underset{r\to 0}{\to} \infty ,$$

which hinders the numerical passage of this vicinity. Furthermore, the characteristic time of velocity variation and, hence, the maximal step are proportional to

$$r^{3/2} \underset{r\to 0}{\to} 0$$

and may be much shorter than the pump field period. For a low frequency of the pump field, $\Omega \ll 1$, the ratio between the time of one impact, $\sim \Omega^3$, and the total scattering time $r_{\rm osc}/v \sim 1/(\Omega^2 v)$ decreases quite rapidly (as Ω^5) with a decrease in frequency Ω! This circumstance compels the code to unjustifiably narrows the time step, which leads to a very long computation time or to an incorrect calculation of the particle motion about the ion and thereby to significant random data errors. We note that the majority of PIC codes do not consider this problem at all, assuming that the fraction of particles that are scattered through large angles is small and may be ignored. The results presented in our review are indicative of the opposite: the contribution from particles scattered through large angles is significant in strong fields.

To eliminate this problem, in the numerical integration of equation (46) use was made of regularization of the equation of motion [52], which consisted in the introduction of fictive time s related to real time t by the differential relationship[5]

$$\mathrm{d}t = f(R)\,\mathrm{d}s\,, \quad f(R) > 0\,. \tag{55}$$

In this case, the equations of motion take on the forms

$$\mathbf{R}' = \mathbf{P} f(R)\,, \quad \mathbf{P}' = \left[-\frac{\mathbf{R}}{R^3} + \mathbf{E}(t)\right] f(R), \quad t' = f(R)\,. \tag{56}$$

Here, the prime denotes differentiation with respect to parameter s, which is sometimes called the fictive time. Furthermore, owing to the explicit time (t) dependence of the equations, an additional equation for the 'real' time t appears.

For a function $f(R)$, one may choose

$$f(R) = \frac{R^2}{1+R^2}\,. \tag{57}$$

This function eliminates the explicit singularity in the equations at $R = 0$ and turns to unity at infinity, where the effect of the Coulomb potential is weak. In addition, this function is rapidly calculated in the numerical simulation.

The purpose of introducing time s is that the system of equations 'selects' the real-time (t) step on its own in the motion along a trajectory. Away from the ion ($R \to \infty$), the time flows in a normal way. As the ion is approached, the time 'slows down'. This corresponds to the fact that in the course of numerical integration in the motion with a constant step in s, the step in real time t automatically splits near the Coulomb singularity. The momenta themselves, unlike those in the case of Levi-Civita regularization [52, 56], may turn to infinity, but they vary slowly on the fictive time scale. This scheme permits the collision-induced particle momentum variation to be calculated more quickly and precisely due to the elimination of explicit singularity from the equations of motion. However, this is achieved at the expense of raising the dimension of the system of equations: a new independent variable t appeared along with the equation for it.

4. High-velocity domain

Let us consider in greater detail the dynamics of electron–ion collisions in each of the above domains (see Fig. 3). We begin with the domain of high electron velocities, $v \gg v_{\rm osc}$. In this case, the influence of an external field $\mathbf{E}$ on the particle trajectory may be disregarded and the particle motion may only be considered in the Coulomb ion potential:

$$\ddot{\mathbf{r}} = -\frac{\mathbf{r}}{r^3}\,. \tag{58}$$

The solution to the problem of a particle motion in the Coulomb potential, which is called the Rutherford problem, is well known [36]. Our concern is only with infinite trajectories. In this case, the motion occurs over a hyperbolic trajectory, which is conveniently represented in the parametric form:

$$r = b_v(\varepsilon\cosh\xi - 1)\,, \quad \varphi = \frac{\varepsilon - \cosh\xi}{\varepsilon\cosh\xi - 1}\,, \qquad t = \frac{b_v}{v}(\varepsilon\sinh\xi - \xi)\,, \tag{59}$$

where $\varepsilon = \sqrt{1 + \rho^2/b_v^2}$ is the orbit eccentricity, and parameter ξ assumes values[6] from $-\infty$ to ∞. The minimum particle–ion distance is expressed as

$$r_{\rm min} = b_v(\varepsilon - 1) = \sqrt{b_v^2 + \rho^2} - b_v \approx \begin{cases} \rho\,, & \rho \gg b_v\,, \\ \dfrac{\rho^2}{2b_v}\,, & \rho \ll b_v\,. \end{cases} \tag{60}$$

The first approximate equality signifies that the impact parameter is hardly changed for $\rho \gg b_v$, i.e., the particle describes a nearly straight line. The second one is indicative of a strong particle attraction by the ion when $\rho \ll b_v$, so that the minimum approach distance to the ion turns out to be much shorter than the initial impact parameter. In particular, by solving the inverse problem — what is the initial impact parameter (or what is the initial area, which is the same thing) of the particle whereby it finds its way into the domain of radius a — it is easy to obtain the formula

$$\rho_{\rm gr} = \sqrt{(a + b_v)^2 - b_v^2} \underset{a \ll b_v}{\simeq} \sqrt{2ab_v} \gg a\,. \tag{61}$$

An estimate of the effective cross section at high ($r_{\rm a} \ll b_v$) frequencies may be obtained even from relation (61):

$$\sigma_{\rm eff} \geqslant 2\pi r_{\rm a} b_v\,, \quad r_{\rm a} \ll b_v\,. \tag{62}$$

True, only those particles that approach the ion to a distance less than the adiabaticity radius $r_{\rm a} = v/\Omega$ can change their energy. From formula (61), for short $r_{\rm a}$ ($r_{\rm a} \ll b_v$) one can see that particles are collected from an area $\pi\rho_{\rm gr}^2 \approx 2\pi r_{\rm a} b_v$.

[5] Since kinetic effects are not described in this section, f in Eqn (55) simply denotes some function in no way related to a distribution function.

[6] Parameter ξ, which is related to time t by the equation $\mathrm{d}t = r\,\mathrm{d}\xi$, is interpreted as the fictive time in going over to Levi-Civita coordinates.

Accordingly, the effective cross section should be no smaller than $\sigma_{\rm eff}$[7] estimated by expression (62). This quantity is appreciably greater [by a factor of $b_v/r_{\rm a}$ $(b_v/r_{\rm a} \gg 1)$] than the effective cross section $r_{\rm a}^2$ derived from the small-angle approximation [15].

The expression for the particle velocity variation $\Delta\mathbf{v}$ in the scattering from a Coulomb center is helpful in the subsequent discussion:

$$\Delta\mathbf{v} = -\frac{\boldsymbol{\rho}\, v}{\rho}\,\frac{2\sqrt{\varepsilon^2-1}}{\varepsilon} - \mathbf{v}\,\frac{2}{\varepsilon^2} = -\frac{2\boldsymbol{\rho}\, v^3}{1+\rho^2 v^4} - \frac{2\mathbf{v}}{1+\rho^2 v^4}\,. \tag{63}$$

In this case, the scattering angle is expressed as $\theta = \pi - 2\arccos(1/\varepsilon) = 2\arctan(b_v/\rho)$. By substituting it into expression (30) for the transport cross section, we arrive at the well-known Rutherford formula [36]:

$$\sigma_{\rm tr} = \frac{2\pi\Lambda}{v^4}\,, \tag{64}$$

which is also valid in the framework of quantum mechanics [57].

From the particle trajectory (59), one can find the energy radiated by one particle in a frequency range $\mathrm{d}\omega$ [49]:

$$\mathrm{d}E_\omega = \frac{\pi\omega^2}{6c^3}\left(H'^2 - \frac{\varepsilon^2-1}{\varepsilon^2}\,H^2\right)\mathrm{d}\omega\,.$$

Here, c is the speed of light in vacuum, $H = H_{\mathrm{i}\nu}(\mathrm{i}\nu\varepsilon)$ is the first-order Hankel function of rank $\mathrm{i}\nu$, and $H' = H'_{\mathrm{i}\nu}(\mathrm{i}\nu\varepsilon)$ is its derivative with respect to argument $\nu = b_v/r_{\rm a}(\omega) \equiv \omega/v^3$. Integrating over many particles permits finding the emission cross section (31) in the scattering of a beam of particles moving in parallel [49]:

$$\chi_{\rm inc} = \frac{4\pi^2\omega}{3c^3v^5}\left|H_{\mathrm{i}\nu}(\mathrm{i}\nu)H'_{\mathrm{i}\nu}(\mathrm{i}\nu)\right|. \tag{65}$$

Using the formula $H_{\mathrm{i}\nu}(\mathrm{i}z) = -(2\mathrm{i}/\pi)\exp(\nu\pi/2)K_{\mathrm{i}\nu}(z)$, the cross section (65) may be rewritten in the form

$$\chi_{\rm inc} = \frac{16}{3}\,\frac{\Phi(\nu)}{c^3v^2}\,,\quad \Phi(\nu) = \nu\exp(\nu\pi)K_{\mathrm{i}\nu}(\nu)\,\frac{K_{1-\mathrm{i}\nu}(\nu)+K_{1+\mathrm{i}\nu}(\nu)}{2}\,. \tag{66}$$

Here, $K_{\mathrm{i}\nu}(z)$ is the modified Bessel function of rank $\mathrm{i}\nu$.

We give special consideration to low- and high-frequency cases. For low frequencies $\nu \ll 1$, one may approximately put $K_{\mathrm{i}\nu}(\nu) \approx K_0(\nu) \approx \ln[2/(\gamma\nu)]$ and $K_{1+\mathrm{i}\nu}(\nu) \approx 1/\nu$, where γ is the Euler constant exponent, $\gamma \approx 1.78107\ldots$. In view of this, we find

$$\chi_{\rm inc} \approx \frac{16}{3v^2c^3}\left(1+\frac{\pi b_v}{r_{\rm a}}\right)\ln\frac{2r_{\rm a}}{\gamma b_v}\,,\quad b_v \ll r_{\rm a}\,. \tag{67}$$

For high frequencies $\nu \gg 1$, we take advantage of the expansions

$$H_{\mathrm{i}\nu}(\mathrm{i}\nu) \approx -\frac{\mathrm{i}}{\pi\sqrt{3}}\left(\frac{6}{\nu}\right)^{1/3}\Gamma\left(\frac{1}{3}\right),$$

$$H'_{\mathrm{i}\nu}(\mathrm{i}\nu) \approx \frac{1}{\pi\sqrt{3}}\left(\frac{6}{\nu}\right)^{1/3}\Gamma\left(\frac{2}{3}\right)\left[1+\frac{7}{90}\left(\frac{6}{\nu}\right)^{1/3}\right]$$

(where Γ is the gamma function). We substitute them into formula (65) to obtain the effective emission cross section at high frequencies:

$$\chi_{\rm inc} \approx \frac{16\pi}{3\sqrt{3}\,c^3v^2}\left(1+\frac{7}{90}\left(\frac{6r_{\rm a}}{b_v}\right)^{2/3}\right),\quad b_v \gg r_{\rm a}\,. \tag{68}$$

The next order of expansion in the small parameter was purposefully retained in formulas (67) and (68) (compare with the corresponding formulas in Ref. [49]) for their further use in the search for the effective collision frequency.

To determine the effective collision frequency in the domain of $v \gg v_{\rm osc}$ under consideration, it is convenient to take advantage of the formula that relates the spontaneous (bremsstrahlung) emission and the stimulated (particle energy variation) emission for an isotropic velocity distribution:

$$\nu_{\rm eff} = \frac{\pi^2c^3n_{\rm i}}{v^2}\,\frac{\partial}{\partial v}(\chi_{\rm inc}v^2)\,, \tag{69}$$

which was derived in Ref. [58] proceeding from the principle of detailed balance (see also Refs [5, 59]). The convenience of formula (69), which was derived from quantum-mechanical considerations, resides in that it relates two nonquantum processes: the dipole radiation of a particle in its trajectory motion, and the variation of particle energy under the action of a weak external field.

In our case, this permits finding the effective collision frequency for a complicated particle trajectory without resorting to unwieldy calculations (under classical or quantum approaches). By applying expression (69) to expression (66) for the radiation cross section, it is possible to find $\nu_{\rm eff}$:

$$\nu_{\rm eff} = \frac{16\pi^2n_{\rm i}}{3v^3}\,\nu\,\frac{\mathrm{d}\Phi(\nu)}{\mathrm{d}\nu}\,. \tag{70}$$

For low and high values of ν, the expression for the effective collision frequency (70) is simplified:

$$\nu_{\rm eff} \approx \begin{cases} 9.45\,n_{\rm i}v\,b_v^2\ln\dfrac{r_{\rm a}}{b_v}\,, & r_{\rm a} \gg b_v\,,\\[2ex] 2.94\,n_{\rm i}v\,b_v^2\left(\dfrac{r_{\rm a}}{b_v}\right)^{2/3}, & r_{\rm a} \ll b_v\,. \end{cases} \tag{71}$$

The first formula in expressions (71) gives the well-known result of the small-angle scattering theory. The second formula, which describes collisions in the case of strong attraction, was obtained proceeding from quantum-mechanical approaches in Refs [50, 51].[8] We note that, owing to substantial attraction, at high frequencies of the external field the collision frequency decreases much more slowly than $1/\omega^2$, as is predicted in the framework of the small-angle scattering theory [15], and so the plasma description calls for the inclusion of large-angle scattering.

5. Averaged description domain

In the case of a strong $(v_{\rm osc} \gg v)$ and high-frequency $(\Omega \gg 1)$ field, the following inequalities hold true:

$$b_v \gg b_{\rm osc} \gg r_{\rm osc}\,, \tag{72}$$

[7] In reality, the particles that approach the ion to a closer distance experience a higher energy change than the small-angle ones, and therefore the effective cross section turns out to be even greater.

[8] The result obtained in Refs [50, 51] differs from ours by a numerical factor.

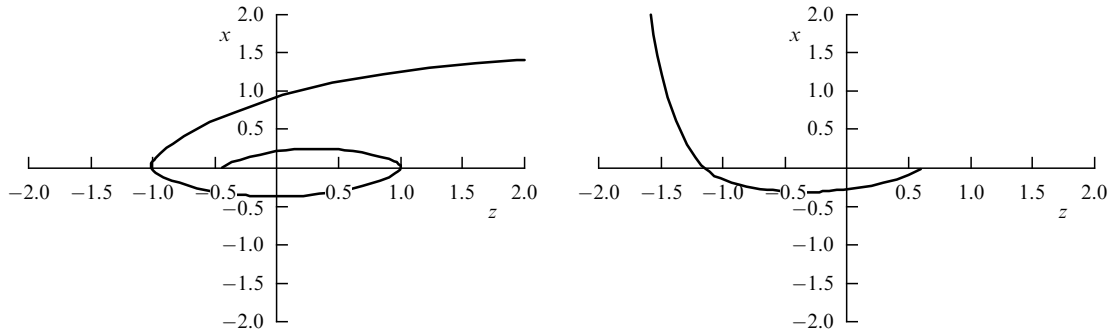

Figure 4. The shape of electron trajectories trapped by the averaged potential in the case of linear field polarization. The coordinates are normalized to radius $r_{\rm osc}$.

and the equations of motion (47) may be simplified. To this end, we expand the potential on the right-hand side of the equation in a Fourier series:

$$\frac{1}{|\mathbf{r}-\mathbf{r}_{\rm osc}(t)|}=\sum_{n=-\infty}^{\infty}U_n(\mathbf{r})\exp(\mathrm{i}\Omega nt)\,,\qquad U_n(\mathbf{r})=\frac{\Omega}{2\pi}\int_0^{2\pi/\Omega}\frac{\exp(-\mathrm{i}\Omega nt)}{|\mathbf{r}-\mathbf{r}_{\rm osc}|}\,\mathrm{d}t\,. \tag{73}$$

Under condition (72), the particle velocity variation over a field cycle $2\pi/\Omega$ is small. Then, we may keep in series (73) only the zero-order term

$$U_0(\mathbf{r})=\frac{\Omega}{2\pi}\int_0^{2\pi/\Omega}\frac{\mathrm{d}t}{|\mathbf{r}-\mathbf{r}_{\rm osc}|}\,, \tag{74}$$

which is also termed the *averaged potential*.

In the case of linear polarization, integral (74) is taken analytically [14]:

$$U_0^{\rm LP}(\mathbf{r})=-\frac{2}{\pi\sqrt{r_+r_-}}\,K\left[\sqrt{\frac{4r_{\rm osc}^2-(r_+-r_-)^2}{4r_+r_-}}\,\right], \tag{75}$$

where $r_\pm=\sqrt{r_\perp^2+(z\pm r_{\rm osc})^2}$, $r_\perp=\sqrt{x^2+y^2}$, and $K(\mu)$ is the complete elliptic integral of the 1st kind. As expected, the averaged potential (75) is axially symmetric about the z-axis and is an even function of z. At the stopping points $r_\pm=0$, the potential has a square-root singularity: $U_0^{\rm LP}\approx-1/\sqrt{r_{\rm osc}r_\pm}$, and a logarithmic singularity on the symmetry axis for $|z|<r_{\rm osc}$:

$$U_0^{\rm LP}\approx-\frac{4}{\pi}\ln\left(\frac{r_\perp r_{\rm osc}}{r_{\rm osc}^2-z^2}\right)(r_+r_-)^{-1/2}\,.$$

However, of greater interest is the expansion of the averaged potential at long distances ($r\gg r_{\rm osc}$):

$$U_0^{\rm LP,\,CP}\approx-\frac{1}{r}\left(1\pm\frac{r_{\rm osc}^2}{r^2}\,\frac{3\cos^2\theta-1}{4}+\ldots\right), \tag{76}$$

where θ is the angle between the electron velocity and the z-axis. The first term in the expansion represents the Coulomb ion field, and the next terms are responsible for the noncentral nature of the averaged potential.

Indeed, it follows from the applicability condition (72) of the averaged description that it makes sense to consider the particle motion with velocities $v\ll\Omega$, i.e., the range $r\gg r_{\rm osc}$ of distances is significant in the particle motion. It can be seen from expansion (76) that the motion of the majority of particles continues to be adequately described by Rutherford formulas. The emergence of a higher-power potential, $\sim 1/r^3$, appears as a new circumstance, which makes possible the *trapping* of transit particles and the fall of particles on the center even for a nonzero impact parameter.

As the center is approached, expansion (76) becomes inapplicable. However, the motion in the exact potential proceeds in a similar manner (Fig. 4) of attraction to the ion.[9] In this case, the attraction in the exact potential turns out to be stronger than in the approximated potential (76).

The particle capture cross section may be estimated from formula (61) as the cross section whereby the minimum approach distance is equal to $r_{\rm osc}$:

$$\sigma_{\rm cap}\simeq\pi\rho_{\rm gr}^2\simeq 2\pi b_v r_{\rm osc}\,,\quad b_v\gg b_{\rm osc}\gg r_{\rm osc}\,. \tag{77}$$

It is easily seen that this cross section increases with a lowering of the particle velocity v or of the field frequency Ω.

We revert to the complete dynamic problem (73) to note that capture cross section (77) yields an estimate from below of the effective cross section $\sigma_{\rm eff}$. Specifically, particles that encounter the singularity of the averaged potential in the dynamic problem experience scattering by large angles and change their energy by a magnitude on the order of the oscillatory energy $mv_{\rm osc}^2$. Therefore, the estimated effective cross section is

$$\sigma_{\rm eff}\geqslant\sigma_{\rm cap}\simeq 2\pi b_v r_{\rm osc}\,,\quad b_v\gg b_{\rm osc}\gg r_{\rm osc}\,. \tag{78}$$

In reality, the effective cross section is larger. Indeed, in the averaged description domain (72), the inequality $b_v\gg r_{\rm a}$ is fulfilled. It permits employing the result for the effective cross section from the Rutherford problem, because, as noted above, the particle motion for $r\gg r_{\rm osc}$ is close to the motion in a stationary Coulomb potential:

$$\sigma_{\rm eff}=\frac{\nu_{\rm eff}}{n_{\rm i}v}\approx 2.94b_v^2\left(\frac{2r_{\rm a}}{b_v}\right)^{2/3}\gg 2\pi b_v r_{\rm osc}\,. \tag{79}$$

[9] Formally, this motion is not at variance with the Liouville theorem on phase volume conservation: as the particles are drawn to the ion, $V_{\mathbf{r}}\to 0$, their velocity rises, $V_{\mathbf{v}}\to\infty$, so that the total phase volume $V_{\mathbf{r}}V_{\mathbf{v}}$ is conserved. Nor does this motion contradict the conservation of angular momentum, since the potential is not centrally symmetric and the centrifugal force can no longer compensate for the nonpoint-like singularity of the potential.

This is because the particles for which the influence of the oscillatory field is significant are collected from a significantly smaller area, $\sim \pi b_v r_{\rm osc}$, than the particles making a contribution to the effective cross section and cannot significantly affect the integral scattering characteristics.

Expansion (76) of the potential permits estimating the transport cross section. Indeed, particle scattering through large angles will occur at the equality between the kinetic and potential energies. Provided that $r_{\rm osc} \ll b_v$, this will take place for impact parameters $r_{\min} \approx b_v \pm (3\cos^2\theta - 1) r_{\rm osc}^2/(4b_v)$. The transport cross section is then expressed as follows:

$$\sigma_{\rm tr} \approx \int_{r_{\min}}^{r_{\max}} \frac{b_v^2\,{\rm d}\rho}{\rho} = b_v^2 \ln \frac{r_{\max}}{b_v \pm (1/4)(3\cos^2\theta - 1) r_{\rm osc}^2/b_v}\,; \quad (80)$$

this quantity is close to the Rutherford cross section (64). The weak anisotropic dependence on the field amplitude $r_{\rm osc}^2(3\cos^2\theta - 1)/b_v$ enters only logarithmically. This result is due to the fact that most of the integral defining the transport cross section acquires its value in distant collisions, which are nicely described by Rutherford trajectories. Furthermore, since distant collisions make the main contribution to the incoherent radiation cross section, as well as to the transport cross section, it may be shown that the incoherent radiation cross section, too, will depend on the pump field logarithmically weakly. Numerical calculations (see Section 8) suggest that these results also persist for low-frequency fields, $b_{\rm osc} \leqslant r_{\rm osc}$.

Therefore, formulas for the effective (79) and transport (80) cross sections suggest that the influence of an external weak high-frequency field ($\Omega \gg 1$) on the particle scattering in the averaged description domain ($b_v \gg b_{\rm osc} \gg r_{\rm osc}$) is insignificant and the particle scattering may be treated in this case as scattering by a stationary Coulomb potential, i.e., in the framework of the Rutherford problem.

6. Domain of multiple returns

So, let us consider what new effects, in comparison with the small-angle approximation, appear at low drift velocities of particles colliding in strong fields, when

$$b_{\rm osc} \ll r_{\rm osc}\,, \quad v \ll v_{\rm osc}\,. \quad (81)$$

The salient feature is a significant bending of trajectories in the course of scattering. This gives rise to new effects: (i) a significant increase in the scattering cross sections due to attraction across the initial beam velocity, and (ii) the appearance of electron bunching along the beam. We discuss them in greater detail. Only a qualitative description of the phenomena is outlined in this section. Their quantitative estimates are given in Section 7.

First, we consider the attraction across the oscillatory velocity direction, whose main consequence is an increase in the particle energy variation and, accordingly, an increase in all scattering cross sections. Figure 5 shows the energy variations on the same scale [in what follows, the darker domains correspond to a higher energy variation (black color corresponds to the oscillatory energy), and the lighter domains to a lower one (white color signifies the absence of energy variation)] as a function of impact parameters, which were obtained numerically and in the framework of the small-angle approximation. It is clear from the drawing that along with the particles having experienced head-on collisions (black circle of size $b_{\rm osc}$ in the center), the particles with

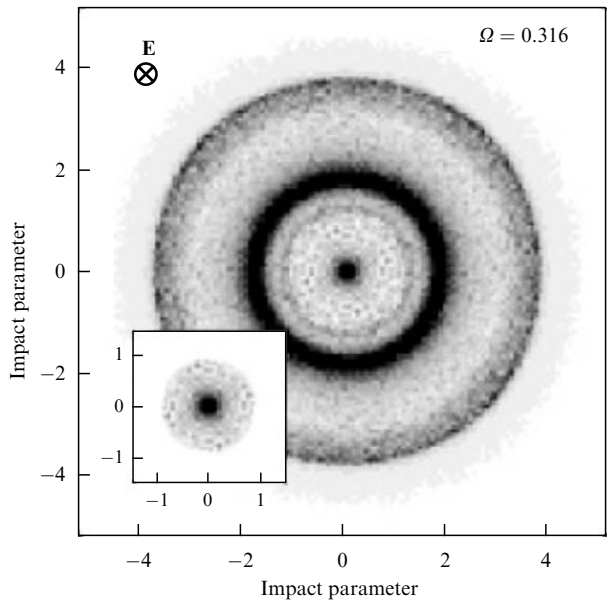

Figure 5. Energy variation as a function of impact parameters at $\Omega = 0.316$ and $v = 1$. Shown in the inset on the same scale is the energy variation obtained in the framework of the small-angle approximation.

impact parameters that are much greater than $b_{\rm osc}$ also experience energy variations on the same order of magnitude. This phenomenon may be termed the 'parachute' effect [37, 38], because the particles gradually, during several flight times, approach the ion (decrease their instantaneous impact parameter). In traditional models we would have observed only head-on collisions. The energy variation of particles from concentric rings would be exponentially small on the strength of the adiabaticity of the motion of distant particles.

One can also see in Fig. 5 the second implication of transverse attraction: the dependence of energy variation on the impact parameters is not a one-to-one function. In strong fields, $\Omega \ll 1$, and at low drift velocities, $v < v_{\rm osc}$, a situation is realized whereby particles with different impact parameters experience the same energy variation. Furthermore, particles with different impact parameters may acquire the same final velocity. In other words, a multiflow state takes place, which is lacking in weak fields. Along with this, stochasticity emerges: a small variation of the initial parameters results in a strong deflection of particle trajectories and a large difference in final particle velocities (Fig. 6). So, if distant particles travel along almost the same line and are well suited to the description in the framework of the small-angle approximation (Fig. 6c), then a strong dispersion of trajectories is observed even at the boundary of the attraction domain. Inside the attraction domain, the trajectories behave stochastically (Fig. 6a). The boundary of the attraction domain may be estimated numerically in a linearly polarized field at $\theta = 0$:

$$\rho_{\rm attr} = \frac{1.5}{\Omega v} \gg b_{\rm osc} = \Omega^2\,. \quad (82)$$

Notice that the attraction domain boundary serves simultaneously as the boundary for a strong particle energy variation. Indeed, to significantly change its energy, a particle should approach the ion, but the particles residing outside the attraction domain cannot approach the ion closely and therefore cannot change their energy considerably.

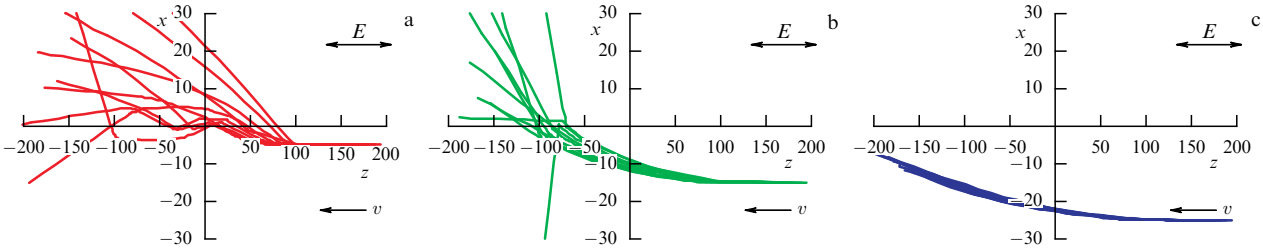

Figure 6. Set of particle drift trajectories with different initial phases for particles traveling inside (a), at the boundary (b), and outside (c) the attraction domain. (Longitudinal fall, linear polarization, $\Omega = 0.1$ and $v = 1$.)

It is noteworthy that the attraction domain boundary for $v \leqslant 1$ turns out to be greater than the adiabaticity radius $r_a = v/\Omega$. Therein lies one of the most nontrivial results of the solution to the problem of energy exchange between electrons and a strong field, which consists in the absence, even for large impact parameters, of the domain corresponding to the so-called Coulomb logarithm (41).

Recall how this domain emerges in weak fields. If the oscillatory electron radius is short in comparison with the distance to a Coulomb center, i.e., the impact parameters are relatively large, then for solving the scattering problem it would suffice to expand the potential in equation (47) for the drift center in powers of the oscillatory radius and take into account the first correction term, which corresponds to the dipole approximation. In this case, the drift center trajectory itself is defined by the static ion field and the energy exchange between an electron and the field by the work of the oscillatory dipole field along this trajectory. This problem is easily solved [5] for impact parameters belonging to the domain of essentially nonadiabatic interactions, $\rho < v/\Omega$. One may verify for oneself that, beginning with relatively small impact parameters corresponding to the Rutherford radius $b_v = 1/v^2$ estimated from the drift velocity, and up to the distances corresponding to the nonadiabaticity domain boundary, $r_a = v/\Omega$, the following estimate applies to the electron energy exchange with the field averaged over incident phases and considered as a function of the impact parameter:

$$\Delta w \simeq m v_{\text{osc}}^2 \frac{b_v^2}{\rho^2} \exp\left(-\frac{\Omega\rho}{v}\right). \tag{83}$$

The exponent on the right-hand side of formula (83) corresponds to the adiabatic electron transit through the interaction domain for impact parameters greater than the size of the adiabaticity domain. Hence, it is clear that integration over the impact parameters, $\int \Delta w \rho \, \mathrm{d}\rho$, gives rise to a logarithmic factor caused by the cutoff of energy exchange at this boundary.

Let us now discuss how this picture changes in strong fields. In the impact parameter domain corresponding to the 'parachute' effect, the impact parameter changes greatly, and this domain is similar in many respects to the domain of small impact parameters in weak fields. It is significant that the drift trajectories deflect greatly in this domain, depending on the field phase, in contrast to the drift trajectories in the case of weak fields. For drift velocities smaller than unity (in dimensionless variables), the boundary of the attraction domain turns out to be further than the adiabaticity domain boundary, and so the exponential cutoff sets in immediately after it. For high drift velocities, $1 < v < 1/\Omega$, a decrease beyond the capture domain obeys a power law and gradually transforms to $1/\rho^2$. Thus, with an increase in velocity we gradually move in this domain to the regime with the Coulomb logarithm.

A similar situation takes place in the case of nonlongitudinal incidence, $\theta \neq 0$ (Fig. 7). Here, concentric rings divide into arcs, with the distance between them decreasing. As would be expected, the effect becomes stronger with a decrease in the initial velocity. For high velocities, the main contribution is made by head-on collisions, and the attraction is insignificant. With a decrease in velocity, the 'segment' (the thin strip in Fig. 7) broadens and, in addition, arcs appear at its ends. In the case of longitudinal incidence, the arcs close up into concentric circles (see Fig. 7). That is, at low velocities the electron drift velocity can no longer be thought of as being straight, and the *bending of the particle drift trajectory* should be taken into account in describing the motion near the Coulomb center.

A similar situation is observed for a circular polarization (CP) (Fig. 8), with the difference being that transverse incidence in the CP case is an analogue of longitudinal incidence for a linear polarization (LP). In the transverse incidence in the circular polarization case, the electron flies past the multiply oscillating ion. As a result, effects of attraction due to periodic returns are most clearly manifested, as is the case in the longitudinal incidence for an LP. In the case of longitudinal incidence for a CP, the attraction effects weaken.

Once again, as in the case of an LP, ellipse splitting shows up (see Fig. 8). The splitting mechanism resembles the one responsible for the appearance of concentric rings in the longitudinal incidence for an LP. The splitting mechanism is due to the fact that a significant energy change is experienced not only by the electron that directly flies into the ion, but also by the electrons that are drawn closer to the ion during several oscillation half-cycles. We note that the picture is asymmetric relative to the x-axis, since the total velocity in the flight past the ion turns out to be different at the two ends of the 'segment'. At one of its ends, the total velocity is equal to the sum of oscillatory and drift velocities, while at the other end the total velocity is equal to their difference.

One of the consequences of particle trajectory bending under the action of Coulomb potential is the manifestation of singularity in the distribution over the minimum approach distance $r_{\min}$ to the ion — the surface particle density at the point where the attractive ion force is maximum. In the case of applicability of the small-angle approximation, this surface density should be constant and equal to the surface density in the plane for $\xi = -\infty$. According to numerical simulation data, the surface density decreases as $1/r_{\min}$ for short $r_{\min}$ (Fig. 9), which is further confirmation that particle trajectory bending in the scattering must be taken into account. For a

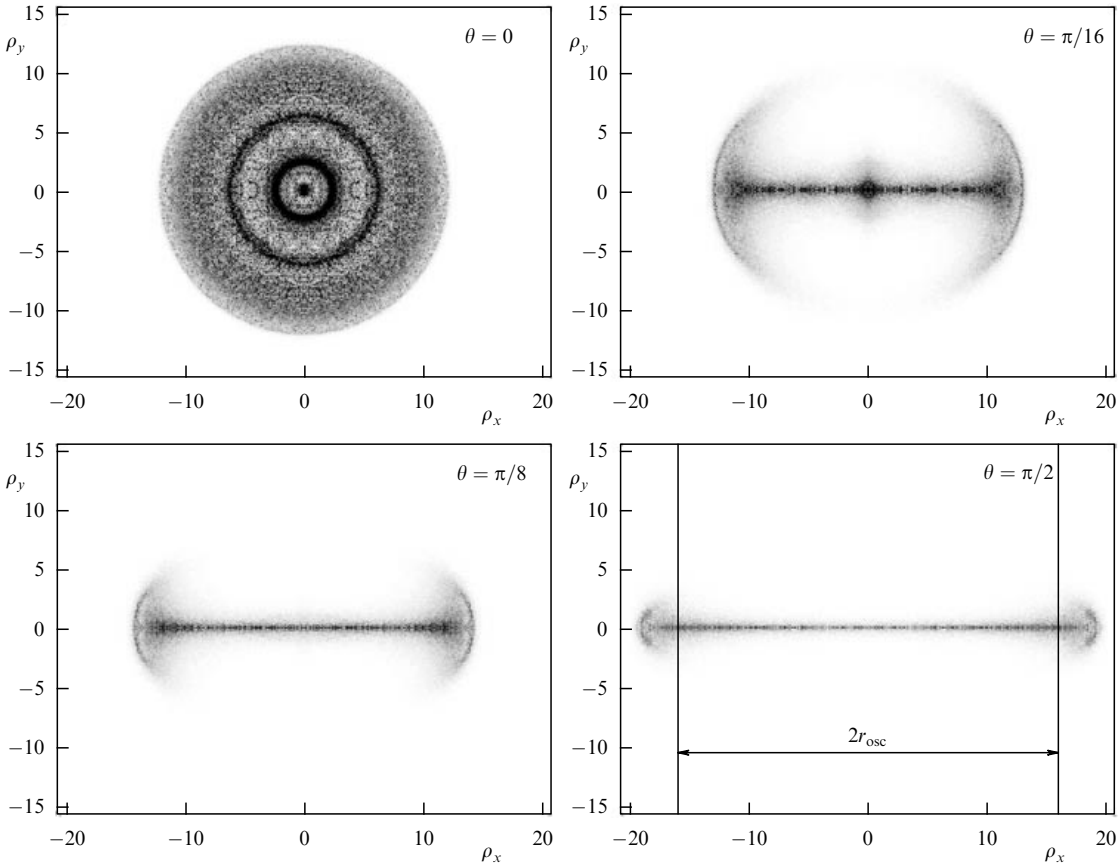

Figure 7. Dependence of energy variation on the impact parameters at various angles of incidence θ for a linear polarization at $\Omega = 0.25$ and $v = 0.5$. The points show the projection of ion oscillations onto the impact parameter plane.

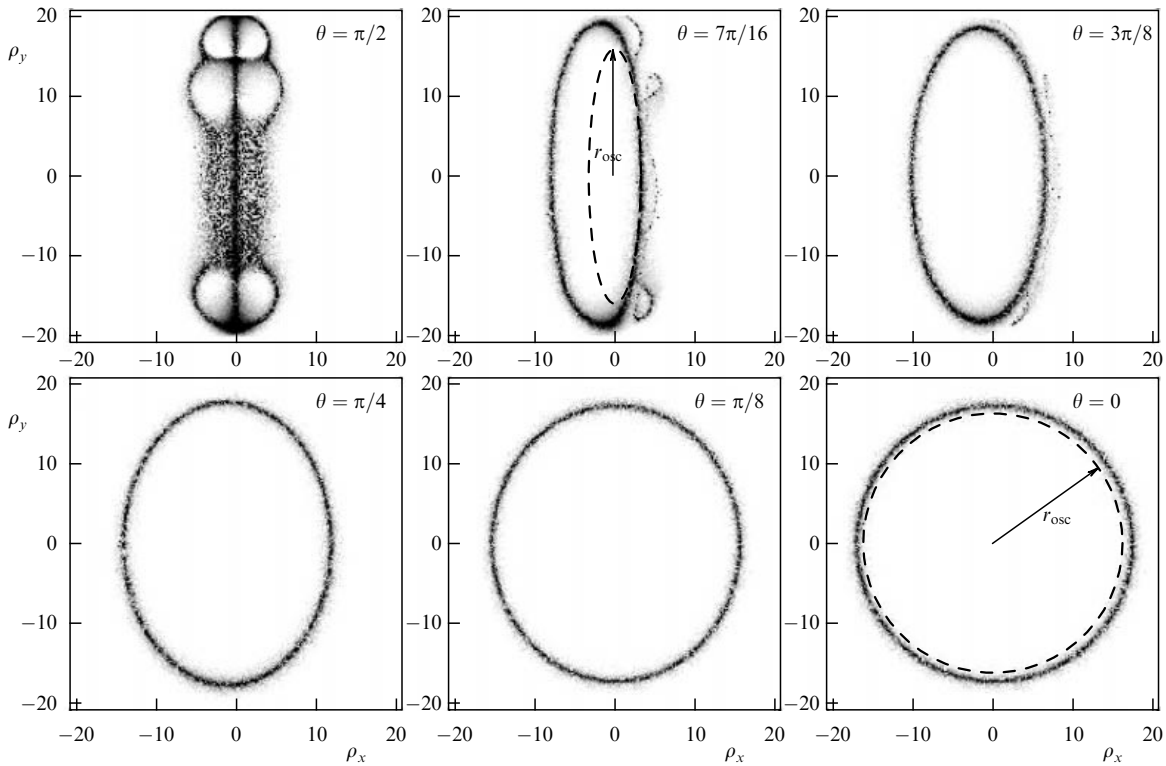

Figure 8. Energy variation as a function of impact parameters for various angles of incidence θ for a CP at $\Omega = 0.25$ and $v = 0.5$.

known $n(r_{\rm min})$ dependence and the assumption that the main energy change is stepwise at $r = r_{\rm min}$, it is possible to estimate the effective cross section $\sigma_{\rm eff}$ (see Section 7). This may be employed for checking the accuracy of calculations.

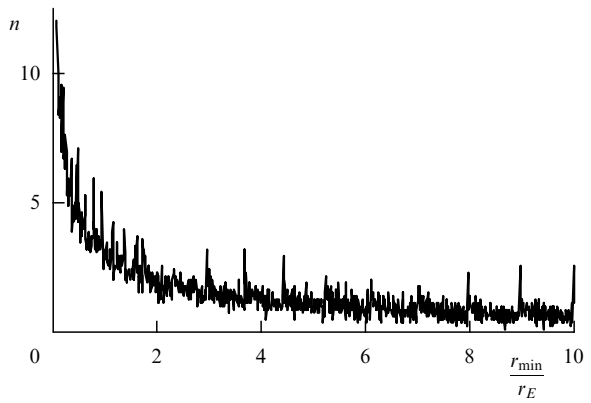

Figure 9. Particle distribution over the minimum approach distance to the ion.

As stated in the foregoing, the Coulomb ion field is responsible not only for the particle 'beam' compression (transverse attraction), but also, jointly with the periodic pump field, for the bunching of particles along the 'beam'. It turns out that virtually all collisions, especially those with a large energy change, occur for quite specific phases of the pump field (Fig. 10). This effect is extraordinary, the more so as it takes place in the scattering of different electrons from different randomly located ions with the only synchronization mechanism — the electric field of the pump wave. All this looks as if a wave of bremsstrahlung 'bursts' is excited in the plasma, which travels along with the pump field wave.

Figure 10 is similar to Fig. 5, but it takes into account the axial symmetry of the problem, which made it possible to derive the dependence of the quantities on the initial incident phase φ of particles as well. Figure 10a displays the energy and Fig. 10b the collision phase as functions of the initial phase and the impact parameter of the electrons being scattered. It is evident that these dependences are periodic in the initial phase due to the periodicity of the pump field. As noted above, in strong fields, due to the 'parachute' effect, an electron may greatly change its energy (the darker color in Fig. 10a), even if its initial impact parameter was far greater than the Rutherford radius b_{osc} estimated from the oscillatory particle velocity (the thin dark strip for $\rho \approx 0$ in the lower part of Fig. 10a). Figure 10b demonstrates much more unexpected fact: the same color corresponds to the same phases at the instant of the last (closest) electron passage near the ion. One can see that all collisions originating from the attraction domain occur practically at only two field phases. This is just the effect of electron bunching.

The bunching consists in the fact that all electrons fly past the ion almost in the same field phase due to adiabatic attraction, despite the initial uniform electron distribution over the field phases. Figure 11 depicts the dependence of the field phase at the instant of the 'last' collision (the instant of closest electron approach to the ion), which is subsequently called the *collision phase*, on the initial field phase. All electrons start moving along the field with an impact parameter $\rho = 3.2$. One can see that the energy exchange between an electron and the field occurs in a narrow band of

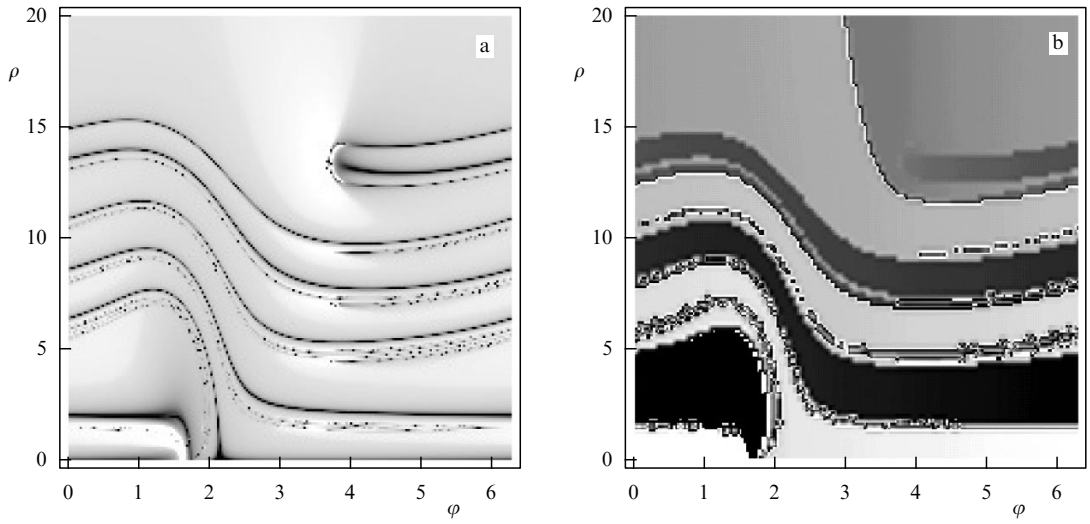

Figure 10. Dependences of the energy variation (a) and collision phase (b) on the impact parameter ρ and the initial incident phase φ of the electrons being scattered at $v = 1$ and $\Omega = 0.1$ (longitudinal scattering, $\mathbf{p}_0 \parallel \mathbf{E}$).

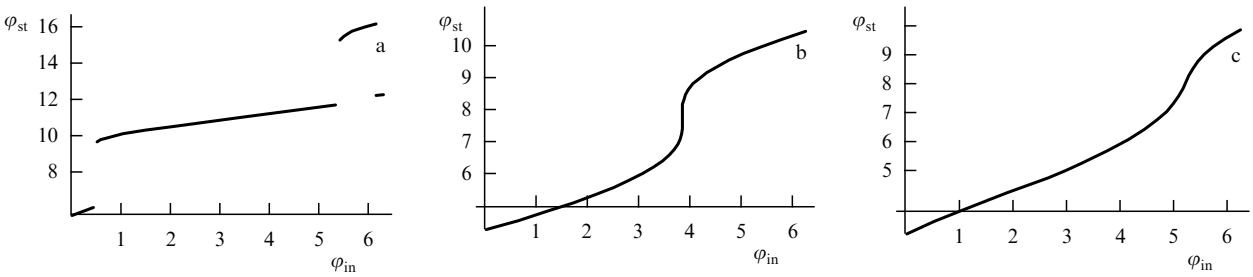

Figure 11. Collision phase as a function of initial phase for velocity values: (a) $v = v_{\text{osc}}/2$, (b) $v = v_{\text{osc}}$, and (c) $v = 3v_{\text{osc}}/2$ at $\Omega = 0.316$.

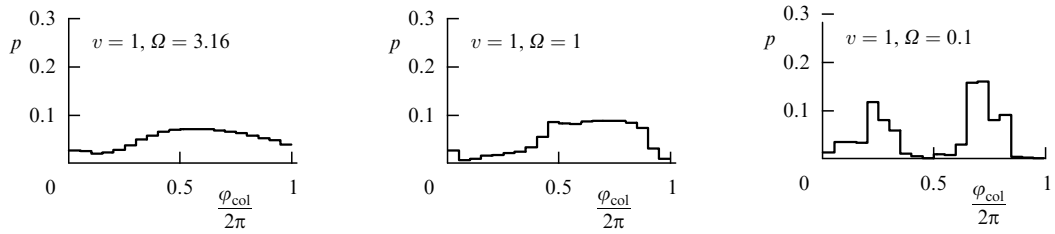

Figure 12. Particle distribution over collision phases in relation to parameter Ω in the case of longitudinal incidence at $v = 1$ and a linear polarization of the pump field.

field phases. The 'steps' in this dependence correspond to the shift of collision instants by a field half-cycle. As the drift velocity rises, the electron bunching in phase vanishes, i.e., collisions begin to occur at arbitrary instants of time, independent of the phase of the external field.

The degree of bunching is demonstrated by the electron distribution function over the collision phase (Fig. 12). As the ratio $v_{\rm osc}/v_T$ increases, all electrons concentrate into two relatively narrow peaks near the maxima of oscillatory velocity (Fig. 12). The width of these peaks is proportional to the ratio $v_T/v_{\rm osc}$. With reference to Fig. 12a, for a high thermal electron velocity, $v_T > v_{\rm osc}$, the effect of bunching in phase vanishes, and the traditional weak-field collision model becomes applicable.

The peak widths in the electron distribution over the collision phase determine the spectral width of coherent radiation. The narrower the peaks in the distribution function, the broader the spectrum of coherent radiation (compare with Fig. 25 in Section 8). In accordance with the above, the number of peaks increases with an increase in the ratio $v_{\rm osc}/v_T$. The bunching, as expected, vanishes completely for $v_T > v_{\rm osc}$. A similar situation takes place in the case of circular polarization. In particular, it is precisely the electron bunching that the generation of coherent radiation is related to for a circular polarization of the pump field (see Section 8). As far as the authors know, this is the only mechanism of coherent radiation generation in a CP field in a transparent plasma.

As regards the qualitative aspect of the bunching effect, a remark is in order. Since the electron scattering angle in each transit depends on its velocity, which in turn depends on the field phase at the instant of closest electron approach to the ion, the energy exchange efficiency, which is determined by the field phase at the instant of collision (the last passage near the ion), depends entirely on the field phase. In essence, herein lies the mechanism of electron separation for the field phases. It has the result that almost all electrons arrive at the ion in specific phases of the external field! This is the effect of phase bunching.

7. Attraction with the inclusion of correlations

The data of numerical simulations outlined in Section 6 may be interpreted proceeding from relatively simple analytical considerations. Specifically, in a strong field (81), the oscillation radius

$$r_{\rm osc} = \frac{1}{\Omega^2} \underset{\Omega\to 0}{\longrightarrow} \infty$$

is quite broad, i.e., most of the time the electron travels away from the Coulomb center, describing a trajectory which oscillates under the action of the pump field. And only once or twice in a cycle can the electron approach the ion and scatter from it in a very short time $\sim b_v/v_{\rm osc} \ll 2\pi/\omega_0$. Accordingly, the electron drift trajectory is a broken line (see Fig. 6). In view of the shortness of the collision time in comparison with the cycle of the pump field, we mark out two time scales corresponding to (1) the instantaneous scattering by the Coulomb center during which the pump field is insignificant, and (2) the motion along the oscillating trajectory disregarding Coulomb attraction.[10] Herein lies the idea of the low-frequency approximation [31]. In the consideration of particle motion, however, the limitation on the number of electron–ion collisions (impacts) will not be imposed, while the model of Ref. [31] implies only a single collision. Moreover, all qualitatively new, unusual effects come out only with the inclusion of multiple collisions. No limitations are imposed on the particle trajectory, either, with the exception of the condition that the time taken by every particle to pass by the ion is much shorter than the field cycle, i.e., the condition for the instantaneous impact parameter is fulfilled:

$$\frac{\rho}{V} \ll \frac{2\pi}{\omega_0} \Longleftrightarrow \rho \ll r_{\rm osc}\,. \tag{84}$$

As earlier, here V is the velocity in the laboratory frame of reference (the total particle velocity).

It should be noted that the assumption of a single electron impact on the ion in the course of collision, which was used in Ref. [31], is equivalent to the straight-line trajectory approximation. The reason lies in the fact that the information about electron motion correlations in the transits past the ion during neighboring field cycles is lost in the single-impact approximation. The effective electron distribution over impact parameters thereby becomes uniform, for which the contribution from electrons scattered through large angles is logarithmically small.

To describe the system of interest in the framework of the low-frequency approximation, advantage is conveniently taken of a point map. The idea is that a discrete set of points $\zeta_n = \zeta(nT)$, where n is an integer, and T is some time interval, is singled out in a continuous trajectory $\zeta(t)$ (as before, $\zeta = \{\mathbf{r}, \mathbf{p}\}$ is the set of particle coordinates and momenta). The relation of the $(n+1)$th point to the nth point is described by a point map:

$$\zeta_{n+1} = \hat{M}[\zeta_n]\,, \text{ or } \bar{\zeta} = \hat{M}[\zeta]\,. \tag{85}$$

[10] The Coulomb attraction for slow particles, $v \leqslant \Omega$, away from the ion may be taken into account by employing the averaged potential (see Section 5).

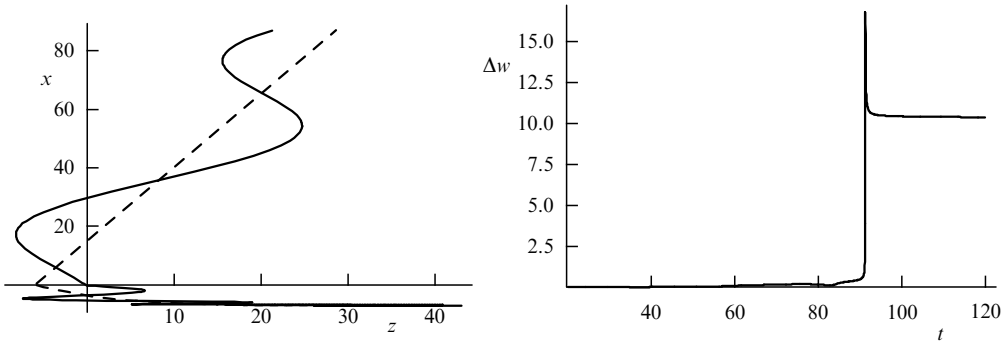

Figure 13. Trajectory of electron motion in a Coulomb field.

The symbol $\bar{\zeta}$ denotes the value of ζ obtained through iterations. For a periodic system, it is expedient to take the time interval T equal to the period $2\pi/\Omega$ of the external field.

In the parameter ranges defined by inequalities (81) and (84), the form of a point mapping (85) is considerably simplified. Condition (81) signifies that the oscillation radius $r_{\rm osc}$ is long, while condition (84) implies that the variation of parameters in every transit occurs quickly on the scales of an oscillation cycle (Fig. 13). In this case, as noted above, two time scales may be marked out: the slow electron oscillation scale, and the fast scale for electron parameter variation in an impact. Assuming that the latter scale is very short (an instantaneous impact), advantage can be taken of the exact solution to the Kepler problem [36], writing down a point mapping through a period in the dimensionless form:

$$\mathbf{r}_{n+1} = \mathbf{r}_n + \mathbf{v}_n t_{\rm c} + \mathbf{v}_{n+1}(T - t_{\rm c})\,, \qquad \mathbf{v}_{n+1} = \mathbf{v}_n - 2\,\frac{V^3\boldsymbol{\rho} + \mathbf{V}}{1+\rho^2 V^4}\,, \tag{86}$$

where $\mathbf{V} = \mathbf{v}_n + \mathbf{v}_{\rm osc}(t_{\rm c})$ and $\mathbf{R} = \mathbf{r}_n + \mathbf{r}_{\rm osc}(t_{\rm c})$ are the particle velocity and coordinate in the laboratory frame of reference at the instant of impact $t_{\rm c}$, and $\boldsymbol{\rho} \equiv \mathbf{R} - \mathbf{V}(\mathbf{R},\mathbf{V})/|V|^2$ is the instantaneous impact parameter.

When a particle experiences two 'collisions' with the ion during a field cycle, the resultant map may be represented as the sequential exercise of two mappings (86) with the instants of collisions taken from the first and second half-cycles, respectively. In view of the previous remark, we are dealing with the mapping in a half-cycle π/Ω for linear polarization of a field. Therefore, the 'period' may be written down as

$$T = \frac{\alpha\pi}{\Omega}\,, \quad \alpha = \begin{cases} 1\,, & \text{for LP}\,, \\ 2\,, & \text{for CP}\,. \end{cases} \tag{87}$$

The mapping as in Eqn (86) is rather complicated in form, but even this one does not describe the entire particle scattering in the presence of a strong pump field. Indeed, the conditions for the construction of mapping (86) are violated at the stopping points ($V(t) \ll v_{\rm osc}$) and, generally speaking, use should be made of the trajectories from the scattering problem in the presence of a constant field [60], which are rather complex in and of themselves.

Despite its simple appearance, a point mapping (86) is quite complex, and its analysis calls for a special investigation. However, several properties of mapping (86) are easily found if the variations of the longitudinal coordinate and total momentum $V \approx v_{\rm osc}$ in the small parameter $v \ll v_{\rm osc}$ are ignored. This results in mapping for longitudinal coordinate ρ

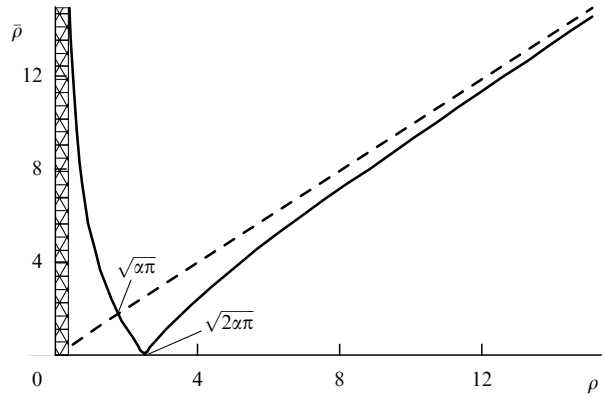

Figure 14. Dependence of the impact parameter $\bar{\rho}$ on the impact parameter ρ through an iteration of mapping (89). The domain of particle loss due to large-angle scattering is crosshatched.

and velocity $u = v_\perp/\Omega$:

$$\bar{\rho} = \rho + \alpha\pi\bar{u}\,, \qquad \bar{u} = u - \frac{2}{\rho} \tag{88}$$

with the generating function $S(\rho,\bar{u}) = \rho\bar{u} + \alpha\pi\bar{u}^2 + 2\ln\rho$.

By disregarding in expressions (88) the particle's shift across the electric field due to the drift velocity $u \ll 2\pi/\rho$ (this is most easily realized in the longitudinal scattering), mapping (88) may be represented in the form of mapping for the variation of only one variable — the local impact parameter $\rho \approx \sqrt{x^2+y^2}$:

$$\bar{\rho} = \left|\rho - \frac{2\alpha\pi}{\rho}\right|. \tag{89}$$

Recall that α is defined by formula (87). Mapping (89) is graphically shown in Fig. 14. Like mapping (86), mapping (89) does not describe the scattering of particles through large angles and their escape from the scattering region. To take into account these particles, a region of loss with an approximate width $b_{\rm osc} = \Omega^2 \to 0$ (the crosshatched domain in Fig. 14) may be introduced, so that particles are assumed to have departed from the scattering domain whenever they enter this region.

Let us consider the properties of mapping (89).

7.1 Multiflow state

First of all, we note the emergence of a multiple flux state (see Section 6), which comprises particles with different impact

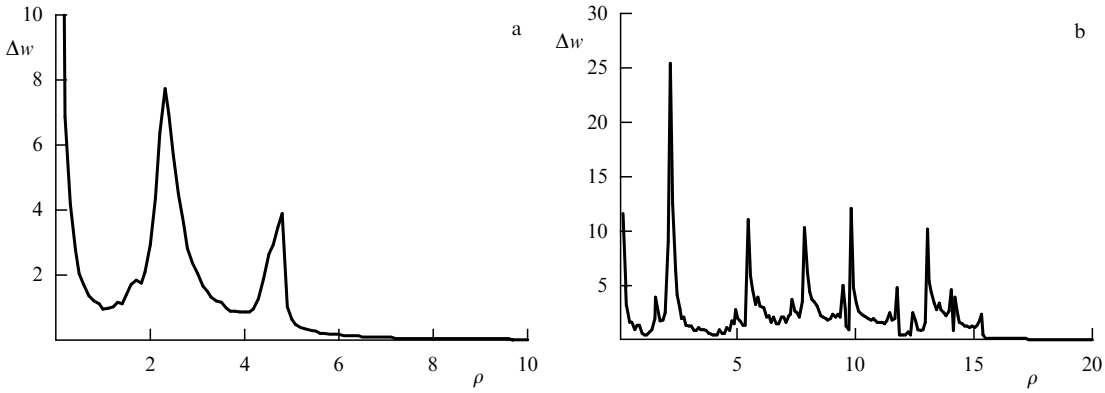

Figure 15. Energy variation Δw averaged over the initial phase as a function of the initial impact parameter ρ for an LP (longitudinal incidence) in panel (a) $\Omega = 0.32$, $v = 1$ and panel (b) $\Omega = 0.1$, $v = 1$.

parameters simultaneously arriving at the same point in space. Let us find the set of initial impact parameters ρ_{ini} whereby the particles enter the domain $\rho \leqslant b_{\text{osc}}$ and, accordingly, experience scattering through large angles, a strong energy change, etc.

The simplest case concerns the particles with small initial parameters $\rho_{\text{ini}} \leqslant b_{\text{osc}}$, i.e., the particles which would 'collide' with the ion in the absence of oscillations induced by the pump field. It is precisely these particles that are described by the small-angle approximation. Apart from them, there are particles that fly past the ion once, scatter through a small angle, and impact the ion on return (see Fig. 1). That is, particles that started moving with different impact parameters arrive at the same point in space. This is what we understand by a multiflow state. The impact parameter ρ_1 corresponding to these particles may be found from the equation

$$\rho_1 - \frac{2\alpha\pi}{\rho_1} = 0 \;\Rightarrow\; \rho_1 = \sqrt{2\alpha\pi}\,. \tag{90}$$

Such is the value of impact parameters in the first peak (compare Fig. 15 with Fig. 5).

Similarly, it is possible to find the values of the initial impact parameters $\rho_2,\ \rho_3, \ldots$ for the 2nd, 3rd, etc. peaks that appear after the 2nd, 3rd, etc. particle return to the ion. The total number of peaks N (or passages over the ion, which is the same thing) may be estimated by the formula

$$N \approx \frac{r_{\text{osc}}}{vT} = \frac{v_{\text{osc}}}{\alpha v}\,. \tag{91}$$

In this case, by analyzing mapping (88) it is possible to obtain the coordinate of the last peak, which is the boundary of the attraction range:

$$\rho_N \equiv \rho_{\text{attr}} \approx \sqrt{2\alpha\pi}\,\frac{v_{\text{osc}}}{v}\,r_E\,, \tag{92}$$

agreeing nicely with the data of numerical simulations (82). It should be noted that determining the location of distant peaks requires taking into account the transverse particle velocity u, i.e., analyzing a more complex mapping (88). Without the inclusion of transverse velocity variation, the coordinates of the peaks and, accordingly, the expression for the attraction boundary would be underrated (Fig. 16).

Estimate (92) may also be obtained in a simpler way. Let us assume that an electron has flown by the ion with a drift velocity v at a distance ρ and was scattered through a small angle $\delta\theta \approx 2/(\rho v)$. To appreciably change its energy, the electron should manage to collide with the ion in a path $2r_{\text{osc}}$. This may be done only by particles with impact parameters that satisfy the condition

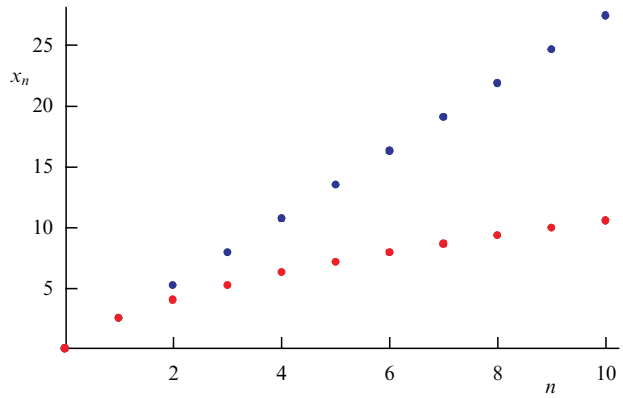

Figure 16. Coordinates of the peaks obtained in the framework of the simplest mapping (89) (lower points) and a more complex mapping (88) (upper points).

$$\rho \leqslant 2r_{\text{osc}}\,\delta\theta \;\Rightarrow\; \rho \leqslant \rho_{\text{attr}} = \frac{2}{\Omega v}\,. \tag{93}$$

Once again, we arrive at an estimate for the boundary of the attraction domain close to estimate (92).

The coordinates of the peaks ρ_n (see Fig. 15) possess one more interesting property: all particles with impact parameters $\rho \in [\rho_n, \rho_{n+1}]$ find themselves within a range $\bar{\rho} \in [\rho_{n-1}, \rho_n]$ after one pass over the ion. This signifies that all particles with impact parameters $\rho \leqslant \rho_{\text{attr}}$ find themselves in a domain $\rho_{\text{fin}} \leqslant \rho_1 = \sqrt{2\alpha\pi}$. Therefore, it is sufficient to consider the scattering of a particle beam with diameter $2\rho_1$ and concentration $n_{\text{eff}} \sim n_0\rho_{\text{attr}}^2/\rho_1^2$ instead of the initial scattering problem for an infinitely broad particle beam with concentration n_0. In the dense plasma case, the effective concentration may lower due to the screening of the ion's Coulomb potential for $\rho \geqslant r_{\text{D}}$ (the Debye radius $r_{\text{D}} = \omega_{\text{p}}/v_T$):

$$n_{\text{eff}} = n_0\,\frac{\min\,(r_{\text{D}}^2, \rho_{\text{attr}}^2)}{\rho_1^2}\,, \quad r_{\text{D}} \geqslant \rho_1\,. \tag{94}$$

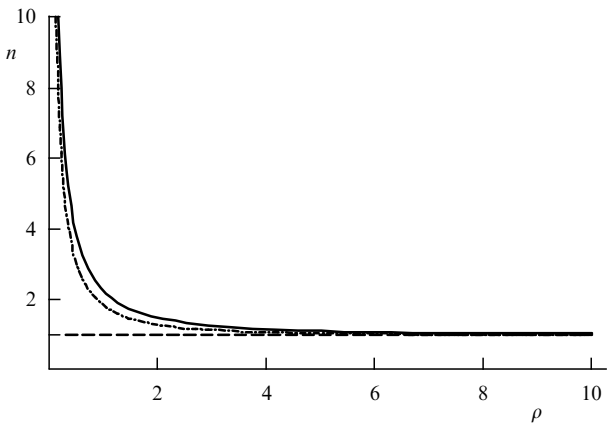

Figure 17. Dependence of the particle concentration on impact parameter ρ for the unperturbed distribution (dashed line), the distribution upon one iteration of mapping (89) (the dashed–dotted line), and the limiting curve after an infinite number of iterations (solid curve), which is the 'norm' of mapping (89).

It follows from formula (94), in particular, that all the effects involving the particle return to the ion upon scattering vanish when $r_{\mathrm{D}} < \rho_1 \approx 2.51 r_E$, while for $r_E \ll r_{\mathrm{D}} \leqslant \rho_{\mathrm{attr}}$ they turn out to be only weakened. In a sufficiently rarefied plasma, $r_{\mathrm{D}} > \rho_{\mathrm{attr}}$, all these effects will show up in full measure.

7.2 Singularity in the correlation function

Another important property of mapping (89) is the appearance of singularity in correlation function (8). As noted in Section 7.1, all particles with impact parameters $\rho \leqslant \rho_{\mathrm{attr}}$ are drawn to the domain $\rho \leqslant \rho_1$ in the course of scattering. It would be instructive to determine the particle distribution prior to the 'last' collision, i.e., in the range $[0, \rho_1]$. To answer this question, we find the variation of concentration (or of the spatial density of the correlation function, which is the same thing) through an iteration of mapping (89) from the particle number conservation law $\bar{n}\bar{\rho}\,\mathrm{d}\bar{\rho} = n\rho\,\mathrm{d}\rho$. Expressing from mapping (89) the old coordinate ρ in terms of the new one $\bar{\rho}$ and using the inequality $\rho > \rho_1$ (we consider particles which have not yet fallen into the $[0, \rho_1]$ domain) one finds (Fig. 17)

$$\bar{n}(\bar{\rho}) = n(\rho_+)\,\frac{\rho_+}{\bar{\rho}}\left|\frac{\mathrm{d}\rho_+}{\mathrm{d}\bar{\rho}}\right| + n(\rho_-)\,\frac{\rho_-}{\bar{\rho}}\left|\frac{\mathrm{d}\rho_-}{\mathrm{d}\bar{\rho}}\right|, \qquad \rho_\pm = \frac{1}{2}\left(\sqrt{\bar{\rho}^{\,2} + 8\alpha\pi} \pm \bar{\rho}\right). \tag{95}$$

In particular, for large impact parameters $\bar{\rho} \gg \sqrt{8\alpha\pi} = 2\rho_1$, the concentration is hardly changed, as would be expected. However, a concentration singularity appears at small impact parameters (compare with Fig. 9):

$$\bar{n} \underset{\bar{\rho} \ll \rho_1}{\simeq} n\,\frac{\rho_1}{2\bar{\rho}}\,. \tag{96}$$

Taking into account relation (94) leads to the formula for the particle distribution over impact parameters after N passages:[11]

$$n_{\mathrm{eff}} \simeq n_0\left(\frac{v_{\mathrm{osc}}}{v} + \frac{b}{\rho}\right) \underset{\rho \ll b}{\simeq} n_0\,\frac{b}{\rho}\,, \quad b = \frac{\rho_{\mathrm{attr}}^2}{2\rho_1}\,. \tag{97}$$

[11] Actually, it is also easy to find from expression (95) the invariant measure $n(\rho) = 1/\rho$ of mapping (89) — the particle distribution which passes into itself after a mapping step.

The appearance of the first term on the right-hand side of formula (97) is due to the fact that distant particles which did not manage to draw closer to the Coulomb center nevertheless experience about $N = v_{\mathrm{osc}}/v$ small-angle collisions during a passage near the ion. For such particles, the effective concentration for one collision with the ion will be of the form of a uniform concentration n_0 multiplied by the number of particle transits past the ion:

$$n_{\mathrm{eff}} \simeq n_0\,\frac{v_{\mathrm{osc}}}{v}\,.$$

Notice. The concentration (97) prior to the 'last' impact is, in essence, the Jacobian for the passage from the initial coordinates $\mathbf{r}_0$ to the coordinates $\mathbf{r}$ of the 'last' impact. In this passage, distant particles, evidently, are not perturbed by the Coulomb field of the ion. Accordingly, the Jacobian is equal to unity as $r \to \infty$. Attraction and bunching of the particles in the vicinity of the ion occur such that the distribution acquires singularity (96) every half-cycle of the field variation. Furthermore, every following cycle more particles experience collisions because of attraction than during the previous one. As a result, the Jacobian assumes the form

$$J(\mathbf{r}_1, \mathbf{r}_0) = 1 + \frac{\rho_1}{\rho}\sum_{n=1}^{2v_{\mathrm{osc}}/v} n\delta\left(\frac{\xi}{r_{\mathrm{a}}} - \frac{n}{2}\right).$$

In this case, the variation range of coordinate ξ is equal to $2r_{\mathrm{osc}}$, while the variation range of the initial coordinate ξ_0 is equal to r_{a} (since we are dealing with the scattering of one layer of thickness r_{a}). Subsequently, of interest will be the integral of the quantities taken over the normalized longitudinal coordinate ξ/r_{a}. The presence of delta functions in the expression for the Jacobian permits performing its integration easily. As a result, we arrive at expression (97) again.

Notice that the particle concentration should be constant when the small-angle approximation is applicable. According to both numerical simulations and analytical estimates (97), the surface density increases as $1/\rho$ for short ρ, which confirms once again the necessity of taking into account the bending of particle trajectories in the scattering.

For a known particle distribution prior to the last 'impact', the use of mapping (86) for the last impact permits finding all scattering characteristics, which will be done in the following sections.

7.3 Stochastic dynamics

The third important property of mapping (89) is the appearance of stochastic dynamics. As noted in Section 6, the dynamics of particle scattering in a strong pump field turn out to be quite complex, stochastic. The same fact is demonstrated by mapping (89). Really, on the one hand, it is globally attractive. On the other hand, the central part of the mapping is locally unstable. This results in particle mixing. This is one of the criteria for stochastic dynamics. In this case, the Coulomb center plays the role of a complex stochastic attractor.

The unusualness of the Coulomb attractor consists in permanent loss of particles due to large-angle scattering. The particles that find their way to the close vicinity of the ion due to attraction in the course of multiple oscillations (for regular dynamics) or due to Arnol'd diffusion (stochastic particle walk in the case of stochastic dynamics) experience large-

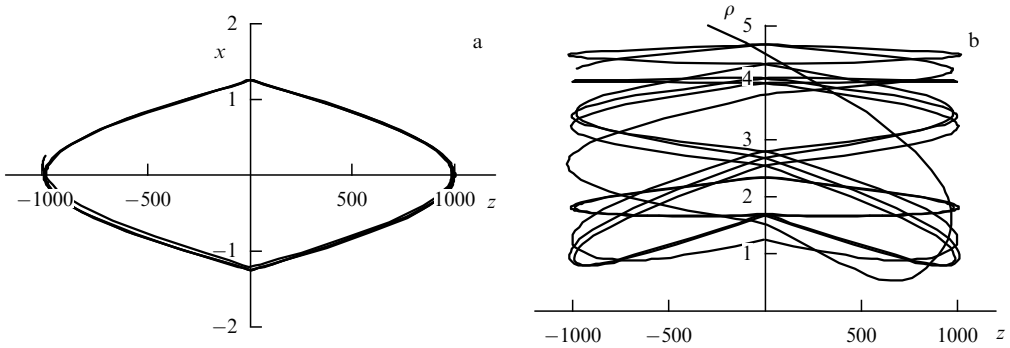

Figure 18. (a) Simplest trajectory of a stationary point $\rho_1^{(1)}$ at $\Omega = 0.0316$. (b) Example of a trajectory 'captured' by the Coulomb attractor.

angle scattering and acquire velocities comparable to the oscillatory one. As a result, these particles, on the one hand, escape from the attractor domain and, on the other, make a contribution to the collisional current and, accordingly, to coherent radiation. Because particles in the scattering through large angles acquire velocities opposed to the instantaneous oscillatory velocity, one would expect the emergence of intensive generation of collisional current (see Section 8.1) and, therefore, of coherent radiation which enhances with the broadening of the stochasticity domain, i.e., with an increase in pump field intensity.

Furthermore, an accumulation of particles in the attractor may take place (Fig. 18). In numerical simulations, this shows up in the appearance of a nonzero capture cross section. This effect corresponds to a so-called dynamic recombination in strong fields. The recombination cross section (or degree) increases with a decrease in flow rate, $v \to 0$, or in field frequency, $\Omega \to 0$. We note that the appearance of particles captured by the potential signifies the necessity of going beyond the framework of binary electron–ion collisions and of including 'collisions' with 'neutral' atoms (i.e., of three-particle collisions). However, as long as the fraction of captured particles is small in comparison with the fraction of particles that make the dominant contribution to the effective cross section (it is precisely this that is demonstrated by numerical simulations), the binary collision approximation can be employed in describing the energy exchange processes.

Mapping (89) also has stationary points, which pass into themselves upon one or several iterations (a particle returns to these points after one or several passes over the ion). These points are easy to find analytically. For a point $\rho_1^{(1)}$, which passes into itself in one iteration (see Fig. 18), we have

$$2\rho_1^{(1)} = \frac{2\alpha\pi}{\rho_1^{(1)}} \Rightarrow \rho_1^{(1)} = \sqrt{\alpha\pi}\,. \tag{98}$$

For points $\rho_1^{(2)}$ and $\rho_2^{(2)}$, which go over into themselves in two iterations, we find

$$\begin{cases} \rho_1^{(2)} + \rho_2^{(2)} = \dfrac{2\alpha\pi}{\rho_1^{(2)}}\,, \\ \rho_1^{(2)} - \rho_2^{(2)} = \dfrac{2\alpha\pi}{\rho_2^{(2)}} \end{cases} \Rightarrow \begin{cases} \rho_1^{(2)} = \dfrac{\sqrt{2\alpha\pi}}{\sqrt{\sqrt{2}+1}}\,, \\ \rho_2^{(2)} = \sqrt{\alpha\pi}\sqrt{\sqrt{2}+1}\,, \end{cases} \tag{99}$$

etc. The trajectory corresponding to the stationary point $\rho_1^{(1)}$ is plotted in Fig. 18. The electron starts moving with a low drift velocity at point $-r_{\rm osc}$, passes over the ion, and scatters through a small angle with total velocity. After that the electron arrives at point $+r_{\rm osc}$ with a velocity opposite to the initial one. The motion reverses.

Unfortunately, all stationary mapping points turn out to be unstable. A small change in the initial conditions 'draws' a particle from the periodic trajectory. Nevertheless, according to the data of dedicated numerical calculations, the majority of particles remain 'trapped' for many field cycles (see Fig. 18). In actual truth, numerical calculations suggest that *all* particles escape from the scattering domain. But the fraction of particles that reside close to the ion longer than some time (for instance, longer than 20 oscillatory radius transit times, $t_{\rm pass} > 20 r_{\rm osc}/v$) rapidly increases with decreasing drift velocity v.

Therefore, we are dealing with a new quasistable electron state in an 'atom', which is realized only in the presence of a strong EM pump wave. This atom measures several r_E. In Ref. [61], such highly excited atoms were investigated in the context of the ionization problem in the field of a strong EM wave. It is likely that the existence of such states may appreciably lower the ionization rate in superstrong low-frequency ($\Omega \ll 1$) fields and favor an increase in the generation of coherent radiation based on the Corkum effect [62] — the radiation emitted in the scattering of the electron which returns to the ion immediately after its detachment (ionization). Recent experimental and analytical investigations into the Corkum effect [63] bear out the importance of accounting for electron returns to the ion.

7.4 Features of transverse scattering

In the general case of a particle incidence across the electric LP field ($\mathbf{v} \perp \mathbf{v}_{\rm osc}$), use should be made of a complete mapping (86) in determining the effective cross section. For a low velocity, $v \ll \Omega$ (or $b_v \geqslant r_{\rm osc} \gg b_{\rm osc}$), advantage can also be taken of simplified one-dimensional mapping (89). Accordingly, the results will be close to those described above. In the opposite limiting case, $b_{\rm osc} < b_v < r_{\rm osc}$, the particle dynamics is different; however, as before, determining the effective cross section calls for the inclusion of large-angle scattering.

To estimate the effective cross section when $b_{\rm osc} < b_v < r_{\rm osc}$, we consider in greater detail particle scattering. Figure 19 depicts particles incident on the ion perpendicular to the field oscillating along the z-axis. The initial impact parameters ρ of the particles are approximately equal to the Rutherford radius $b_v \gg b_{\rm osc}$, so that the particles are scattered by the immobile ion [12] with an angular variation of the drift velocity by more than $\pi/2$.

[12] A case in point is motion near the stopping points, where the ion is practically immobile for a greater part of the period [60].

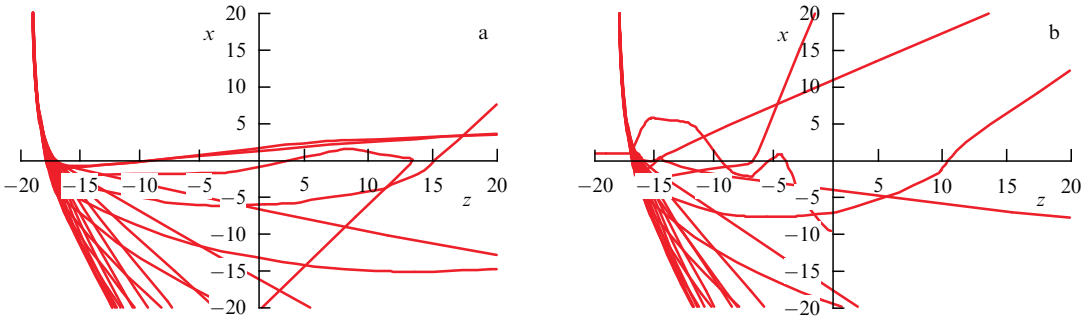

Figure 19. Set of drift trajectories for particles with different initial phases, which fly (a) at the boundary of and (b) inside the attraction domain. Particle parameters are $\Omega = 0.25$, and $v = 0.5$. Transverse beam incidence in a LP field.

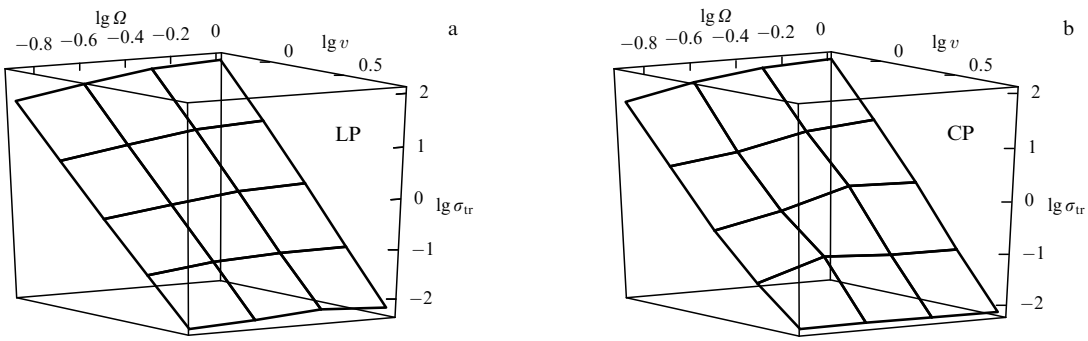

Figure 20. Logarithm of the transport cross section $\sigma_{\rm tr}$ as a function of velocity v and frequency Ω for LP (a) and CP (b) pump fields.

After the first collision, which changes the particle energy only slightly, the particles move along a straight line and travel a distance of about $\pi r_{\rm a} = \pi v/\Omega$ during a half-cycle. In a cycle, the particle collides at point $z = r_{\rm osc} - \pi r_{\rm a}$ with the 'returning' ion, which has velocity $v_* = \sqrt{2\pi v v_{\rm osc}} \gg v$. A second collision occurs, which changes the particle energy to a value on the order of $v_*^2 \simeq 2\pi v_{\rm osc} v$. Notice that by the second collision the particles, in fact, find themselves in the longitudinal scattering mode described in Section 7.1, since the transverse velocity of such particles is low. This also signifies that a particle may actually experience many collisions, rather than one, prior to changing its energy significantly and leaving the scattering domain (see Fig. 19).

It is worthy of note, however, that such energy variation is not acquired by all particles but only those which reach the ion neighborhood of $b_* = 1/v_*^2$ in the second collision. On the strength of condition $b_* \ll b_v$, this is possible only for particles from a region of width b_*. This permits estimating the effective cross section as the product of the area $b_v b_*$ from which the particles are collected and the relative change in their energy $2\pi v v_{\rm osc}/v_{\rm osc}^2$:

$$\sigma_{\rm eff} = \frac{2\pi v v_{\rm osc}}{v_{\rm osc}^2}\, b_v b_* = 2\pi b_v b_{\rm osc}\,. \qquad (100)$$

Numerical integration in the case of transverse beam incidence yields precisely the same result.

8. Collision cross sections. Radiation emission in collisions

We now turn to a discussion of the period-averaged moments of the collision operator: the transport ($\sigma_{\rm tr}$) and effective ($\sigma_{\rm eff}$) cross sections.

First, we consider the transport cross section $\sigma_{\rm tr}$ (30), responsible for the directional variation of electron momentum in the scattering from an ion. Figure 20 shows the transport cross section on a log-log scale obtained by numerical integration for a linearly and circularly polarized pump field [38, 39]. One can see from the drawing that the transport cross section is hardly affected by an external field. An exception is provided by the domain $v \simeq v_{\rm osc}$, in which the transport cross section increases due to a significant contribution from the *stopping points* — the points at which the total electron velocity $\mathbf{V} = \mathbf{v} + \mathbf{v}_{\rm osc}$ is close to zero. For a high thermal velocity $v \gg v_{\rm osc}$, the cross section $\sigma_{\rm tr}$ is close to the zero-field value, since the effect of the pump field may be ignored in this case. For low velocities $v \ll v_{\rm osc}$, the cross section is proportional to $1/v^4$ again, since the main contribution to the cross section is made by distant particles, for which the effect of an external field on their trajectories is also weak. Therefore, numerical calculations suggest the following approximation for the transport cross section:

$$\sigma_{\rm tr} \approx \frac{4\pi\Lambda}{v^4}\,, \qquad v \ll v_{\rm osc} \quad \text{and} \quad v \gg v_{\rm osc} \qquad (101)$$

(where Λ is a logarithmic factor), which applies to both linearly and circularly polarized pump waves. Formula (101) is supposedly true for an arbitrarily polarized pump wave as well.

We now turn to a discussion of the more important effective cross section (23), which characterizes the energy exchange between electrons and the pump field. Plotted in Fig. 21 is the quantity $\lg|\sigma_{\rm eff}|$ in relation to the logarithm of velocity v and frequency Ω. First, we consider the case of linear field polarization (Fig. 21a).

For high velocities $v \gg v_{\rm osc}$, the dependence of the effective cross section on velocity v and frequency Ω is

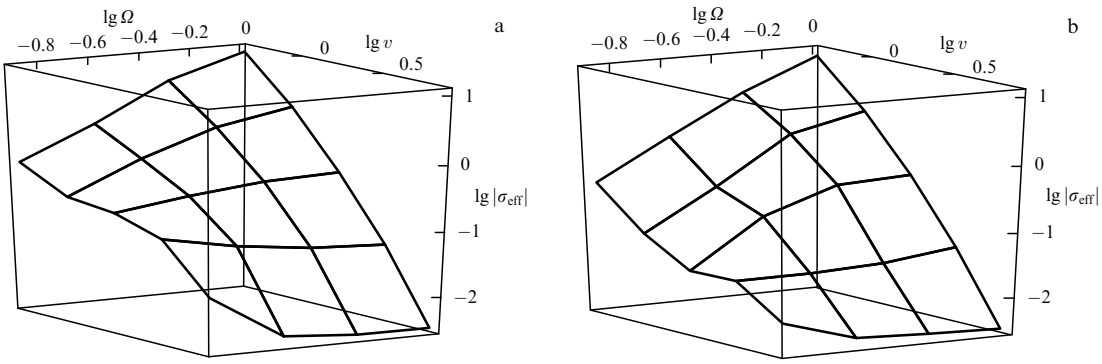

Figure 21. Logarithm of the modulus of the effective cross section σ_{eff} as a function of velocity v and frequency Ω for a pump field with linear (a) and circular (b) polarizations.

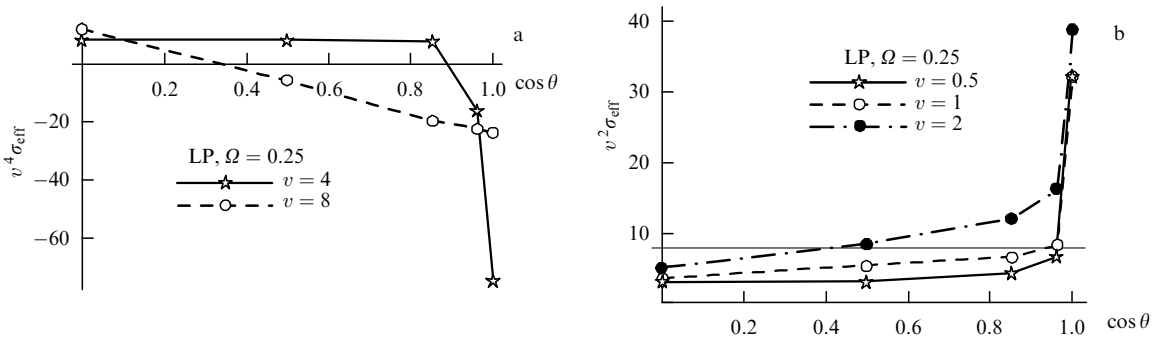

Figure 22. Effective cross section σ_{eff} as a function of angle θ for an LP pump field under the conditions $v \geqslant v_{\text{osc}}$ (a) and $v \ll v_{\text{osc}}$ (b) at $\Omega = 0.25$.

approximated by the formula

$$\sigma_{\text{eff}} \approx \frac{4\pi\Lambda}{v^4} \Leftrightarrow \nu_{\text{eff}} \approx \frac{\Lambda}{v^3}\,, \quad v \gg v_{\text{osc}}\,, \tag{102}$$

which is similar to the formula which is derived in the framework of the small-angle approximation [3–5, 33]. This is due to the fact that the main contribution to the integral for σ_{eff} in this case is made by distant small-angle collisions ($r_{\text{a}} \gg b_v$). Consequently, the transport and effective cross sections should be of the same order of magnitude, which is numerically borne out. The dependence of the cross section σ_{eff} on angle θ (Fig. 22a) is also in good agreement with the small-angle approximation:

$$\sigma_{\text{eff}} \approx 2 - 3\cos^2\theta\,, \quad v \gg v_{\text{osc}}\,. \tag{103}$$

In the strong-field domain, $v \ll v_{\text{osc}}$ and $v > \Omega$, numerical integration yields an estimate for the effective cross section in the form

$$\sigma_{\text{eff}} \approx \frac{\Omega^2}{v^2} = b_v b_{\text{osc}} \;\Leftrightarrow\; \nu_{\text{eff}} \approx \frac{1}{v v_{\text{osc}}^2}\,, \quad v \ll v_{\text{osc}}\,. \tag{104}$$

We note that ν_{eff} is $v_{\text{osc}}/v \gg 1$ times higher than the collision frequency obtained in the generalization of the small-angle approximation to the strong field case [3, 13]:

$$\nu_{\text{trad}} \sim \frac{\Lambda}{v_{\text{osc}}^3}\,, \quad v \ll v_{\text{osc}}\,. \tag{105}$$

The reason for so strong a discrepancy between the data of numerical integration and traditional models is discussed in Section 6.

Furthermore, in the case of longitudinal ($\theta = 0$) particle incidence, the effective cross section considerably hightens:

$$\sigma_{\text{eff}} \approx \frac{1}{v^2}\,, \quad v \ll v_{\text{osc}}\,, \quad \theta = 0\,. \tag{106}$$

To state it in different terms, a strong anisotropy of σ_{eff} is observed (Fig. 22b), which vanishes at high frequencies. The central peak width $\delta\theta$ may be estimated as

$$\delta\theta \leqslant \sqrt{\frac{\sigma_{\text{eff}}}{\sigma_{\text{eff}}(\theta = 0)}} \approx \Omega \ll 1\,. \tag{107}$$

It is easily seen that the width $\delta\theta$ tends to zero upon increasing the pump field amplitude ($\Omega \to 0$).

Another feature of the effective cross section in the high-field domain is its positiveness for all angles θ [compare with formula (103)], which is due to the fact that the scattered electron energy is low in comparison with the oscillatory energy. As a consequence, energy-loss collisions decrease σ_{eff} only slightly. By contrast, energy-gain collisions [especially the not-small-angle ones (see Section 6)] substantially increase the effective cross section.

Similar dependences are obtained as well with the use of formula (97) for the effective particle density $n(\rho)$. Indeed, the particle energy change as a function of impact parameter ρ may be found from the formula

$$\Delta w = \frac{4v_{\text{osc}}^2}{1 + \rho^2/b_{\text{osc}}^2}\,, \tag{108}$$

which gives a one-to-one relationship between the particle energy change and the impact parameter ρ. In this case, it is assumed that the main contribution is only made by the last

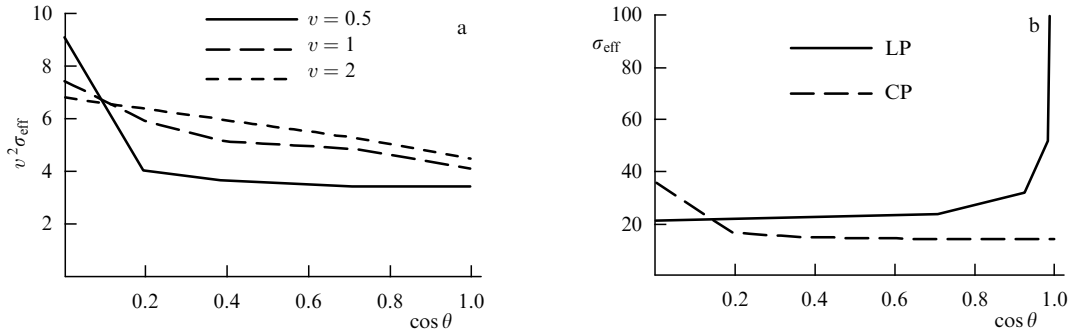

Figure 23. (a) Dependence of the effective cross section $\sigma_{\rm eff}$ on angle θ for a CP pump field when $v \ll v_{\rm osc}$ at different frequencies Ω. (b) Comparison of the angular dependences of $\sigma_{\rm eff}$ for linearly and circularly polarized pump fields at $\Omega = 0.25$ and $v = 0.5$.

impact (see Fig. 13) and that 'soft' impacts lead to only a variation of the spatial particle distribution. As a result, the cross section is found as the integral[13]

$$\sigma_{\rm eff} = \frac{2\pi}{v_{\rm osc}^2}\int_0^{r_{\rm a}} n(\rho)\rho\,{\rm d}\rho\,\frac{4v_{\rm osc}^2}{1+\rho^2/b_{\rm osc}^2} \underset{r_{\rm a}\gg b_{\rm osc}}{\simeq} 4\pi\,\frac{v_{\rm osc}}{v}\,b_{\rm osc}^2\Lambda + 4\pi^2 b b_{\rm osc} \underset{b\gg\sqrt{b_{\rm osc}b_v}\Lambda}{\approx} 4\pi^2 b b_{\rm osc}\,, \tag{109}$$

and the effective collision frequency is written out as

$$\nu_{\rm eff} = 4\pi v n_{\rm i}\sigma_{\rm eff} \simeq 4\pi n_{\rm i} v_{\rm osc} b_{\rm osc}^2\Lambda + 4\pi^2 n_{\rm i} v b b_{\rm osc} \underset{b\gg\sqrt{b_{\rm osc}b_v}\Lambda}{\approx} 4\pi^2 n_{\rm i} v b b_{\rm osc} \propto \frac{1}{v v_{\rm osc}^2}\,. \tag{110}$$

Here, $b = 1/\Omega^2 v^2$ for longitudinal particle incidence (97), and $b = b_v = 1/v^2$ for the transverse one (100).

Quantitatively similar results are also obtained for a CP pump field (Fig. 21b). Good agreement with the small-angle approximation (102) is again observed for high velocities $v \gg v_{\rm osc}$. For low velocities, the integral magnitude of the effective cross section is described by formula (104). However, the angular dependence $\sigma_{\rm eff}(\theta)$ is fundamentally different: tt is smoother (Fig. 23a), and the magnitude of $\sigma_{\rm eff}(\theta = \pi/2)$ for a CP is higher than for an LP. The two plots are compared in Fig. 23b. Again, as with an LP, the anisotropy of $\sigma_{\rm eff}$ vanishes with increasing frequency Ω.

So appreciable an increase in collision frequency (104) in strong fields in comparison with that in traditional (small-angle) models has the following implications: (1) the amount of energy acquired by the plasma due to collisions will not decrease with an increase in the pump field amplitude; (2) the rate of plasma heating

$$Q = \nu_{\rm eff}\,\frac{p_{\rm osc}^2}{2m} \sim \frac{1}{\sqrt{T}} \tag{111}$$

is defined only by the temperature and is independent of the pump field intensity. With the use of formula (104), it may be estimated that plasma heating to the oscillatory temperature proceeds 4–5 times faster than in the context of traditional models.

Radiation emission in collisions. Let us turn to a discussion of the results on integrating incoherent bremsstrahlung (31)

[13] In reality, the energy variation of particles with impact parameters $\rho \geqslant r_{\rm a}$ is exponentially small and, therefore, the integration should be restricted to the $\rho < r_{\rm a}$ domain.

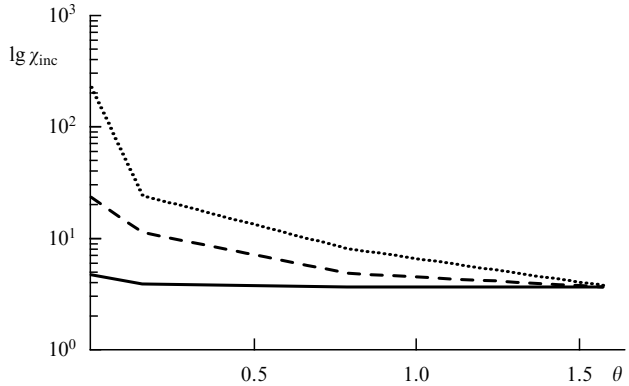

Figure 24. Dependence of the incoherent radiation cross section on the angle between the initial beam velocity and the field vector at $v = 1$ and different amplitudes of the pump wave: $\Omega = 1$ (weak field case) — solid curve, $\Omega = 0.316$ — dashed curve, and $\Omega = 0.1$ — dotted curve.

and collisional current (29), which is responsible for the coherent bremsstrahlung. We first consider the incoherent radiation. Numerical integration of formula (31) [40, 64] shows that complete (integrated over the incidence angle) incoherent radiation is, to logarithmic accuracy, independent of the pump field amplitude and is nicely approximated by the formula

$$\chi_{\rm inc} \approx \frac{\Lambda}{v^2}\,, \tag{112}$$

where Λ is a logarithmic factor, i.e., the formula of traditional weak-field models [49] remains valid. Here, the situation resembles that with the transport cross section (101), which also varies only slightly with increasing field amplitude. As with the transport cross section $\sigma_{\rm tr}$, a strong anisotropy of the emission cross section $\chi_{\rm inc}$ appears (Fig. 24). The radiation emission at longitudinal incidence ($\theta = 0$) may be approximated by the formula

$${\rm d}\chi_{\rm inc} \approx \frac{\Lambda}{\Omega^2 v^2}\,{\rm d}o\,. \tag{113}$$

In this case, the central peak width is again defined by formula (107).

Of considerably greater interest is the emergence of collisional current and coherent bremsstrahlung induced by it. First, we consider the LP case depicted in Fig. 25 on a logarithmic scale. For high velocities $v \geqslant v_{\rm osc}$, the collisional

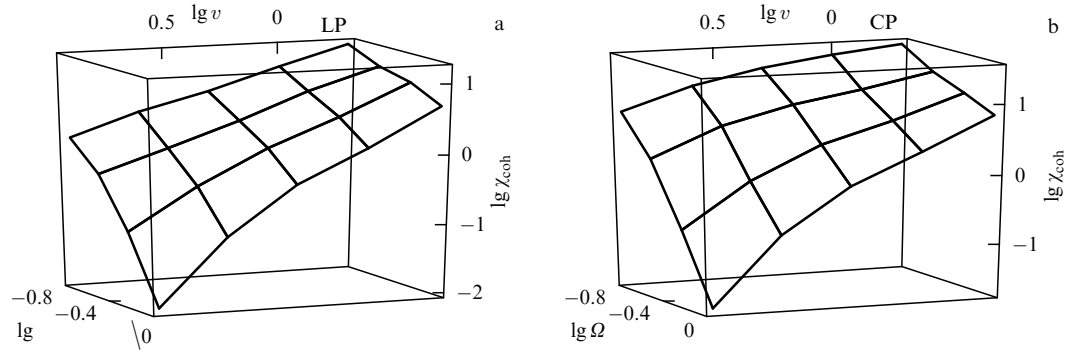

Figure 25. Dependence of the coherent emission cross section on velocity v and frequency Ω for linearly (a) and circularly (b) polarized pump fields.

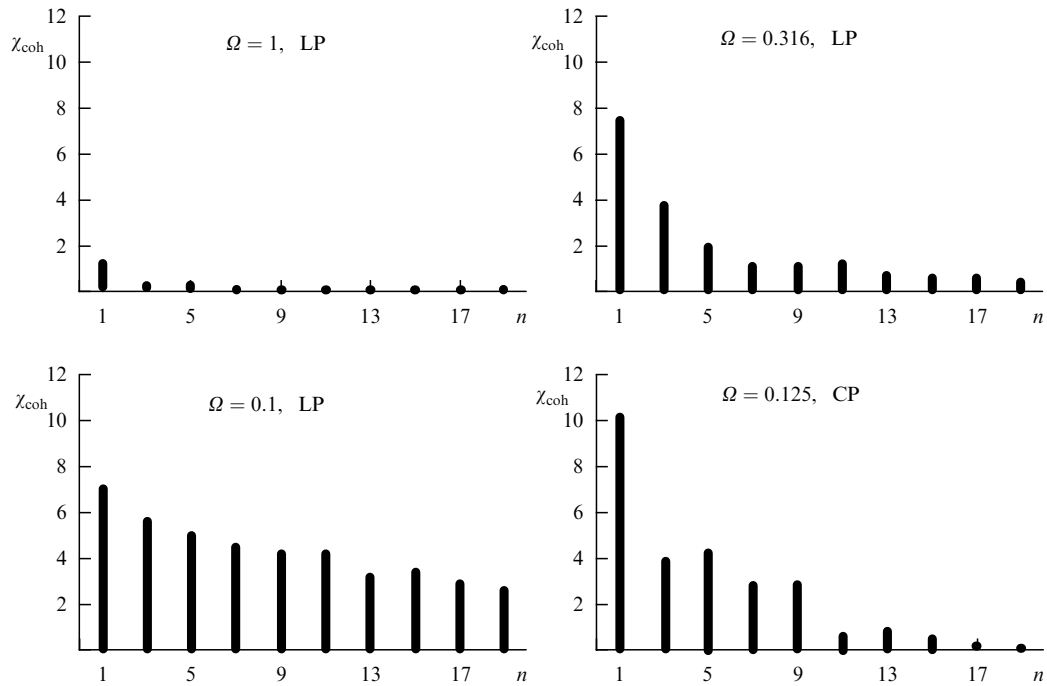

Figure 26. Coherent emission cross section as a function of the harmonic number radiated at different frequencies of the pump field Ω at $v = 1$.

current is low, which is quite consistent with the assumption made in traditional models that the instants of electron–ion collisions are random (uncorrelated):

$$\chi_{\rm coh} = 0\,, \quad v \geqslant v_{\rm osc}\,. \tag{114}$$

In the strong-field domain, $v \ll v_{\rm osc}$, $r_{\rm a} > b_{\rm osc}$, numerical integration yields an estimate for $\chi_{\rm coh}$ in the form

$$\chi_{\rm coh} \sim \frac{1}{\Omega v n}\,. \tag{115}$$

The frequency spectrum displays a plateau with the number of harmonics of order $v_{\rm osc}/v$ (Fig. 26). As would be expected, coherent radiation vanishes completely when $v > v_{\rm osc}$. The presence of primarily the odd harmonics in the spectrum of the coherent current component is due to the fact that bunching is realized twice during one half-cycle near the maxima of total electron velocity (see Fig. 12). This signifies that during each bunching peak the electrons are scattered in the direction opposite to the instantaneous oscillatory velocity. Thus, in each cycle the collisional current is represented in the form of two peaks of opposite polarity shifted by a half-cycle.

In the case of a CP pump field, qualitatively and quantitatively similar effects are observed (see Fig. 25). For high velocities, again, the collisional current is not present (114). For low velocities, formula (115) is applicable, with the reservations made below it. The frequency spectrum also resembles the spectrum concerned in the LP case (see Fig. 26). We note that, to the authors' knowledge, this is the only mechanism of coherent radiation generation in plasma exposed to a circularly polarized pump field.

9. Particle acceleration in collisions

Collisions are responsible not only for background plasma heating and radiation emission, but also for the emergence of fast particles. In the nonrelativistic case, the highest particle momentum is limited by a value of $2p_{\rm osc} = 2mca$. (Introduced here is the frequently exploited notation for the normalized

vector potential $a \equiv p_{\rm osc}/(mc) = eA/(mc^2)$.) However, ionization [65] in relativistically strong fields ($a \gg 1$) may give rise to particles with momenta on the order of $p_{\rm osc}^2/(mc) = mca^2$. This brings up the question: what is the highest energy which a particle with a kinematic momentum equal to the oscillatory one may acquire after an instantaneous elastic collision?

The answer is trivially obtained from formulas for charged particle motion in the field of a plane monochromatic EM wave [49]:

$$\mathbf{p}_\perp = \mathbf{q} + \mathbf{p}_{\rm osc}\,, \quad p_\parallel = \frac{p_0^2 + q^2 + 2\mathbf{q}\mathbf{p}_{\rm osc} + p_{\rm osc}^2}{2\alpha} - \frac{\alpha}{2}\,, \quad (116)$$

where $p_0 = mc$ is the rest momentum, $\mathbf{q}$ and α are the integrals of motion, and $\mathbf{p}_\perp$ and $p_\parallel$ are the kinematic particle momenta along and across the wave vector in the laboratory frame of reference.

It is easy to obtain the answer to the question posed above by considering the stepwise change in the particle momentum ('injection' of a particle with new momenta) and *taking into account* conservation in the adiabatic approximation (see Section 9.2) of the phase-averaged momentum after passage of the wave packet. The highest after-collision energy corresponds to the 'production' of a particle with the initial momenta $p_\perp = 0$ and $p_\parallel = p_{\rm osc}$, which in turn corresponds to $\mathbf{q} = -\mathbf{p}_{\rm osc}$ and $\alpha \approx p_0^2/(2p_{\rm osc})$. The longitudinal momentum averaged over the phase of the wave (i.e., the drift one) is of the form

$$\langle p_\parallel \rangle \approx \frac{p_{\rm osc}^2 + \langle p_{\rm osc}^2 \rangle}{2\alpha} = \frac{p_{\rm osc}\big(p_{\rm osc}^2 + \langle p_{\rm osc}^2 \rangle\big)}{p_0^2}\,. \quad (117)$$

Expressing formula (117) in terms of a, i.e.

$$H_{\max} = c\langle p \rangle_{\max} \approx mc^2 a\big(a^2 + \langle a^2 \rangle\big) \sim 2mc^2 a^3\,,$$

allows understanding that the increase in highest energy is proportional to a^3 [66]. Interestingly, with increasing EM wave amplitude $p_{\rm osc}$ the energy threshold rises even faster than in the nonrelativistic case ($H_{\rm nonrel}^{\max} \leqslant 2p_{\rm osc}^2/p_0$).

Broadly speaking, we may whence obtain a rather unexpected result about the possibility that even stronger particle acceleration can occur in the field of an EM wave. Let a particle scatter (for instance, by an ion) and acquire a momentum $\mathbf{p}$. Then, using formulas (116) and (117), one finds that the phase-averaged momentum equals

$$\langle \mathbf{p}_\perp \rangle = \mathbf{q}\,, \quad \langle p_\parallel \rangle = p_\parallel - \frac{p_{\rm osc}^2 + 2\mathbf{q}\mathbf{p}_{\rm osc} - \langle p_{\rm osc}^2 \rangle}{2(p_\parallel - w)}\,. \quad (118)$$

The integrals of motion are $\mathbf{q} = \mathbf{p}_\perp - \mathbf{p}_{\rm osc}$ and $\alpha = w - p_\parallel$, and the energy $w = (p^2 + p_0^2)^{1/2}$. Taken for the value of $\mathbf{p}_{\rm osc}$ are the values of the oscillatory momentum at the instant of scattering.

By putting $\mathbf{p}_\perp = 0$ (the particle scattered along $\mathbf{k}$) and assuming that the momentum is high enough, $p \gg p_0$, we conclude that the average momentum (and, hence, the final particle energy) will be a^2 times higher than after scattering! This process may be termed a 'Coulomb accelerator'.

But here other points arise. To what degree does the phase-averaged momentum persist after passage of the wave packet, and what are the limits on energy increase? To provide answers to these questions, it is convenient to go over to canonical variables, in which the Hamiltonian of the problem is independent of the rapidly oscillating external field. In the nonrelativistic case, this frame of reference is termed the drift frame. We also adhere to this term in the general relativistic case.

9.1 Drift coordinates in a relativistically strong electromagnetic wave

The form of drift coordinates in the relativistic case and the transformation to them are nontrivial. For the initial Hamiltonian, we take that describing the free motion in the field of an electromagnetic wave packet in generalized coordinates (in this case, not only the customary canonical momenta $\mathbf{P}$ and coordinates $\mathbf{r}$ are the canonically conjugate coordinate and momentum, respectively, but so are the time ct and the energy Hc (see, for instance, Ref. [67])):

$$\mathcal{H} = \frac{\big(\mathbf{P} + \mathbf{p}_{\rm osc}(\mathbf{r}, t)\big)^2 + p_0^2 - H^2}{2p_0}\,. \quad (119)$$

The role of time for this generalized Hamiltonian is played by parameter s — the 'intrinsic' time — so that the equations of motion take on the form

$$\frac{\mathrm{d}\mathbf{r}}{\mathrm{d}s} = \frac{\partial \mathcal{H}}{\partial \mathbf{P}}\,, \quad \frac{\mathrm{d}\mathbf{P}}{\mathrm{d}s} = -\frac{\partial \mathcal{H}}{\partial \mathbf{r}}\,,$$
$$\frac{\mathrm{d}t}{\mathrm{d}s} = \frac{\partial \mathcal{H}}{\partial H}\,, \quad \frac{\mathrm{d}H}{\mathrm{d}s} = -\frac{\partial \mathcal{H}}{\partial t}\,.$$

Whence follows, in particular, that the quantity $H = -[(\mathbf{P} + \mathbf{p}_{\rm osc})^2 + p_0^2]^{1/2}/p_0$ is negative for increasing time: $\mathrm{d}t/\mathrm{d}s = -H/p_0 > 0$. We note that the employment of generalized coordinates [49, 67] made it possible to represent the Hamiltonian in a simple quadratic form without using cumbersome square-root dependences. The Hamiltonian $\mathcal{H}$ possesses an important property: it is identically equal to zero in the trajectory of motion. Indeed, Hamiltonian $\mathcal{H}$ is constant, since it does not depend explicitly on parameter s; furthermore, this constant is equal to zero on the strength of the expression for the particle energy in the relativistic case.

Transformation to the drift coordinates requires performing a canonical transformation to eliminate the explicit dependence on the fast phase from the free-motion Hamiltonian $\mathcal{H}$. In this case, the free motion itself in drift coordinates in the field of a plane uniform EM wave should be a straight line with particle momentum conservation. In the general form, the generating function of this transformation may be found by solving the Hamilton–Jacobi equation for our Hamiltonian and the intrinsic time s. Actually, this problem has long been solved [49]. However, since we are also concerned with nonadiabatic corrections, we outline the requisite calculations and slightly modify the procedure. To this end, let us choose the system of coordinates in which the x-axis is aligned with the wave vector $\mathbf{k}$ of the EM wave. In this laboratory reference system, the Hamiltonian assumes the form

$$2p_0\mathcal{H} = \big(\mathbf{P}_\perp + \mathbf{p}_{\rm osc}(x - t)\big)^2 + P_x^2 + p_0^2 - H^2\,, \quad (120)$$

where the time coordinate ct is denoted, as before, by t for brevity.

In the co-moving frame of reference $\{\xi, \eta\}$ with

$$\xi = x - t\,, \quad \eta = x + t\,, \quad P_x = P_\xi + P_\eta\,, \quad H = P_\eta - P_\xi\,,$$

the Hamiltonian may be written out as[14]

$$2p_0\mathcal{H} = \left(\mathbf{P}_\perp + \mathbf{p}_{\rm osc}(\xi)\right)^2 + p_0^2 + 4P_\xi P_\eta \,. \tag{121}$$

Next, performing a canonical transformation with the use of the generating function

$$F = \bar{\mathbf{p}}_\perp\left(\mathbf{r}_\perp - \mathbf{r}_{\rm osc}(\xi,\bar{p}_\eta)\right) + \bar{p}_\eta\eta + \bar{p}_\xi\xi - \int\frac{p_{\rm osc}^2 - \langle p_{\rm osc}^2\rangle}{4\bar{p}_\eta}\,{\rm d}\xi \tag{122}$$

(the angle brackets imply averaging over coordinate ξ, i.e., over the wave phase) and taking into consideration the definition

$$r_{\rm osc} = \int\frac{p_{\rm osc}}{2P_\eta}\,{\rm d}\xi\,, \tag{123}$$

one obtains the change of variables in the form

$$\begin{aligned}
&\bar{\mathbf{p}}_\perp = \mathbf{P}_\perp\,, \quad \bar{\mathbf{r}}_\perp = \mathbf{r}_\perp - \mathbf{r}_{\rm osc}\,, \quad \bar{p}_\eta = P_\eta\,,\\
&\bar{\eta} = \eta + \frac{1}{4p_\eta^2}\int\left(p_{\rm osc}^2 + 2\mathbf{p}_\perp\mathbf{p}_{\rm osc} - \langle p_{\rm osc}^2\rangle\right){\rm d}\xi\,,\\
&\bar{p}_\xi = P_\xi - \frac{p_{\rm osc}^2 + 2\mathbf{p}_\perp\mathbf{p}_{\rm osc} - \langle p_{\rm osc}^2\rangle}{4p_\eta}\,, \quad \bar{\xi} = \xi\,.
\end{aligned} \tag{124}$$

Then, the coordinate-independent Hamiltonian assumes the form

$$2p_0\mathcal{H} = p_\perp^2 + p_0^2 + \langle p_{\rm osc}^2\rangle + 4p_\xi p_\eta\,. \tag{125}$$

It is noteworthy that the canonical transformation made using expressions (122) and (123) may be performed for an *arbitrary* (not necessarily harmonic) dependence of the vector potential $\mathbf{A} = -c\mathbf{p}_{\rm osc}/e$ on the coordinate ξ.

Finally, reverting to the usual coordinates x, t allows obtaining the relationship between the momenta $\mathbf{p}$ and $\mathbf{P}$, respectively, in the drift and laboratory systems of coordinates, as well as the expression for Hamiltonian [66]:

$$\mathbf{p}_\perp = \mathbf{P}_\perp\,, \quad p_x = P_x - \frac{p_{\rm osc}^2 + 2\mathbf{p}_\perp\mathbf{p}_{\rm osc} - \langle p_{\rm osc}^2\rangle}{2(p_x + h)}\,, \tag{126}$$

$$\mathcal{H} = \frac{p_\perp^2 + p_x^2 + p_0^2 + \langle p_{\rm osc}^2\rangle - h^2}{2p_0}\,. \tag{127}$$

Here, we purposefully singled out the term $\langle p_{\rm osc}^2\rangle$, which conforms to the effective particle 'making heavier' in relativistically strong fields. This term may smoothly depend on coordinates, which corresponds to the appearance of a pondermotive potential. Notice that expressions (126) for the drift momenta coincide with the kinematic momenta (118) *averaged over the wave phase* (recall that the drift 'energy' h is negative).

It should be noted that several interesting features of the drift coordinates show their worth in the relativistic limit, in which the amplitude of oscillations in the coordinate and momentum, unlike that in the nonrelativistic limit, depends significantly on the particle energy. This is easily seen from expression (123), because in the general case p_η is defined by the particle energy, and not only by its rest mass. Furthermore, the real particle time $t(s)$ flows nonuniformly due to the periodic change of the particle momentum in the external field. Thus, the 'drift' (uniform) time turns out to be different for different oscillating particles. This signifies that there is no way of introducing, as is done in the nonrelativistic case, a drift system of coordinates in the universal (laboratory, real) time t for all particles.

For a particle traveling in the field of only one wave, Hamiltonian (127) may be presented in a more familiar form $h = -(p^2 + p_0^2 + \langle p_{\rm osc}^2\rangle)^{1/2}$, with momentum h expressed explicitly. Recall that any canonical variable (most often momentum) expressed as a function of the remaining canonical variables may fulfill the function of the Hamiltonian. This form of Hamiltonian is encountered in many papers on the averaged description of particle motion in a wave field (see, for instance, Refs [65, 68] and references cited therein). The appearance of an additional potential $\mathcal{V}$ (for instance, of the Coulomb potential of an ion) in the equation will complicate the form of the Hamiltonian (127):

$$\begin{aligned}
\mathcal{H} = {}& \frac{p_\perp^2 + p_x^2 + p_0^2 + \langle p_{\rm osc}^2\rangle - h^2}{2p_0} + \frac{2h\mathcal{V} - \mathcal{V}^2}{2p_0}\\
&+ \mathcal{V}\,\frac{p_{\rm osc}^2 + 2\mathbf{p}_\perp\mathbf{p}_{\rm osc} - \langle p_{\rm osc}^2\rangle}{2p_0(p_x + h)}\,,
\end{aligned} \tag{128}$$

and will not permit writing down the Hamiltonian in a familiar form, because expressing momentum h becomes much more difficult. On the other hand, the use of generalized Hamiltonian (128) in numerical simulations permits eliminating errors in the determination of the drift momentum, when calculating relativistic particle collisions [69].

9.2 Adiabaticity conditions

Another difference between our proposed approach and the averaged description is the possibility of considering the field of a wave packet and not only of a plane monochromatic wave. As noted in Section 9.1, formulas (126) and (127) remain invariant in the presence of an arbitrary dependence on the 'longitudinal' coordinate ξ. Introduction of an additional dependence on the remaining coordinates will lead to the emergence of oscillating terms in the drift momentum $p_{\perp,\eta} = P_{\perp,\eta} - \delta p_{\perp,\eta}$ and in the Hamiltonian

$$\begin{aligned}
\mathcal{H} = {}& \frac{p_\perp^2 + p_x^2 + p_0^2 + \langle p_{\rm osc}^2\rangle - h^2}{2p_0} + \delta p_\eta\,\frac{p_x - h + 2\mathcal{U}}{p_0}\\
&+ \delta\mathbf{p}_\perp\,\frac{2\mathbf{p}_\perp - 2\mathbf{p}_{\rm osc} + \delta\mathbf{p}_\perp}{2p_0}\,,
\end{aligned} \tag{129}$$

where

$$\delta p_i = \int\frac{\partial\mathcal{U}}{\partial r_i}\,{\rm d}\xi\,, \quad \mathcal{U} = \frac{2\mathbf{p}_\perp\mathbf{p}_{\rm osc} + p_{\rm osc}^2 - \langle p_{\rm osc}^2\rangle}{4p_\eta}\,. \tag{130}$$

These terms are small in comparison with the radiation wavelength in the case of a smooth dependence on transverse coordinates, which permits evaluating the nonadiabatic corrections to the averaged description in the framework of the perturbation theory. Moreover, if it turns out that these corrections are insignificant, we will be able to continue the chain of canonical transformations and find second-order corrections to the drift Hamiltonian, etc. [70].

The conditions for the adiabatic approximation in the particle's motion in a wave packet are also easily found

[14] This is a canonical change of variables with the generating function $F_\xi = \bar{\mathbf{p}}_\perp\mathbf{r}_\perp + \bar{p}_\xi(x - t) + \bar{p}_\eta(x + t)$.

from general considerations. Specifically, the variation of momenta will be adiabatically (exponentially) small when the intrinsic time of traversing the packet along coordinates $\mathbf{r}_\perp, \eta$ is much longer than the intrinsic transit time of a field cycle. These times are easy to estimate: $s_0 = \lambda/v_\xi$ is the intrinsic transit time of a field cycle, while $s_1 = L_\perp/v_\perp$ and $s_2 = L_\parallel/v_\eta$ are the intrinsic transit times along the transverse and 'longitudinal' coordinates. The transit velocities in intrinsic time are defined by standard formulas $\mathrm{d}r_i/\mathrm{d}s = v_i = \partial\mathcal{H}/\partial p_i$ and assume the form [as follows from formula (125)]

$$v_\perp = \frac{p_\perp}{p_0} \approx a\,, \quad v_\xi = \frac{2p_\eta}{p_0}\,, \quad v_\eta = \frac{2p_\xi}{p_0}\,.$$

We additionally take into account the relationship between momenta $p_{\max} \approx p_\xi \approx p_{\mathrm{osc}}^2/p_\eta \gg p_0$ for the ultrarelativistic case and write the adiabaticity conditions in the following simple form [66]:

$$p_{\max} \ll \frac{2L_\perp}{\lambda}\, p_{\mathrm{osc}}\,, \quad p_{\max} \ll \sqrt{\frac{L_\parallel}{\lambda}}\, p_{\mathrm{osc}}\,. \tag{131}$$

These are essentially the same conditions which were earlier given by other authors [65], though expressed in terms of the maximum particle momentum.

The physical meaning of conditions (131) is rather clear. An ultrafast particle travels almost together with the wave, and due to the relativistic time dilation it needs a longer intrinsic time to transit the field oscillations than it does in the nonrelativistic case. Meanwhile, the particle escape across the packet is as quick as in the nonrelativistic case. This is precisely the reason why the ordinary nonrelativistic adiabaticity condition $L_\perp, L_\parallel \gg \lambda$ is replaced by condition (131), which contains the particle momentum. Similarly it is possible to obtain the conditions for adiabaticity violation in the propagation of a wave packet through a medium (plasma, for instance). In this case, the limitation actually consists in the fact that the particle velocity may not exceed the wave group velocity.

9.3 Energy change during a prompt impact

We write out the energy relations in the sharp stepwise variation of the total particle momentum due to an elastic collision. Let the kinematic particle momentum prior to the collision be equal to $\{h, \mathbf{p}\}$ in the laboratory frame of reference and let the momentum immediately after (on the scale of the field cycle) the collision be $\{h, \mathbf{p} + \delta\mathbf{p}\}$. As an important example of such collisions, we refer to electron–ion collisions disregarding ion momentum variation (an infinitely heavy ion). As is well known, the energies of particles are conserved in their scattering by the ion Coulomb potential in the absence of external fields [49]. This follows directly from the stationarity of the corresponding Hamiltonian of the particle interaction.

Let us find the variation of the particle drift momentum $\Delta\mathbf{p}$. The variation of transverse drift momentum of the particle is precisely $\Delta\mathbf{p}_\perp = \delta\mathbf{p}_\perp$. Furthermore, since p_η is not transformed in switching to the drift coordinates, we obtain

$$\Delta p_\eta = \frac{\delta p_x}{2} = \frac{\Delta p_x + \Delta h}{2}\,.$$

The variation of the remaining momentum component $\Delta p_\xi = (\Delta p_x - \Delta h)/2$ should be expressed with consideration for formulas (124) describing the transition to drift coordinates:

$$\Delta p_\xi = \frac{\delta p_x}{2} - \frac{p_{\mathrm{osc}}^2 + 2(\mathbf{p}_\perp + \delta\mathbf{p}_\perp)\mathbf{p}_{\mathrm{osc}} - \langle p_{\mathrm{osc}}^2\rangle}{4(p_\eta + \delta p_x/2)} + \frac{p_{\mathrm{osc}}^2 + 2\mathbf{p}_\perp\mathbf{p}_{\mathrm{osc}} - \langle p_{\mathrm{osc}}^2\rangle}{4p_\eta}\,.$$

Hence, we obtain for the energy variation

$$\Delta h = \frac{1}{2(p_x + h + \delta p_x)} \times \left[2\delta\mathbf{p}\mathbf{p}_{\mathrm{osc}} - \frac{\delta p_x}{p_x + h}\left(p_{\mathrm{osc}}^2 + 2\mathbf{p}_\perp\mathbf{p}_{\mathrm{osc}} - \langle p_{\mathrm{osc}}^2\rangle\right)\right]. \tag{132}$$

In the nonrelativistic limit, $p_x, |h - p_0| \ll p_0$, we obtain the well-known expression for the energy variation:

$$\Delta h = -\frac{\Delta\mathcal{E}}{c} \simeq \frac{\delta\mathbf{p}\mathbf{p}_{\mathrm{osc}}}{p_0}\,, \tag{133}$$

which reflects the fact that the particle energy change equals the work done by the field on the particle. The energy change is highest in the backward particle scattering, when $\delta\mathbf{p} = -2\mathbf{p}_{\mathrm{osc}}$. From now on, unless otherwise stated, we assume that the initial drift momentum is small in comparison with the oscillatory momentum. However, in the case of relativistic motion, it is easily seen that an appreciable energy variation is also possible in transverse scattering (along $\mathbf{k}$ — especially when $\delta p_x \sim p_0, p_x$) due to a change in particle 'mass' and, accordingly, the oscillatory trajectory, because the oscillation amplitude depends on the particle drift momentum in the relativistic case.

Let us analyze expression (132). It is seen that the expression in square brackets is limited in amplitude and may not be greater than a value of order p_{osc}^2. This follows directly from the smallness of the initial drift momenta, $p \ll p_{\mathrm{osc}}$, and an energy estimate $h \approx p_{\mathrm{osc}} \gg p_0$. Assuming that the variation of momentum along $\mathbf{k}$ is small ($\delta p_x \ll h \approx p_{\mathrm{osc}}$), we immediately arrive at the limitation of the highest acquired energy by a value of order p_{osc}^2, as noted above.

However, let a particle scatter by nearly 90° from its initial velocity ($\delta\mathbf{p}_\perp = -\mathbf{p}_{\mathrm{osc}}$) and fly *along* the wave vector of an EM wave. Then, the denominator of expression (132) will turn out small: $2(p_x + h + \delta p_x) \approx p_0^2/p_{\mathrm{osc}} \ll p_{\mathrm{osc}}$. As a result, the highest possible particle energy will be on the order of

$$\Delta h_{\max} = \frac{p_{\mathrm{osc}}}{p_0^2}\left(p_{\mathrm{osc}}^2 + \langle p_{\mathrm{osc}}^2\rangle\right) \approx \frac{2p_{\mathrm{osc}}^3}{p_0^2} \gg p_{\mathrm{osc}}\,. \tag{134}$$

This is the earlier obtained estimate (117).

We note that it is sometimes more convenient to use formulas for drift coordinates than expressions for the variation of momenta. In particular, the formulas for drift coordinates make it possible to rather easily obtain the particle energy distribution after a collision. Furthermore, the drift coordinates are convenient in the numerical simulation of particle collisions in relativistically strong fields.

9.4 Ultrafast particle distribution

Let us find the energy distribution of ultrafast particles emerging in electron–ion collisions per unit time. To do this

requires calculating the integral

$$g(h) = n_{\mathrm{i}} \iint n(\rho) v \delta(h - \Delta h) \rho \, \mathrm{d}\rho \, \mathrm{d}\phi \,, \tag{135}$$

where $n_{\mathrm{i}} = n_{\mathrm{e}}/Z$ is the ion concentration, $n(\rho)$ is the particle density prior to the last impact, and h is the drift energy variation in a relativistic Coulomb collision.

The particle density prior to the last impact may be determined from the following considerations. Notice that relativistically strong laser fields correspond to the conditions

$$p_{\mathrm{osc}} = \frac{eA}{c} \gg m v_T = \sqrt{\frac{mT}{2}}, \quad r_{\mathrm{osc}} \approx \frac{c}{\omega} \gg b_{\mathrm{osc}} \approx \frac{e^2 Z}{p_{\mathrm{osc}} c} \,. \tag{136}$$

The approximate expressions for the oscillation radius r_{osc} and the Rutherford radius b_{osc} [unlike those in inequalities (81)] are given for the ultrarelativistic intensity case of $p_{\mathrm{osc}} \gg mc$.

We assume that the particle scattering in relativistically strong fields occurs in two stages and the particle concentration $n(\mathbf{r})$ prior to the last hard impact is given by formulas (97). In relativistically strong fields, distribution (97) will supposedly remain, since this is the simplest form of distribution in conditions whereby particles gather at a point from a circle. Since the law of increasing the scattered momentum with decreasing impact parameter holds in the relativistic case, distribution (97) will therefore take place for kinematic reasons. The distribution form (97) is also borne out by numerical calculations of collisions in relativistically strong fields (see Section 10).

To determine the variation of momentum which enters in expression (132) for h, we will take advantage of the exact formulas for relativistic particle scattering from a Coulomb center [49]. The utilization of these formulas is justified by the circumstance that the last, 'hard', impact occurs on time and spatial scales much shorter than the EM wave scale (period and wavelength). Naturally, this is true for collisions occurring away from the particle stopping points (when the total particle velocity is equal to zero), which are nonexistent in relativistically strong fields. The particle longitudinal[15] momentum δp_x has the form

$$\delta p_x = p_{\mathrm{osc}} \cos\phi \sin\theta(\rho) \,, \tag{137}$$

where the scattering angle

$$\theta = \pi - \frac{2}{\sqrt{1 - \beta^2/\rho^2}} \arccos \frac{-\beta\sqrt{p_{\mathrm{osc}}^2 + p_0^2}}{\sqrt{p_{\mathrm{osc}}^2 \rho^2 + p_0^2 \beta^2}} \,. \tag{138}$$

Here, β is the characteristic parameter of the scattering problem, defined as

$$\beta = \frac{e^2 Z}{p_{\mathrm{osc}} c} \underset{p_{\mathrm{osc}} \gg p_0}{\approx} b_{\mathrm{osc}} \,.$$

We note an important feature of scattering with relativistic velocities. Forward scattering becomes possible at small impact parameters $\rho \sim \beta$. Moreover, with decreasing impact parameter, $\rho \to \beta$, the scattering acquires a rapidly oscillating nature, because the denominator $(1 - \beta^2/\rho^2)^{1/2}$ tends to zero in formula (138) for the scattering angle. Particles with an impact parameter $\rho < \beta$ fall on the Coulomb center and are given no consideration in what follows.

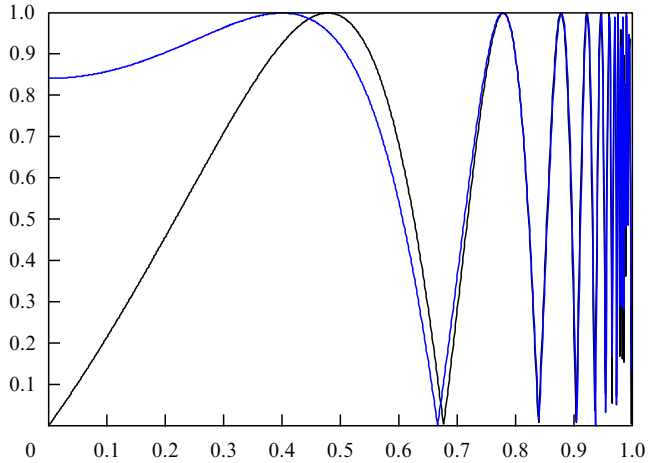

Figure 27. (Color online.) Function $\sin\theta$ for the argument expressions (139) (black curve) and (141).

If the scattering in ultrarelativistic fields ($p_{\mathrm{osc}} \gg p_0$) is of interest, expression (138) for the scattering angle becomes simpler:

$$\theta = \pi - \frac{2}{\sqrt{1 - \eta^2}} \arccos(-\eta) \,, \tag{139}$$

where $\eta = \beta/\rho \geqslant 1$. In this case, integral (135) for a circularly[16] polarized electromagnetic wave assumes the form

$$g(h) = v n_{\mathrm{e}} n_{\mathrm{i}} \iint \delta\left(h - \frac{p_{\mathrm{osc}}(2 + \cos\theta)}{1 - \sin\theta\cos\phi + \mu}\right) \frac{b\eta}{\beta} \frac{\mathrm{d}\eta \, \mathrm{d}\phi}{\eta^3} \,, \tag{140}$$

where μ is the small parameter of the problem, and $\mu = p_0^2/(2p_{\mathrm{osc}}^2) = 1/(2a^2) \ll 1$. To evaluate this integral requires expressing the integration parameter η in terms of h. However, this is rather hard to do analytically because of the transcendental nature of the scattering angle dependence (139) on η.

Let us consider in greater detail the quantity $\sin\theta$ (Fig. 27). Of primary interest to us are the energies on the order of $h \sim p_{\mathrm{osc}}/\mu$, which corresponds to the values $|\sin\theta| \approx 1$. In this case, due to the rapid oscillations of this function, the possibility arises to replace it with some approximate function of a simpler form. As an example of such a function, we take (see Fig. 27)

$$\sin\theta = \sin\left(1 + \frac{2\pi}{\sqrt{1 - \eta^2}}\right) \,. \tag{141}$$

Evidently, the domain of small values of $\eta \ll 1$ responsible for a relatively small energy change will be incorrectly described in this case, i.e., we must restrict ourselves to energies $h \geqslant 2p_{\mathrm{osc}}$.

[15] The variation of the remaining components will be small for the particles of interest.

[16] Similarly, it is possible to write down expressions for an arbitrarily polarized wave, which will give rise to the additional integral accounting for the dependence on the field phase at the instant of collision. Circular polarization is different in that the modulus of the oscillatory velocity is independent of the field phase, which eliminates one integration.

As a result, integral (140) assumes the form

$$g(h) \approx 2vn_e n_i \sum_{k=1}^{\infty} \int \frac{b\eta_k}{\beta} \frac{\partial\theta^*}{\partial h} \frac{1}{\eta_k^4} \frac{4\pi^2\,\mathrm{d}\phi}{\left(\theta^* + \pi(k+1)\right)^3}$$
$$\approx vn_e n_i \left(\frac{4}{5}\right)^3 \frac{2}{\pi\eta_1^4} \frac{b\eta_1}{\beta} \int \frac{\partial\theta^*}{\partial h}\,\mathrm{d}\phi\,. \qquad (142)$$

Here, η_k is a value of $\eta \in (0.4, 1)$ at which $\sin\theta = 1$, and θ^* is the scattering angle at which the argument of the delta function in integral (140) turns to zero:

$$\theta^* \approx \arcsin \frac{1 + \mu - 2p_{\mathrm{osc}}/h}{|\sin\phi|}\,. \qquad (143)$$

We note that the limitation on the maximum energy gain is easily obtainable from this expression, again proceeding from the arcsine function domain: $h \leqslant 2p_{\mathrm{osc}}/\mu$.

Finally, the particle energy distribution takes on the form

$$g(h) = vn_e n_i \left(\frac{4}{5}\right)^3 \frac{2}{\pi\eta_1^4} \frac{b\eta_1}{\beta} \frac{p_{\mathrm{osc}}}{h^2}\, K\left[1 - \left(1 + \mu - 2\,\frac{p_{\mathrm{osc}}}{h}\right)^2\right], \qquad (144)$$

where $K(x)$ is the complete elliptic integral of the first kind. On singling out the dependence on the main plasma parameters, the energy distribution assumes the following simple form

$$g(h) \sim \frac{n_i^2 Z^3 \Lambda}{h^2}\,, \qquad (145)$$

where Λ is a logarithmic factor. This formula is convenient for making experimental estimates. For instance, by changing the type of gas (i.e., the value of Z) we obtain a cubic dependence on the ion charge. Furthermore, seen clearly is the power law for a decrease in $g(h)$ with increasing particle energy. Notice that such particles will hardly experience collisions in the plasma subsequently due to their high energy, which will conserve their energy distribution law. The dependence on the gas density (on n_i) is not quite evident, because high concentrations entail the violation of adiabaticity conditions (131).

Estimate (145) may actually be obtained from quite simple considerations. Assume that a particle is isotropically scattered if its impact parameter is small, $\rho \sim \beta$ (see Fig. 27). Then, in view of formulas (97) and (118), the energy distribution takes on a simple form for high-energy particles, $p > p_{\mathrm{osc}}$:

$$g(h) = 2\pi vn_i n_e b\beta \int \delta\left(h - \frac{p_{\mathrm{osc}}}{1 + \mu - \cos\vartheta}\right) \sin\vartheta\,\mathrm{d}\vartheta\,.$$

Here, ϑ is the angle between the wave vector and the kinematic particle momentum after a collision, and $p_x = p_{\mathrm{osc}}\cos\vartheta$. The integral is easily computed with the help of the delta-function definition, when the particle energy satisfies the conditions $h > p_{\mathrm{osc}}$, $h < 2p_{\mathrm{osc}}a^2$:

$$g(h) = 4\pi vn_i n_e b\beta\,\frac{p_{\mathrm{osc}}}{h^2} \sim \frac{n_i^2 Z^3}{h^2}\,. \qquad (146)$$

Interestingly, the crude assumption of scattering isotropy has led to the loss of the logarithmic factor [compare with expression (145)], but the dependence on the main parameters has remained correct.

10. Collisions in relativistically strong fields

Electron scattering dynamics in relativistic and strong nonrelativistic fields is similar in many respects. The effects of attraction and bunching take place in just the same way [69]. Accordingly, the statement that the straight-line approximation is inapplicable for describing collisions in such fields remains valid. Specifically, in strong fields, $\Omega \ll 1$, account should be taken of the attraction stage — the phase of motion during which an electron in the oscillating field is attracted to a close neighborhood of an ion from large impact parameters. The energy of an electron is hardly changed at this stage, but its position in space relative to the ion changes appreciably. Only then does the strong ('hard', last) electron impact on the ion occur with a significant change of the electron energy and the electron velocity direction.

The attraction effect, which is purely kinematic in nature, is due to the attraction of an oscillating electron to the ion. In this case, the presence of two conditions is significant at the stage of electron attraction, which persist in the relativistic case, too: the attractive ion center, and the periodic external field. Although the particle oscillations will be highly complicated, the qualitative pattern of collisions will remain unaltered. Moreover, since the effect is determined by the *drift* velocity[17] of the incident electrons, the characteristic scales and dependences remain the same as in nonrelativistic fields. Only the character of the last ('hard') electron impact on the ion will actually change. It is in this case that relativistic formulas have to be used for resolving the scattering problem [49].

Let us show, for instance, the presence of the attraction effect in relativistically strong fields (compare with the consideration in Section 7). From exact formulas for the scattering of a relativistic particle in the ion field [49] there follows a simple relationship between the particle momentum variation $\Delta p_\perp$ and its impact parameter ρ:

$$\Delta p_\perp = \frac{p_{\mathrm{osc}} b_{\mathrm{osc}}}{\rho} \ll p_{\mathrm{osc}}\,. \qquad (147)$$

However, for $b_{\mathrm{osc}} = e^2 Z/p_{\mathrm{osc}} v_{\mathrm{osc}}$, one must substitute the relativistic expression, which takes into account the electron velocity–momentum relation: $v_{\mathrm{osc}} = p_{\mathrm{osc}} c/(p_{\mathrm{osc}}^2 + p_0^2)^{1/2}$. On finding from this the magnitude of transverse velocity variation $\Delta v_\perp = \Delta p_\perp c/(p_{\mathrm{osc}}^2 + p_0^2)^{1/2}$, it is easy to see that the particles with the instantaneous impact parameter $\rho_1 = \sqrt{2\pi} r_E$ will arrive exactly at the ion in a field cycle $2\pi/\omega$. We emphasize that definition (52) of the quantity r_E retains the same form as in the nonrelativistic case, though with the substitution of relativistic expressions for the oscillation radius and the Rutherford radius:

$$r_{\mathrm{osc}} = \frac{p_{\mathrm{osc}} c}{\omega\sqrt{p_{\mathrm{osc}}^2 + p_0^2}}\,, \quad b_{\mathrm{osc}} = \frac{e^2 Z\sqrt{p_{\mathrm{osc}}^2 + p_0^2}}{p_{\mathrm{osc}}^2 c}\,. \qquad (148)$$

Similarly, it is possible to find the instantaneous impact parameters whereby the electron will arrive exactly at the ion in two, three, etc. oscillations, the expressions for these parameters being precisely the same as in the nonrelativistic case.

[17] For typical plasma parameters with a temperature ranging from several electron-volts to several hundred electron-volts, the electron drift velocity may be treated as nonrelativistic.

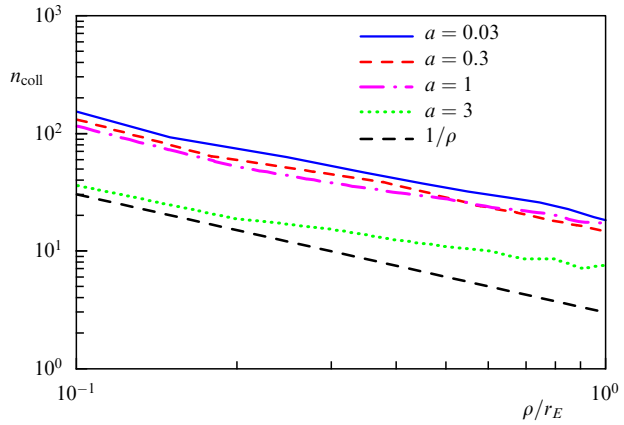

Figure 28. Density prior to a hard impact as a function of the distance to the ion for different a values. The lower dashed line stands for the model dependence.

Therefore, all inferences of the nonrelativistic scattering problem remain in force with consideration for the relativistic definition of parameters in the scattering problem (148). The results of numerical simulations bear out this statement. For instance, the particle distribution prior to a 'hard' impact has the same singularity (Fig. 28) as in the nonrelativistic case (97). Some decrease in the number of particles is due to the appearance of an oscillation finite width in the coordinate along the direction of wave propagation. As a result, the mode of 'longitudinal' collisions in a linearly polarized field, when the particles move along the symmetry axis of the electric field and are under conditions most favorable for gaining energy, is replaced with the scattering mode similar to that in a circularly polarized wave. In this case, the maximum value of coefficient b becomes smaller, but its dependence on the angle θ of particle incidence becomes smoother, so that the integral value $\int b \sin\theta \, d\theta$ remains almost constant. The magnitude of b turns out to depend only slightly on the angle of particle incidence and is approximately equal to $b_v = e^2 Z/(mv^2)$. It is precisely this picture that is observed for the dependence of the effective (energy) collision cross section on the particle incidence angle with increasing parameter a (see Section 10.1).

Despite the relatively simple form of the particle energy distribution (97) prior to the last impact, the dynamics of the scattered particles is rather complex. This is illustrated by Fig. 29, which shows the energy variation in relation to the initial impact parameter for different entrance angles and amplitudes a of the pump field. Darker domains correspond to greater energy changes. In the nonrelativistic case, $a \approx 0$, one can view concentric rings in the longitudinal particle incidence and a dumbbell-shaped distribution in the lateral one. With increasing pump field amplitude, the rings in the longitudinal incidence begin to 'blur', which corresponds to the appearance of a 'figure-eight' in the oscillatory electron motion — the passage to a scattering mode similar to the scattering mode in the circularly symmetric case. This figure-eight is seen well in Fig. 29b for the transverse scattering. Furthermore, the oscillatory radius somewhat shortens in comparison with that in the nonrelativistic case [in perfect agreement with formula (148)]. Lastly, in an ultrarelativistic pump field ($a = 3$), the dynamics becomes even more complicated — the difference between the longitudinal and lateral particle incidences becomes insignificant. The particles

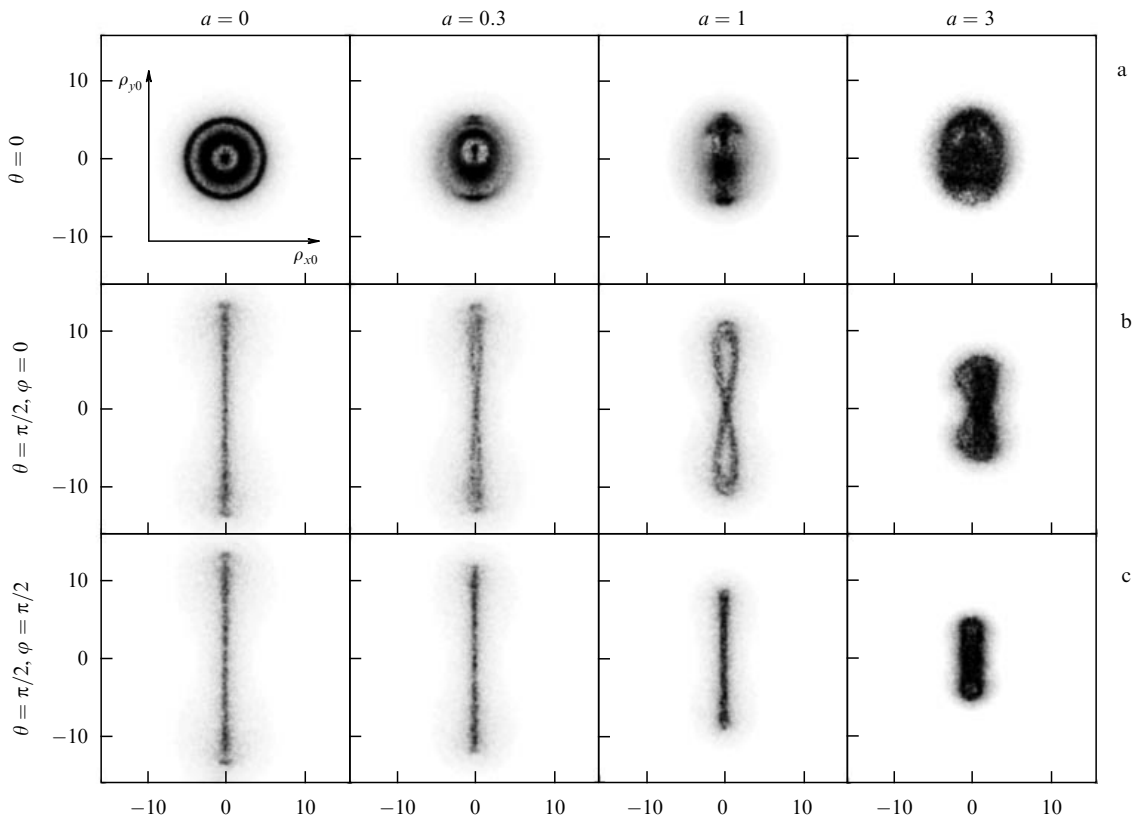

Figure 29. Dependence of the energy variation on the impact parameters normalized to the oscillatory radius for various incidence angles and values of parameter a at $\Omega = 0.3$.

begin to gain more energy (the darker color in Fig. 29; lines thicken), which is indicative of an increase in the oscillatory Rutherford radius $b_{\rm osc}$ with increasing $a > 1$, in accordance with formula (148).

10.1 Joule heating

The integral characteristics of scattering behave quite similarly. First, we consider the energy-related scattering cross section (23), which may be estimated from simple analytical considerations. We assume that the main contribution to heating in the last impact is made by small-angle scatterings with a momentum variation (147). The particle density (97) prior to the last impact on the ion is known from numerical simulations. Then, the scattering cross section takes on the form

$$\sigma_{\rm eff} \approx \int_{b_{\rm osc}}^{\infty} n(\rho)\,\frac{\Delta p_{\perp}^2}{p_{\rm osc}^2}\,\rho\,{\rm d}\rho = b_v b_{\rm osc} \sim \frac{\sqrt{1+a^2}}{T_{\rm e} p_{\rm osc}^2}\,. \qquad (149)$$

The results of numerical simulations bear out estimate (149) completely. One can see in Fig. 30 that the collision cross section is almost constant for underrelativistic intensities, $a < 1$. For relativistic intensities $(a \geqslant 1)$, the cross section starts to rise in proportion to $\sqrt{1+a^2}$, this dependence taking place for all polarizations of the pump field.

Figure 31 depicts the effective cross section as a function of the entrance angles of scattered particles for a linearly polarized pump field. In the nonrelativistic limit $(a \approx 0)$, one can see a strong anisotropy of the cross section in relation to the angle θ between the particle momentum and the direction of the electric field. The anisotropy stems from the following fact: all particles that travel along the field find themselves in a mode which favors multiple scattering by the ion. Conversely,

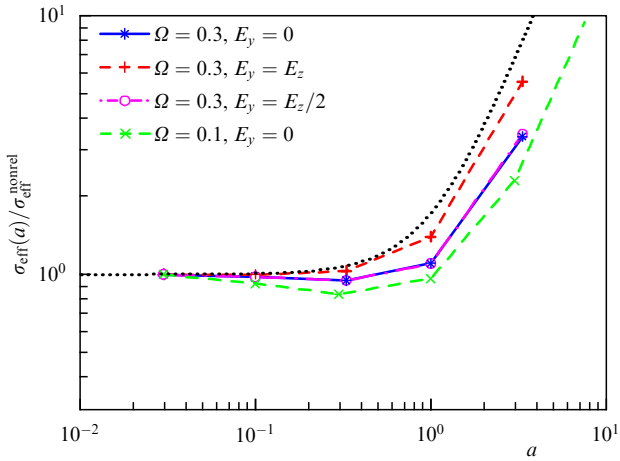

Figure 30. (Color online.) Dependence of the integral scattering cross section on a for different polarizations [linear $(E_y = 0)$, circular $(E_y = E_z)$, and elliptical $(E_y = E_z/2)$] of the pump field and Ω parameter values. The dotted curve shows the model dependence $\sqrt{1+a^2}$.

only a relatively small fraction of particles experience multiple collisions at an incidence perpendicular to the electric field.

If the relativistic effects are included, the passage from sinusoidal oscillations to figure-eight oscillations entails three implications. First, an increasingly large fraction of particles begin to experience multiple collisions at an incidence at an angle to the electric field, which broadens the dependence of the scattering cross section on angle θ. Second, the longitudinal incidence $(\theta = 0)$ becomes progressively less preferred than nonzero-angle incidence, and only a part of the electrons experience multiple impacts on the ion in this case.

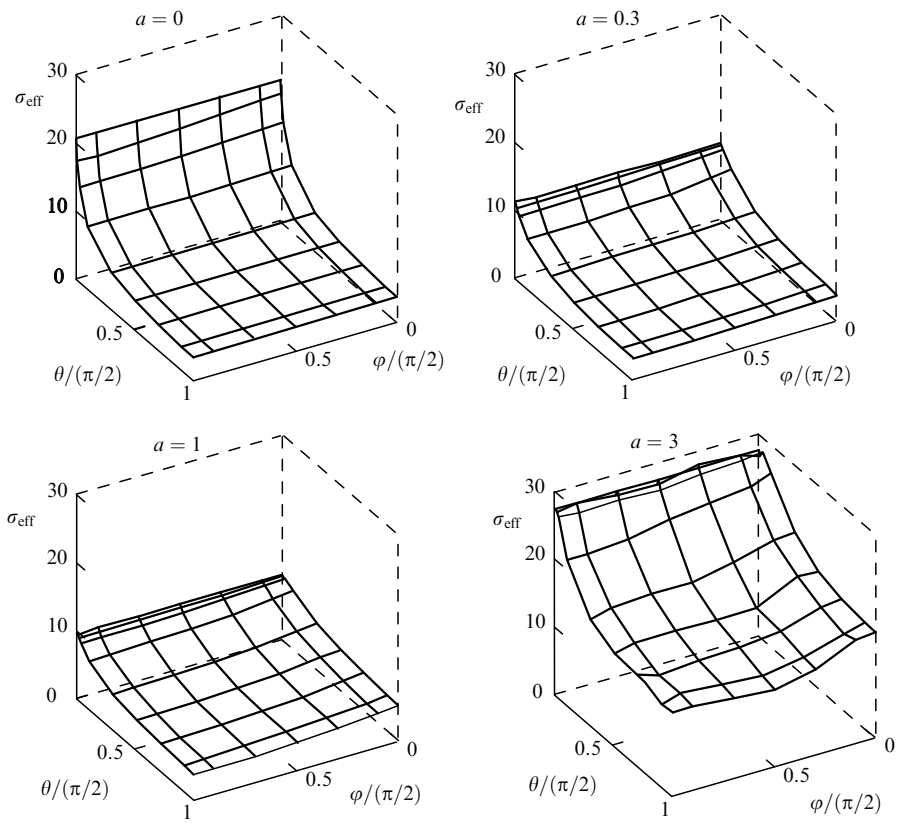

Figure 31. Dependence of the effective cross section on the incidence angles at $\Omega = 0.3$ and different values of a indicated in the panels.

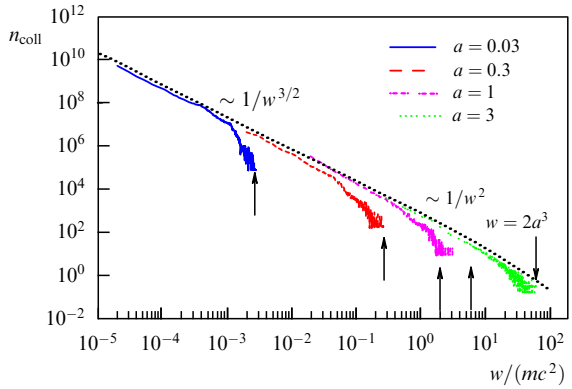

Figure 32. (Color online.) Particle energy-change distribution for various values of a at $\Omega = 0.3$. The dotted line (lying above all the other curves) stands for the model dependence (150). The arrows at the bottom mark the energy of particles with the greatest momentum change $2p_{\rm osc}$.

As a consequence, the cross section at $\theta = 0$ becomes smaller. A passage to the mode of collisions in a circularly polarized field actually occurs. Third, there appears a weak dependence of the cross section on the angle ϕ between the direction of the initial particle momentum and the wave vector of the pump field. Lastly, in ultrarelativistic fields ($a \gg 1$) the cross section rises as a whole proportionally to $\sqrt{1+a^2}$. In this case, the heating rate $\mathrm{d}T/\mathrm{d}t$ does not depend as well on the EM wave amplitude due to the 'lowering' of transferred (oscillatory) energy $\sim \sqrt{1+a^2} - 1$, with exception of the transition domain with $a \sim 1$.

10.2 Production of fast particles

By proceeding from the considerations stated at length in Section 10.1, it is also possible to obtain the particle energy distribution $w = c((p_0^2 + p^2)^{1/2} - p_0)$ (Fig. 32). For a relatively small momentum variation, $w \ll mc^2$, the particle distribution function decreases as $\sim 1/w^{3/2}$. Conversely, at high energies, $w \gg mc^2$, this function becomes proportional to $\sim 1/w^2$ and bounded from above by an energy $2a^2 p_{\rm osc} c \gg p_{\rm osc} c$. The behavior of the particle energy distribution function for both small and large momentum changes is in complete agreement with theoretical expectations.

Specifically, for $p < p_{\rm osc}$, advantage can be taken of formula (147) to calculate the distribution

$$g(\mathbf{q}) = n_{\rm i} n_{\rm e} v_{Te} \int \delta(\mathbf{q} - \mathbf{p}_+)\, \mathrm{d}^2\rho\, \mathrm{d}\phi\,.$$

By using the definition of the delta function, we obtain the particle energy distribution in the form

$$g(\Delta p_\perp) = n_{\rm i} n_{\rm e} v_{Te} \frac{n(\rho)\rho}{\mathrm{d}\Delta p_\perp/\mathrm{d}\rho}\,,$$

where the impact parameter

$$\rho = \frac{b_{\rm osc}\, p_{\rm osc}}{\Delta p_\perp} = \frac{b_{\rm osc}\, p_{\rm osc} c}{\sqrt{w^2 + 2wcp_0}}$$

should be expressed in terms of the final momentum $\Delta p_\perp$ or energy w (we assume that $w \gg T_{\rm e}$), and the particle concentration $n(\rho)$ prior to the hard impact is defined by formula (97). Since the fast particle fraction is small, the background plasma may be considered as a 'source' and its parameters to be invariable. Moreover, the fast particles do not experience subsequent collisions due to their high energy. As a result, the energy distribution function assumes the form [71]

$$g(p) \sim \frac{1}{p^3} \quad \text{or} \quad g(w) \sim \frac{w + p_0}{(w^2 + 2p_0 w)^{3/2}} \sim \begin{cases} \dfrac{1}{w^{3/2}}\,, & w \ll mc^2, \\ \dfrac{1}{w^2}\,, & w \gg mc^2. \end{cases} \tag{150}$$

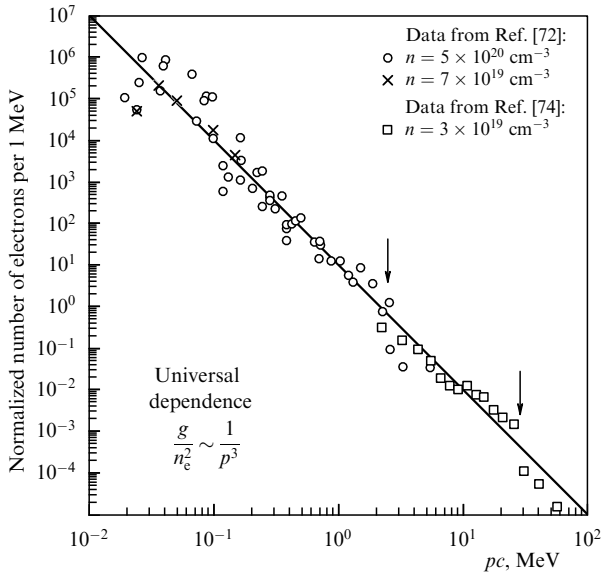

Figure 33. Comparison of the experimental data of Refs [72–74] and the theoretical dependence (150) (solid line) for the distribution of hot electrons over the 'energy momentum' pc. The arrows indicate the cutoffs $2p_{\rm osc}$.

Precisely this distribution of scattered particles was obtained in the experiments [72–74], i.e., the momentum distribution (150). In Fig. 33, one can see good agreement between the theoretical dependence (150) and the experimental data. Note that four different series of experimental measurements are combined in Fig. 33 [72–74]. Figure 33 provides another indication of precisely collisional hot electrons. Collisional heating has a natural upper threshold for the electron momentum — $2p_{\rm osc}$. The corresponding highest energies are indicated by arrows in Fig. 33. One can see that they correspond to a sharp decrease in the number of observed hot electrons.[18] We emphasize that Fig. 33 demonstrates the dependence on the 'energy momentum' pc and not on the particle energy. These quantities are equal only in the ultrarelativistic limit [72, 73]. The possibility of interpreting experimental data in this way is also due to the fact that the authors of Ref. [74] employed magnetic scintillators, which measured precisely the particle momentum rather than particle energy. When all of this is taken into account, one may draw a conclusion that there was a calibration error in the distributions obtained in Ref. [74].

In the other limiting case of $p_0 \leqslant p_{\rm osc} < w/c < a^2 p_{\rm osc}$, the energy–momentum relationship is linear: $w = pc$. The momentum distribution of such ultrafast particles, which was

[18] It is pertinent to note that particles with a far higher energy (up to $p_{\rm osc}^2/m$ or $p_{\rm osc}^3/m^2c$) may be produced in electron–ion collisions in the ultrarelativistic case.

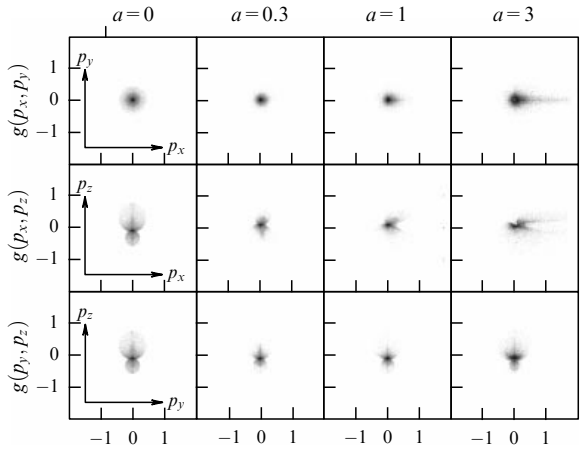

Figure 34. Particle momentum-change distribution for various values of a. Shown are the distributions in planes $p_x \times p_y$, $p_x \times p_z$, and $p_y \times p_z$. The particle momenta are normalized to the oscillatory momentum.

found earlier [see formula (145)], is proportional to $\sim 1/p^2$. The direction of particle escape is almost parallel to the wave vector of an EM wave. Accordingly, the particle energy distribution takes the form

$$g(w) \sim \frac{1}{p^2}\,\frac{\mathrm{d}p}{\mathrm{d}w} = \frac{1}{w^2}\,, \quad w \gg p_{\mathrm{osc}}\,. \tag{151}$$

In this case, the highest particle energy is limited by the value of $2p_{\mathrm{osc}}^3/p_0^2$. It is precisely such a 'tail' that is demonstrated also by numerical simulations (see Fig. 32).

Figure 34 depicts the variation of the angular distribution of scattered particles with increasing parameter a. The color gradation serves to show the scattered electron density (the more particles with a given momentum, the darker the color) in relation to the momentum projections for different values of the normalized vector potential a. It can be seen that the scattered electron distribution is almost isotropic across the wave electric field, although there is a small fraction of electrons with $p_z \neq 0$ scattered along the wave electric field. With increasing a, the electron distribution becomes anisotropic and, for $a \geqslant 1$, an appreciable 'tail' appears directed along the EM wave propagation — to the $p_x > 0$ domain. Actually, confined in this tail are superhigh-energy electrons with energies $w > p_{\mathrm{osc}}$ — the so-called a^3 effect.

Electrons with energies of several hundred megaelectron-volts were observed with precisely distribution law (151) in the experiment [75]. Seen in Fig. 35 is the power-law electron energy distribution, as well as a kink arising from the nonadiabaticity of motion in a wave packet for electrons with too high an energy (131). The disappearance of this kink with increasing density may be due to the fact that the attraction effect vanishes in dense plasma, because the binary collision approximation becomes invalid.

Apart from the graphic comparison of experimental data and the theoretical curve, it is possible to find and compare the heating rate (temperature after a pulse propagation) and the number (net charge) of fast electrons. The rate of heating in the nonrelativistic and relativistic cases is easy to obtain by putting $b = b_v$:

$$Q \simeq 4\pi n_{\mathrm{i}} n_{\mathrm{e}} m c^3 b_{\mathrm{c}}^2\,\frac{c}{v}\,. \tag{152}$$

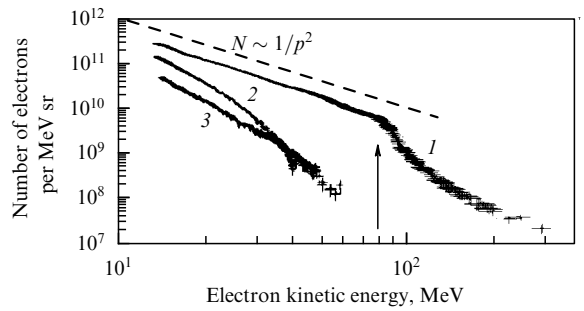

Figure 35. Electron energy distribution for $n_{\mathrm{e}} = 5.4 \times 10^{18}$ cm^{-3} (curve *1*), $n_{\mathrm{e}} = 7.7 \times 10^{18}$ cm^{-3} (curve *2*), and $n_{\mathrm{e}} = 83 \times 10^{18}$ cm^{-3} (curve *3*) [75]. One can see a kink in the transition to the nonadiabatic mode (indicated by an arrow) and the disappearance of this kink with increasing particle concentration. The dashed line matches the $1/p^2$ law. The arrow indicates the adiabaticity boundary (131).

Here, $b_{\mathrm{c}} = e^2 Z/(mc^2)$ is the Rutherford radius for $p = mc$, equal to the classical electron radius at $Z = 1$.

We note that the heating rate (152) is independent of the EM field amplitude in both the nonrelativistic and relativistic cases. A dimensional estimate of the heating rate per unit volume, namely

$$Q = 10^{13}\,\frac{nZ}{\sqrt{T}}\,[\mathrm{eV\ cm^{-3}\ s^{-1}}]\,, \tag{153}$$

permits estimating the plasma temperature after the passage of an EM pulse. In particular, for 1-ps long pulses (which corresponds to the experimental conditions in Refs [72, 73]), formula (153) yields an electron temperature on the order of several hundred electron-volts, which conforms to the available experimental data (200–600 eV).

11. Collision operator in strong fields

Formally, the collision operator has the form of expression (17). However, its direct employment is hindered by the complex, inherently stochastic shape of test particle trajectories. Expression (17) may be simplified by taking into consideration the features of particle dynamics in strong electric fields. The dynamics of such particles represent a pulling towards the ion with hardly any variation in the modulus of the drift velocity, a sharp 'hard' impact on the ion, and an escape from the scattering domain.

The escaped particle momentum is hardly changed. This permits replacing the final momentum $\mathbf{p}(t = +\infty)$ by the momentum after the hard impact. Furthermore, by replacing the integration variable $\mathbf{r}_0$ with the coordinate $\mathbf{r}_{\mathrm{c}}$ prior to the hard impact, we obtain

$$\langle w_{\mathrm{ei}}(\mathbf{p}, \mathbf{p}_0, t)\rangle = \frac{n_{\mathrm{i}}}{T}\int J(\mathbf{r}_{\mathrm{c}}, \mathbf{p}_0)\big(\delta(\mathbf{p}_0 + \delta\mathbf{p} + \Delta\mathbf{p} - \mathbf{p}) - \delta(\mathbf{p}_0 - \mathbf{p})\big)\,\mathrm{d}^3 r_{\mathrm{c}}\,. \tag{154}$$

Here, $\delta\mathbf{p}$ is a small variation of the particle momentum at the stage of pulling towards the ion, $J(\mathbf{r}_{\mathrm{c}}, \mathbf{p}_0)$ is the Jacobian[19] of a transition from $\mathbf{r}_0$ to $\mathbf{r}_{\mathrm{c}}$, $\Delta\mathbf{p}$ is the momentum change in the

[19] A note is in order: in the case of multiflow particle dynamics (which takes place in strong fields), summation over ambiguity regions should be performed in the Jacobian.

hard impact, and

$$\Delta\mathbf{p} = -\left(\frac{2\boldsymbol{\rho}\, mP/b}{1+\rho^2/b^2} + \frac{2m\mathbf{P}}{1+\rho^2/b^2}\right) \underset{\rho \gg b}{\approx} -2mP\,\frac{\boldsymbol{\rho}}{\rho}\,\frac{b}{\rho}\,, \quad (155)$$

where $\rho = \mathbf{R}_c - \mathbf{P}(\mathbf{R}_c, \mathbf{P})/|P|^2$ and $b = e^2 Z/(mP^2)$ are the impact parameter prior to the hard impact and the Rutherford radius determined from the total particle velocity. As before, $\mathbf{R}$ and $\mathbf{P}$ are the complete coordinate and momentum at the instant of impact. For low velocities, $p \ll p_{\rm osc}$, and a linearly polarized pump wave, $\mathbf{E} = E\mathbf{z}_0$, the expressions for $\boldsymbol{\rho}$ and $\mathbf{P}$ become simpler:

$$\mathbf{P} \simeq \mathbf{z}_0 p_{\rm osc}(z)\,, \quad \boldsymbol{\rho} \simeq x\mathbf{x}_0 + y\mathbf{y}_0\,. \quad (156)$$

To calculate the Jacobian, advantage can be taken of the fact that the physical meaning of the Jacobian is reduced to the particle concentration in new variables, which was already found in Section 7. In general, the concentration in the case of a linearly polarized field may be represented in the form

$$J(\mathbf{r}_c, \mathbf{p}_0) = n_0\left(1 + \frac{p}{p_{\rm osc}}\,\frac{a(\mathbf{p}_0)}{\rho}\right) \approx \alpha(\mathbf{p}_0)\,\frac{b_{\rm osc}}{\rho}\,, \quad (157)$$

where $\alpha(\mathbf{p}_0) \sim p_{\rm osc}/p \gg 1$ is a factor which describes the anisotropy of the attraction effect in relation to the particle velocity prior to scattering (to the initial velocity). Furthermore, owing to the smallness of particle velocity variation at the stage of attraction, we may put $\delta\mathbf{p} \approx 0$. As a result, the expression for the collision kernel takes on the form

$$\langle w_{\rm ei}\rangle = \frac{n_{\rm i}}{T}\int J(\mathbf{r}_c, \mathbf{p}_0)\Big(\delta\big(\mathbf{p}_0 + \Delta\mathbf{p}(\mathbf{r}_c, \mathbf{v}_0) - \mathbf{p}\big) - \delta(\mathbf{p}_0 - \mathbf{p})\Big)\,{\rm d}^3 r_c\,. \quad (158)$$

Disregarding particle velocity variation is insignificant in the consideration of energy exchange with the field, when the characteristic particle energy variation is comparable to or exceeds the initial energy (for instance, in the description of particles on the tail of the distribution function) but may introduce errors in transport scattering characteristics, which get the bulk of the contribution, as in weak fields, from long-range small-angle scatterings.

Expression (158) for the collision kernel resembles formula (17) but has a significant difference: the *explicit stochasticity* of particle dynamics is excluded from the integrand. In reality, expression (158) describes the stochastic mode, but does so implicitly: in terms of the particle concentration $n(\mathbf{r}, \mathbf{p}_0)$ prior to the last impact. In this case, the density must be exactly calculated, considering the complexity of stochastic particle dynamics. One may take a simpler road: take some approximation of expression (157) for the concentration prior to the last impact and exploit the fact that $J(\mathbf{r})$ appears in the integrand, and the inaccuracies of the approximation will 'smooth out' in the integration.

Expression (158) is sufficient for calculating the diffusion part of the collision operator in small-angle scattering. Specifically, from expression (17) it differs by only the integrand factor $J \sim 1/\rho$, which describes the attraction of particles at the aiming stage. In this case, use can be made of the perturbation method in small-angle scattering once again, but for the particles already pulled.

In this case, calculations are similar to those in Refs [5, 76]. The collision operator assumes the Landau form:

$$\mathrm{St}_{\rm ei}\,[f] = \frac{\partial}{\partial p_i}\,B_{ij}\,\frac{\partial f(\mathbf{p})}{\partial p_j}\,,$$

where coefficient B_{ij} is defined by the integral [77]

$$\begin{aligned} B_{ij} &= n_{\rm i}\int_{b_{\rm osc}}^{\infty} \frac{\alpha b_{\rm osc}}{\rho}\,\frac{\partial\mathcal{V}}{\partial r_i}\,\frac{\partial\mathcal{V}}{\partial r_j}\bigg|_{\mathbf{r}\to\mathbf{r}_0+\mathbf{v}t}\,{\rm d}t\,{\rm d}^3 r \\ &= \frac{2\pi\alpha n_{\rm i} e^4 Z^2 m}{p_{\rm osc}}\left(\delta_{ij} - \frac{P_i P_j}{|P|^2}\right)\int_{b_{\rm osc}}^{\infty}\frac{b_{\rm osc}\,{\rm d}r}{r^2} \\ &\simeq \frac{\pi^2\alpha n_{\rm i} e^4 Z^2 m}{p_{\rm osc}}\left(\delta_{ij} - \frac{P_i P_j}{|P|^2}\right). \end{aligned} \quad (159)$$

The last expression comprises integral $\int b_{\rm osc}\,{\rm d}r/r^2$, which diverges at the lower limit of integration. As its lower limit in the integration, we took the Rutherford radius corresponding to total velocity, $b \approx b_{\rm osc}$ — the limit of pulse variation expansion (155) in the scattering through small angles ($\rho \gg b \approx b_{\rm osc}$).

Tensor (159) exhibits the only form of the simplest differential operator that yields the correct result for the collision frequency in strong fields under the assumption that the scattering occurs primarily across the electric field of an EM wave. We note that precisely the same 'diffusion' part also results for the instantaneous (not time-averaged) collision operator. In the latter case, however, the total particle momentum P will also depend on time.

In reality, the divergence at the lower limit in expression (159) is rather strong, i.e., the contribution from close collisions is comparable to the contribution from distant, small-angle scatterings. Specifically, by applying the method of moments to expression (158), we obtain the expression for the first moment:

$$\frac{{\rm d}\langle p_i\rangle}{{\rm d}t} = \frac{\pi^2 n_{\rm i} e^4 Z^2 \alpha m}{p_{\rm osc}^3}\,p_{{\rm osc},\,i}(t) = \frac{\partial B_{ij}}{\partial p_j}\,,$$

which coincides with the similar expression from integral (159). However, even for the second moment,

$$\frac{{\rm d}\langle p_i p_j\rangle}{{\rm d}t} = \frac{\pi^2 n_{\rm i} e^4 Z^2 \alpha m}{p_{\rm osc}}\,(\delta_{ij} + \delta_{iz}\delta_{jz}) \neq B_{ij}\,,$$

an expression results corresponding to a nearly isotropic scattering rather than the scattering (see Fig. 34 at $a = 0$) across the instantaneous (oscillatory) velocity, as would follow from expression (159).

The main difficulty in expression (159) is concerned with the integral $\int_{b_{\rm osc}}^{\infty}{\rm d}r/r^2$, which diverges at the lower limit. This divergence is due to the appreciable contribution made by particles scattered through large angles. For an accurate (not estimative) description of collisions, complete integral (158) must therefore be employed.

We write out integral (158) in an explicit form, taking into account the bunching of particles near the phases of peak oscillatory velocity:

$$\begin{aligned} \langle w_{\rm ei}\rangle = \frac{v_{\rm osc} n_{\rm i}}{2\pi}\int J(\mathbf{r}, \mathbf{v}_0)\bigg[\delta\left(\delta\mathbf{p}_\perp - \frac{2p_{\rm osc} b_{\rm osc}\boldsymbol{\rho}}{\rho^2 + b_{\rm osc}^2}\right) \\ \times\,\delta\left(\delta p_z \pm \frac{p_{\rm osc} b_{\rm osc}^2}{\rho^2 + b_{\rm osc}^2}\right) - \delta(\delta\mathbf{p})\bigg]\,{\rm d}x\,{\rm d}y\,, \end{aligned} \quad (160)$$

where $\delta\mathbf{p} = \mathbf{p}_0 - \mathbf{p}$. The plus and minus signs correspond to the electron bunches near the highest values of the oscillatory momentum along and opposite to the direction

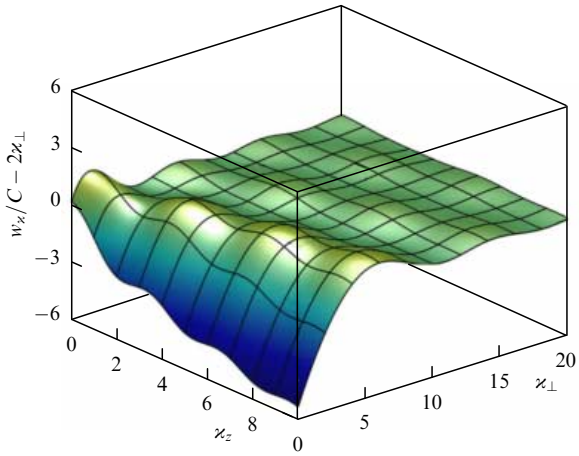

Figure 36. Fourier transform of collision function (161).

of their motion, since the modulus of oscillatory velocity $v_{\rm osc}(t) \sim |\sin(\Omega^* t)|$ in a linearly polarized field reaches its maximum twice a period.

To calculate expression (160), we go over to the Fourier transform

$$w_\varkappa = \int \langle w(\delta\mathbf{p})\rangle \exp\left(\frac{\mathrm{i}\boldsymbol{\varkappa}\delta\mathbf{p}}{p_{\rm osc}}\right) \mathrm{d}^3\delta p\,.$$

As a result, after a change $\rho \to b_{\rm osc}\tan(\varphi/2)$, expression (160) reduces to a single integral:

$$w_\varkappa = C\int_0^\pi \frac{J_0(\varkappa_\perp \sin\varphi)\cos\left[\varkappa_z(1+\cos\varphi)\right] - 1}{1+\cos\varphi}\,\mathrm{d}\varphi\,, \quad (161)$$

where $C = v_{\rm osc}\alpha n_{\rm i} b_{\rm osc}^2/(2\pi)$. Unfortunately, attempts to calculate integral (161) analytically do not meet with success. The result of numerical integration of expression (161) is plotted in Fig. 36. However, analytical calculation is possible in two important cases.

The first covers the expansion of expression (161) at small $\varkappa$:

$$w_\varkappa \approx -\frac{\pi C}{4}(2\varkappa_z^2 + \varkappa_\perp^2) + \ldots\,. \quad (162)$$

This expansion corresponds to diffusion in a momentum space:

$$\frac{\partial^2 \tilde{B}_{ij} f(\mathbf{p})}{\partial p_i\,\partial p_j}\,, \quad \tilde{B}_{ij} = \frac{\pi^2\alpha n_{\rm i} e^4 Z^2 m}{4p_{\rm osc}}\left(\delta_{ij} + \frac{p_{{\rm osc},i}\,p_{{\rm osc},j}}{|p_{\rm osc}|^2}\right). \quad (163)$$

The second case concerns the expansion as $\varkappa_\perp \to \infty$. Numerical integration yields a linear dependence (see Fig. 36). True, the second derivative of expression (161) has the form

$$\frac{\mathrm{d}^2 w_\varkappa}{\mathrm{d}\varkappa_\perp^2} = \pi\left(J_1^2\left(\frac{\varkappa_\perp}{2}\right) - J_0^2\left(\frac{\varkappa_\perp}{2}\right)\right) \underset{\varkappa_\perp\to\infty}{\to} 0\,.$$

This signifies that $w_\varkappa$ is a linear function of $\varkappa_\perp$ for $\varkappa_\perp \to \infty$. Moreover, it may be shown (see Fig. 36) that

$$w_\varkappa \underset{\varkappa_\perp\to\infty}{\approx} 2\varkappa_\perp\,.$$

Using this dependence and the integral

$$\int_0^\infty r^2 J_0(kr)\,\mathrm{d}r = -\frac{1}{k^3}\,,$$

the possibility arises to find an approximate expression for the collision operator in strong fields:

$$\langle w_{\rm ei}\rangle \approx \frac{2C\delta(\Delta P_\parallel/p_{\rm osc})}{\Delta P_\perp^3}\,. \quad (164)$$

Assuming the momentum of scattered electrons to be much greater than their thermal velocity, the collision operator may be simplified by replacing the distribution function $f(p_0)$ with the delta function [77]:

$$\left\langle \mathrm{St}\,[f]_{\rm hot}\right\rangle = \int f(\mathbf{p}_0)\,F(\mathbf{p})\,\mathrm{d}^3 p_0\,, \quad F(\mathbf{p}) = \frac{2Cp_{\rm osc}\delta(p_\parallel)}{p_\perp^3}\,. \quad (165)$$

This is the power-law fast-electron distribution obtained in Section 10.2.

Since the velocity of such particles after the collision is high and, accordingly, their collision frequency is negligibly small, there is good reason to speak about 'runaway' electrons. These particles experience hardly any collisions with ions in an alternating EM field and, in a way, are subsequently 'lost' for energy exchange processes, similarly to the runaway electrons produced in collisions in a static field [5]. The loss frequency μ — the frequency of appearance of electrons in the tail of the distribution function — may be estimated by the formula

$$\mu \equiv \int_{p>p_T} F(\mathbf{p})\,\mathrm{d}^2 p = \frac{n_{\rm i}\,p_{\rm osc}}{\pi}\,b_{\rm osc} b_v. \quad (166)$$

The runaway particle distribution per unit time in a momentum space is given by expression (165).

So, the collision operator may be qualitatively represented as the sum of two terms — a 'diffusion' term, and a fast particle 'generator':

$$\mathrm{St}_{\rm ei}\,[f] = \frac{\partial^2 \tilde{B}_{ij} f(\mathbf{p})}{\partial p_i\,\partial p_j} + \int f(\mathbf{p}_0)F(\mathbf{p})\,\mathrm{d}^3 p_0 - \mu f(\mathbf{p})\,. \quad (167)$$

This representation yields correct values for the plasma heating rate, as well as for the number and distribution law of the fast particles produced in collisions in the plasma. However, it is not entirely correct from the standpoint of kinetic peculiarities of scattering. When an issue of central interest is kinetics and it is required to accurately describe the plasma kinetics, use should be made of integral form (18) with kernel (160) or (161).

12. Applicability domain

We write down in dimensional form the applicability conditions of the results outlined in Sections 8–11. In the subsequent formulas, the electron temperature T is expressed in [eV], the power P in [10^{16} W cm^{-2}], all frequencies in [10^{15} Hz], wavelengths λ in [μm], the rest of the lengths in [cm], particle concentrations n in [10^{18} cm^{-3}], and the pulse duration τ in [10^{-15} s].

All calculations were performed in the strong field domain under the conditions expressed in dimensional form as

follows:

$$v \ll v_{\rm osc} \Leftrightarrow T \ll 6.7 \times 10^3 \, \frac{P}{\omega_0^2} \,, \tag{168}$$

$$\omega_0 \ll \omega_E \Leftrightarrow \omega_0 \ll 20 \, P^{3/8} \,. \tag{169}$$

Another important condition is imposed on the pulse duration. The pulse duration τ should be longer than the time taken to transit the characteristic region of interaction with the ion (on the order of two oscillatory radii) with a drift velocity: [20]

$$\tau \gg \frac{v_{\rm osc}}{v} \frac{2\pi}{\omega_0} \Leftrightarrow \tau \gg 510 \sqrt{\frac{P}{T}} \frac{1}{\omega_0^2} \,. \tag{170}$$

Another condition arises from the classical description we employed. It may be shown that this condition is equivalent to the following one:

$$r_E \gg \lambda_{\rm osc} = \frac{\hbar}{m v_{\rm osc}} \;\Leftrightarrow\; P \gg 2.4 \times 10^{-6} \, \frac{\omega_0^4}{Z^2} \,. \tag{171}$$

Therefore, with increasing field the applicability conditions for the classical description of the binary collision problem are improved. From a qualitative viewpoint, the issue is that the energy exchange occurs in a region of size r_E (48), which is inversely proportional to the square root of the field amplitude. Since the electron de Broglie wavelength estimated from the oscillatory velocity decreases even faster ($\sim 1/E$), quantum corrections should be insignificant, which is confirmed by the data of numerical simulations [42–44].

The condition imposed on the particle concentration is the most rigorous. The results outlined here are formally valid only for a sufficiently rarefied plasma, $n r_{\rm osc}^3 \ll 1$ (Table 1). However, similar effects would be expected to take place in denser plasmas as well. Specifically, of significance is only the assumption that there is only one ion in the volume $r_{\rm osc} \rho_{\rm attr}^2$ which defines the attraction domain, since the presence of another ion in the path of the electron scattered by the ion may radically change the collision dynamics and minimize correlation effects [78]. In dimensional variables, this condition has the form

$$n \leqslant 6 \times 10^{17} \, \frac{T \omega_0^4}{PZ} \simeq 8 \times 10^{18} \, \frac{T}{\lambda^4 PZ} \,. \tag{172}$$

In higher-density plasmas, the effects described in our review will not show up completely (will turn out to be weakened, while their parameter dependence will change), but will take place up to concentrations $n b_{\rm osc} r_{\rm osc}^2 \equiv n r_E^2 r_{\rm osc} \leqslant 1$, albeit in a rather weak form. In such a plasma, the neighboring ions have no effect on the electron trajectory during the external field cycle and permit the electron to execute one oscillation and be attracted to the ion from a distance on the order of $r_E = \sqrt{b_{\rm osc} r_{\rm osc}}$. We did not perform

Table 1. Limiting concentrations (in cm^{-3}).

	Formula	Estimation formula
Dense plasma for $v \gg v_{\rm osc}$	$1/b_v^3$	$3 \times 10^{20} \, \frac{T^3}{Z^3}$
Dense plasma for $v \ll v_{\rm osc}$	$1/b_{\rm osc}^3$	$9 \times 10^{31} \, \frac{P^3}{Z^3 \omega^6}$
Boundary of correlation effects ($r_E \ll r_{\rm D}$)	$1/(r_E^2 b_v)$	$9 \times 10^{22} \, \frac{T\sqrt{P}}{Z^2}$
Applicability domain of numerical data	$1/(r_{\rm osc} \rho_{\rm attr}^2)$	$6 \times 10^{17} \, \frac{T\omega^4}{PZ}$
Highly rarefied plasma	$1/r_{\rm osc}^3$	$2 \times 10^{16} \, \frac{\omega^6}{P^{3/2}}$

Table 2. Characteristic scales in electron–ion collisions.

Quantity	Notation*	Formula	Estimation formula
Spatial scale			
Pulse length	L	$c\tau$	$2.99 \times 10^{-5} \tau$
Oscillation radius	$r_{\rm osc} = \frac{1}{\Omega^2}$	$\frac{eE}{m\omega^2}$	$3.41 \times 10^{-6} \, \frac{P^{1/2}}{\omega^2}$
Rutherford radius in v_T	$b_v = \frac{1}{v^2}$	$\frac{Ze^2}{m v_T^2}$	$1.44 \times 10^{-7} \, \frac{Z}{T}$
Rutherford radius in $v_{\rm osc}$	$b_{\rm osc} = \Omega^2$	$\frac{Ze^2}{m v_{\rm osc}^2}$	$2.17 \times 10^{-11} \, \frac{Z\omega^2}{P}$
Return radius	$r_E = 1$	$\sqrt{\frac{Ze}{E}}$	$8.61 \times 10^{-9} \, \frac{Z^{1/2}}{P^{1/4}}$
Attraction radius	$\rho_{\rm attr} = \frac{1}{\Omega v}$	$\sqrt{b_v r_{\rm osc}}$	$7.02 \times 10^{-7} \, \frac{P^{1/4} Z^{1/2}}{\omega T^{1/2}}$
Coherence radius	$r_{\rm a}$	$\frac{2\pi c}{\omega_{\rm p}}$	$3.34 \times 10^{-3} \, \frac{1}{\sqrt{n}}$
Debye radius	$r_{\rm D}$	$\frac{v_T}{\omega_{\rm p}}$	$7.41 \times 10^{-7} \, \frac{\sqrt{T}}{\sqrt{n}}$
Compton length	$\lambda_{\rm C}$	$\frac{h}{mc}$	3.86×10^{-11}
de Broglie length in v_T	λ_v	$\frac{h}{m v_T}$	$2.76 \times 10^{-8} \, \frac{1}{\sqrt{T}}$
de Broglie length in $v_{\rm osc}$	$\lambda_{\rm osc}$	$\frac{h}{m v_{\rm osc}}$	$3.39 \times 10^{-10} \, \frac{\omega}{\sqrt{P}}$
Velocities			
Thermal velocity	$v_T = v$	$\sqrt{\frac{2T}{m}}$	$4.19 \times 10^7 \sqrt{T}$
Oscillatory velocity	$v_{\rm osc} = \frac{1}{\Omega}$	$\frac{eE}{m\omega}$	$3.41 \times 10^9 \, \frac{\sqrt{P}}{\omega}$
Normalization velocity	$v_E = 1$	$r_E \omega_E$	$1.71 \times 10^8 P^{1/8} Z^{1/4}$
Critical velocity	$v_\Omega = \Omega$	$r_E \omega$	$8.61 \times 10^7 \, \frac{\sqrt{Z}\omega}{P^{1/4}}$
Frequencies			
Field frequency	$\omega = \Omega$	$\frac{2\pi c}{\lambda}$	$\frac{1.88}{\lambda}$
Plasma frequency	$\omega_{\rm p} = \sqrt{4\pi n}$	$\sqrt{\frac{4\pi e^2 n}{m}}$	$5.64 \times 10^{-2} \sqrt{n}$
Normalization frequency	$\omega_E = 1$	$\sqrt[4]{\frac{eE^3}{m^2 Z}}$	$19.9 \, \frac{P^{3/8}}{Z^{1/4}}$

* For some quantities, their dependence on parameters v and Ω is given in dimensionless form.

[20] It is pertinent to note that an appreciable fraction of 'captured' electrons — the particles which would not leave the interaction region $r_{\rm osc}$ for a time considerably longer than the transit time $2r_{\rm osc}/v_T$ for this region — was observed in numerical simulations. The fraction of such electrons increases with field intensity.

detailed calculations for this case but, according to general considerations, incoherent bremsstrahlung will be enhanced by a factor of $r_{\rm osc}/b_{\rm osc}$ [by analogy with the increase in the effective cross section (see Section 8)] in comparison with that in traditional models, and a weak coherent radiation will emerge (see Section 8). In a plasma of even higher density ($nb_{\rm osc}^3 \sim 1$), correlation effects vanish completely and traditional models become applicable [79–84].

To summarize this section, we give estimates for characteristic quantities (spatial dimensions, velocities, and frequencies) in dimensional form (Table 2).

13. Conclusions

Our review presents the current state of research on electron–ion collisions in strong electromagnetic fields. The emphasis was placed on the description of relativistic- and nonrelativistic-velocity electrons colliding with ions. Of the most important results included in our review, we highlight the following ones.

We have classified the types of electron motion and expected effects in the electron scattering by an ion in the presence of an EM field. The equation of test electron motion and, accordingly, the structure of phase space were shown to depend on one dimensionless parameter, which is defined by the ratio of the potential energy at a range of the oscillatory radius from the ion to the electron oscillatory energy.

We have analyzed the strong field case under those conditions where the oscillatory velocity is far greater than the drift one. We have obtained analytical and numerical estimates of the effective collision frequency, the intensity of coherent harmonic emission, and the energy distribution of fast particles. We showed that, unlike traditional notions, the efficiency of these processes does not become lower with increasing intensity of the pump field. A common feature of the above effects is their weak dependence on the polarization of the pump field.

A general expression was derived for the integral of binary electron–ion collisions in the kinetic equation for the single-particle distribution function in the drift coordinates and velocities of electrons in the field of an arbitrary EM wave. For strong EM fields, the expression for the collision operator was represented in the form of the sum of a diffusion term and a fast particle source.

An investigation of the applicability conditions for the results outlined in our review shows that they remain valid for a transparent plasma and an EM wave of arbitrary (including relativistic) intensity.

References

1. Silin V P *Sov. Phys. JETP* **11** 1277 (1960); *Zh. Eksp. Teor. Fiz.* **38** 1771 (1960)
2. Silin V P *Sov. Phys. JETP* **14** 617 (1962); *Zh. Eksp. Teor. Fiz.* **41** 861 (1961)
3. Silin V P *Sov. Phys. JETP* **20** 1510 (1965); *Zh. Eksp. Teor. Fiz.* **47** 2254 (1964)
4. Dawson J, Oberman C *Phys. Fluids* **5** 517 (1962)
5. Lifshitz E M, Pitaevskii L P *Physical Kinetics* (Oxford: Pergamon Press, 1981); Translated from Russian: *Fizicheskaya Kinetika* (Moscow: Nauka, 1979)
6. Silin V P, Uryupin S A *Sov. Phys. JETP* **54** 485 (1981); *Zh. Eksp. Teor. Fiz.* **81** 910 (1981)
7. Bunkin F V, Fedorov M V *Sov. Phys. JETP* **22** 844 (1966); *Zh. Eksp. Teor. Fiz.* **49** 1215 (1965)
8. Pert G J *J. Phys. A* **5** 506 (1972)
9. Schlessinger L, Wright J *Phys. Rev. A* **20** 1934 (1979)
10. Rae S C, Burnett K *Phys. Rev. A* **46** 2077 (1992)
11. Pflalzner S *Appl. Phys. B* **55** 368 (1992)
12. Fedorov M V *Elektron v Sil'nom Svetovom Pole* (Electron in a Strong Light Field) (Moscow: Nauka, 1991)
13. Shvets G, Fisch N J *Phys. Plasmas* **4** 428 (1997)
14. Mittleman M H *Introduction to the Theory of Laser-Atom Interactions* (New York: Plenum Press, 1993)
15. Pert G J *Phys. Rev. E* **51** 4778 (1995)
16. Silin V P *Vvedenie v Kineticheskuyu Teoriyu Gazov* (Introduction to the Kinetic Theory of Gases) (Moscow: Nauka, 1971)
17. Kostyukov I Yu, Rax J-M *Phys. Rev. E* **59** 1122 (1999)
18. Christov I P, Murnane M M, Kapteyn H C *Phys. Rev. Lett.* **78** 1251 (1997)
19. Kolbenstvedt H, Olsen H A *Phys. Rev.* **175** 11 (1968)
20. Faehl R J, Roderick N F *Phys. Fluids* **21** 793 (1978)
21. Jones R D, Lee K *Phys. Fluids* **25** 2307 (1982)
22. Polishchuk A Ya, Meyer-Ter-Vehn J *Phys. Rev. E* **49** 663 (1994)
23. Pert G J *J. Phys. B* **8** 3069 (1975)
24. Pert G J *J. Phys. B* **12** 2755 (1979)
25. Pert G J *J. Phys. A* **9** 1797 (1976)
26. Bunkin F V, Kazakov A E, Fedorov M V *Sov. Phys. Usp.* **15** 416 (1973); *Usp. Fiz. Nauk* **107** 559 (1972)
27. Fedorov M V *Sov. Phys. JETP* **24** 529 (1967); *Zh. Eksp. Teor. Fiz.* **51** 795 (1966)
28. Pert G J *J. Phys. B* **29** 1135 (1996)
29. Reiss H R *Prog. Quantum Electron.* **16** 1 (1992)
30. Nikishov A I, Ritus V I *Sov. Phys. JETP* **19** 529 (1964); *Zh. Eksp. Teor. Fiz.* **46** 776 (1964)
31. Kroll N M, Watson K M *Phys. Rev. A* **8** 804 (1973)
32. Silin V P *JETP* **84** 262 (1997); *Zh. Eksp. Teor. Fiz.* **111** 478 (1997)
33. Silin V P *JETP* **87** 468 (1998); *Zh. Eksp. Teor. Fiz.* **114** 864 (1998)
34. Decker C D et al. *Phys. Plasmas* **1** 4043 (1994)
35. Wiesenfeld L *Phys. Lett. A* **144** 467 (1990)
36. Landau L D, Lifshitz E M *Mechanics* (Oxford: Pergamon Press, 1976); Translated from Russian: *Mekhanika* (Moscow: Nauka, 1988)
37. Fraiman G M, Mironov V A, Balakin A A *Phys. Rev. Lett.* **82** 319 (1999)
38. Fraiman G M, Mironov V A, Balakin A A *JETP* **88** 254 (1999); *Zh. Eksp. Teor. Fiz.* **115** 463 (1999)
39. Fraiman G M, Balakin A A *Physica D* **152 – 153** 731 (2001)
40. Fraiman G M, Balakin A A, Mironov V A *Plasma Phys.* **8** 2502 (2001)
41. Brantov A et al. *Phys. Plasmas* **10** 3385 (2003)
42. Rascol G et al. *Phys. Plasmas* **13** 103108 (2006)
43. Baumann C, Kull H-J, Fraiman G M *Phys. Rev. A* **92** 063420 (2015)
44. Serebryakov D A, Balakin A A, Fraiman G M *Plasma Phys. Rep.* **40** 705 (2014); *Fiz. Plazmy* **40** 807 (2014)
45. Bogoliubov N N *The Dynamical Theory in Statistical Physics* (Delhi: Hindustan Publ. Corp., 1965); *Problemy Dinamicheskoi Teorii v Statisticheskoi Fizike* (Moscow: Gostekhizdat, 1946)
46. Balakin A A *Plasma Phys. Rep.* **34** 1046 (2008); *Fiz. Plazmy* **34** 1129 (2008)
47. Langdon A B *Phys. Rev. Lett.* **44** 575 (1980)
48. Albritton J R *Phys. Rev. Lett.* **50** 2078 (1983)
49. Landau L D, Lifshitz E M *The Classical Theory of Fields* (Oxford: Butterworth-Heinemann, 2000); Translated from Russian: *Teoriya Polya* (Moscow: Nauka, 1973)
50. Krainov V P *J. Phys. B* **33** 1585 (2000)
51. Krainov V P *JETP* **92** 960 (2001); *Zh. Eksp. Teor. Fiz.* **119** 1109 (2001)
52. Balakin A A, Fraiman G M *Comput. Phys. Commun.* **164** 46 (2004)
53. Bell A R, Evans R G, Nicholas D J *Phys. Rev. Lett.* **46** 243 (1981)
54. Matte J P et al. *Plasma Phys. Control. Fusion* **30** 1665 (1988)
55. Epperlein E M, Rickard G J, Bell A R *Phys. Rev. Lett.* **61** 2453 (1988)
56. Stiefel E L, Scheifele G *Linear and Regular Celestial Mechanics; Perturbed Two-Body Motion, Numerical Methods, Canonical Theory* (Berlin: Springer-Verlag, 1971); Translated into Russian *Lineinaya i Regulyarnaya Nebesnaya Mekhanika* (Moscow: Nauka, 1975)
57. Landau L D, Lifshitz E M *Quantum Mechanics: Non-Relativistic Theory* (Oxford: Pergamon Press, 1977); Translated from Russian:

Kvantovaya Mekhanika: *Nerelyativistskaya Teoriya* (Moscow: Nauka, 1989)
58. Madey J M J *Nuovo Cimento B* **50** 64 (1979)
59. Fraiman G M, Kostyukov I Yu *Phys. Plasmas* **2** 923 (1995)
60. Balakin A A, Mironov V A, Fraiman G M *Plasma Phys. Rep.* **27** 462 (2001); *Fiz. Plazmy* **27** 491 (2001)
61. Krainov V P *JETP* **111** 171 (2010); *Zh. Eksp. Teor. Fiz.* **138** 196 (2010)
62. Corkum P B, Burnett N H, Ivanov M Y *Opt. Lett.* **19** 1870 (1994)
63. Yudin G L, Ivanov M Y *Phys. Rev. A* **63** 033404 (2001)
64. Balakin A A, Fraiman G M *JETP* **93** 695 (2001); *Zh. Eksp. Teor. Fiz.* **120** 797 (2001)
65. Dodin I Y, Fisch N J, Fraiman G M *JETP Lett.* **78** 202 (2003); *Pis'ma Zh. Eksp. Teor. Fiz.* **78** 238 (2003)
66. Balakin A A, Fraiman G M *JETP* **103** 370 (2006); *Zh. Eksp. Teor. Fiz.* **130** 426 (2006)
67. Charlier C L *Die Mechanik des Himmels* (Berlin: W. de Gruyter, 1927); Translated into Russian: *Nebesnaya Mekhanika* (Moscow: Nauka, 1966)
68. Tokman M D *Plasma Phys. Rep.* **25** 140 (1999); *Fiz. Plazmy* **25** 160 (1999)
69. Balakin A A *Plasma Phys. Rep.* **34** 296 (2008); *Fiz. Plazmy* **34** 330 (2008)
70. Arnold V I, Kozlov V V, Neishtadt A I *Mathematical Aspects of Classical and Celestial Mechanics* (Berlin: Springer, 2006); *Matematicheskie Aspekty Klassicheskoi i Nebesnoi Mekhaniki* (Itogi Nauki i Tekhniki. Sovremennye Problemy Matematiki. Fundamental'nye Napravleniya) Vol. 3 (Ed. R V Galekrelidze) (Moscow: VINITI, 1985)
71. Balakin A A, Fraiman G M, Fisch N J *JETP Lett.* **81** 1 (2005); *Pis'ma Zh. Eksp. Teor. Fiz.* **81** 3 (2005)
72. Key M H et al. *Phys. Plasmas* **5** 1966 (1998)
73. Hatchett S P et al. *Phys. Plasmas* **7** 2076 (2000)
74. Koyama K, Saito N, Tanimoto M, in *ICPP 2000, Quebec, Canada* (2000) p. MP1.067, ICPP No. 4051
75. Mangles S P D et al. *Phys. Rev. Lett.* **94** 245001 (2005)
76. Balescu R *Statistical Mechanics of Charged Particles* (Amsterdam: North-Holland, 1965); Translated into Russian: *Statisticheskaya Mekhanika Zaryazhennykh Chastits* (Moscow: Mir, 1967)
77. Balakin A A, Fraiman G M *Europhys. Lett.* **93** 35001 (2011)
78. Balakin A A, Tolmachev M G *Plasma Phys. Rep.* **34** 658 (2008); *Fiz. Plazmy* **34** 716 (2008)
79. Pfalzner S, Gibbon P *Phys. Rev. E* **57** 4698 (1998)
80. Mostovych A N et al. *Phys. Rev. Lett.* **66** 612 (1991)
81. Cauble R, Rozmus W *Phys. Fluids* **28** 3387 (1985)
82. Ichimaru S, Tanaka S *Phys. Rev. A* **32** 1790 (1985)
83. Bornath T et al. *Phys. Rev. E* **64** 026414 (2001)
84. Haberland H, Bonitz M, Kremp D *Phys. Rev. E* **64** 026405 (2001)